

Dynamics of Parallel Manipulators with Hybrid Complex Limbs – Modular Modeling and Parallel Computing –

Andreas Müller

JKU Johannes Kepler University, Linz, Austria, a.mueller@jku.at

ABSTRACT

Parallel manipulators, also called parallel kinematics machines (PKM), enable robotic solutions for highly dynamic handling and machining applications. The safe and accurate design and control necessitates high-fidelity dynamics models. Such modeling approaches have already been presented for PKM with simple limbs (i.e. each limb is a serial kinematic chain). A systematic modeling approach for PKM with complex limbs (i.e. limbs that possess kinematic loops) was not yet proposed despite the fact that many successful PKM comprise complex limbs.

This paper presents a systematic modular approach to the kinematics and dynamics modeling of PKM with complex limbs that are built as serial arrangement of closed loops. The latter are referred to as hybrid limbs, and can be found in almost all PKM with complex limbs, such as the Delta robot. The proposed method generalizes the formulation for PKM with simple limbs by means of local resolution of loop constraints, which is known as constraint embedding in multibody dynamics. The constituent elements of the method are the kinematic and dynamic equations of motions (EOM), and the inverse kinematics solution of the limbs, i.e. the relation of platform motion and the motion of the limbs. While the approach is conceptually independent of the used kinematics and dynamics formulation, a Lie group formulation is employed for deriving the EOM. The frame invariance of the Lie group formulation is used for devising a modular modeling method where the EOM of a representative limb are used to derive the EOM of the limbs of a particular PKM. The PKM topology is exploited in a parallel computation scheme that shall allow for computationally efficient distributed evaluation of the overall EOM of the PKM. Finally, the method is applied to the IRSBot-2 and a 3RR[2RR]R Delta robot, which is presented in detail.

Keywords–Parallel kinematics machines, parallel robots, complex limbs, hybrid robots, dynamics, kinematics, control, screws, Lie group $SE(3)$, parallel computing

1 Introduction

Many of the successfully applied PKM possess limbs with kinematic loops, which will be referred to as *complex limbs*. The best known example is the Delta robot introduced by Clavel [1, 2], which generates a Schönflies motion (also called SCARA motion [3]). The Delta has exactly one kinematic loop per limb. Other PKM were proposed whose limbs possess several loops, which are called fundamental cycles (FCs). Almost all such PKM possess complex multi-loop limbs where the loops are arranged in series within the limbs, i.e. the FC share at most one common link. Such limbs are called *hybrid*. From a modeling and analysis perspective this allows treating the loops independently so that the loop constraints can be solved separately. The concept of 'locally' solving loop constraints was proposed in [4] for general multibody system as *constraint embedding*. A similar approach will be employed in this paper for PKM modeling.

The main feature of Delta robots is that each limb resembles a 4-bar linkage that is hinged at the base and the moving platform. The parallelogram(s) within a limb are often regarded as a kinematic joint referred to as Π -joint [3] (notice that this compound joint contributes its own inherent dynamics, which must be accounted for by the dynamics formulation). Various PKM whose limbs comprise parallelogram linkages were reported in the literature. A PKM with two parallelogram limbs generating Schönflies motions was proposed in [5, 6], and another Schönflies motion PKM with four limbs in [7]. The Orthoglide, a 3-DOF translational PKM, was proposed in [8, 9]. Another 3-DOF example is the CaPaMan robot [10]. A kinematically redundant PKM involving parallelogram loops was presented in [11]. A redundantly actuated planar PKM with two parallelogram limbs intended as machine tool was proposed in [12]. Parallelogram limbs were used in [13, 14] as building blocks for synthesizing spatial 3-DOF translational PKM actuated with prismatic joints. A planar 3-DOF PKM with a hybrid arrangement of parallelograms is the NaVaRo robot [15]. The Par2 robot [16, 17] is an example for a 2-DOF Delta variant. The 4-DOF H4 robot [18] and the Par4 [19] are modifications of the Delta where the end-effector rotation is controlled by an articulated platform. The relevance of a (conceptually simple) parallelogram arrangement within the limbs is documented by patents such as [20] on a 2-DOF PKM and [21] on a 4-DOF Schönflies motion PKM, in addition to the original patent by Clavel [22]. To exploit the full spectrum of PKM with complex limbs, however, other robots were proposed. The IRSBot-2 [23] is a 2-DOF PKM where each limb comprises a planar parallelogram as well as a loop

with four U joints. To increase the workspace, in [24, 25, 15] a 3-DOF translational PKM was presented whose limbs are constructed from scissor mechanisms, which leads to a multi-loop complex limb. The systematic design and modeling of PKM with complex limbs is a relatively new field of research, and more general designs with closed loops, other than simple parallelogram linkages, will yield novel PKM. This paper shall provide a basis for modeling such general PKM.

The type synthesis of PKM with complex limbs is more involved than it is for simple limbs due to the much larger varieties of closed loop mechanisms that can generate the platform motion. A synthesis method for 2-DOF PKM comprising complex limbs with two loops was reported in [26], but a dedicated approach for PKM with complex limbs has not yet been proposed. In principle, the general method based on linear transformations [27, 28] and the synthesis based on the virtual chain concept [29] or screw system based approaches [30] can be applied. The Lie group methods based on displacement groups should be applicable. It could in particular lead to a modular synthesis method by synthesizing and combining loops with certain motion space, as it was pursued in [30] based on instantaneous screw systems.

The dynamics modeling is an integral part of the design and analysis process of PKM in order to exploit their acceleration and load capacity. There are many publications that addressed the derivation of dynamic EOM for specific PKM with simple limbs, e.g. [31, 32, 33, 34, 35, 36, 37, 38, 39, 40]. The EOM for Delta robots were derived in [2, 41, 42, 43, 44] starting from the kinetic and potential energy and then analytically deriving the Lagrange equations. To make this tractable, simplifying assumptions are made. In [2, 45], for instance, the inertia of the lower arm parallelogram is split and is distributed to the upper arm and the platform, respectively. Lagrange equations were derived analytically in [7] to formulate the dynamic EOM in terms of actuator coordinates for a 4-DOF Schönflies motion PKM with parallelogram joints. Aiming at general PKM with simple limbs without the need for model simplifications, systematic modeling approaches were proposed in [3, 46, 47, 48, 49]. These methods have in common that they take into account the special kinematic structure of PKM. To this end, the kinematics and dynamics model of the individual limbs, and of the platform, are derived and are used to formulate the overall EOM by imposing the loop closure conditions. The differences are found mainly in the kinematics modeling. Key element is the forward and inverse kinematics of the individual limbs. The latter refers to the relation of the motion of all joints of the limb and the platform motion, which is used to express the PKM motion in terms of taskspace coordinates. It should be mentioned that the bond graph modeling technique was applied to PKM with simple and complex limbs in [50, 51].

This paper presents a systematic generally applicable modeling approach for rigid body PKM with complex limbs, following the basic concept of the formulation for PKM with simple limbs in [47, 49]. The modularity is exploited for modeling the kinematics and dynamics of the (possibly structurally identical) limbs. The approach is independent of the particular formulation used for kinematics and dynamics modeling. Its application is described in detail when using the screw and Lie group formulation, which can be directly related to the formulation in [3, 49] for PKM with simple limbs. Special emphasis is given to the computational aspects, and its applicability for parallel computation is explored. The main steps for deriving the task space formulation of the EOM can be summarized as follows:

1. Analyze PKM topology, and partition into separate subgraphs representing the limbs (sec. 2). Identify FCs, and construct a tree-topology system (sec. 3.1).
2. Express the forward kinematics of the tree-topology system (sec. 3.2)
3. Separately solve the velocity constraints of each FC in all limbs (sec. 3.3, 3.4)
4. Incorporate the constraint solution into the forward kinematics of the tree-topology system (sec. 3.5-3.7)
5. Solve the inverse kinematics of the mechanism (sec. 4).
6. Pursue the kinematics and dynamics modeling as for the PKM with simple limbs (sec. 6)

The paper is organized as follows. The graph representation of kinematic topology, its partitioning into subgraphs corresponding to the limbs, and the introduction of a tree-topology kinematics are recalled in sec. 2. The kinematics modeling of the tree-topology system is presented in sec. 3.2 in terms of joint screw coordinates and the product of exponentials (POE). The constraints for kinematic loops within the limbs are presented in sec. 3.3 and 3.4. In sec. 3.3 the cut-joint formulation is presented as the method of choice, which is widely used in MBS dynamics. The cut-body formulation is recalled in sec. 3.4 for completeness only as it allows application of the reciprocal screw method to formulate the constraint Jacobian, which is an established approach to linkage analysis. It does, however, not directly lead to an efficient implementation. A formulation for the inverse kinematics of the mechanism is presented in sec. 4, and for the inverse kinematic of the manipulator in sec. 5. The formulation in sec. 4 is then employed for deriving the dynamic EOM in sec. 6. A task space formulation is presented in sec. 6.5, and a formulation in actuator coordinates is derived in sec. 6.6. The inherent modularity of PKM is exploited in sec. 7 for a modular modeling approach. Applications of the dynamics model are discussed in sec. 8. The system of EOM applicable to time integration (to solve the forward dynamics) is presented in sec. 8.1. The inverse dynamics formulation is summarized in 8.2 and its use for parallel computation is discussed. The method is demonstrated in detail for the 3RR[2RR]R Delta robot in sec. 9. The paper closes with a short conclusion and outlook in sec. 10. For completeness, appendix A summarizes the Lie group formulation of linkage kinematics in terms of joint screws, which is then used in appendix B to briefly summarize the Lie group formulation of EOM. The notation and list of symbols is summarized in appendix C.

2 Kinematic Topology

The topological graph, denoted Γ , describes the arrangement of bodies and joints [52,53,54]. Vertices represent bodies, and edges represent joints. Edges of Γ represent joints with general DOF, but are often used to represent 1-DOF joints, which are used to model multi-DOF joints. The topological graph possesses γ fundamental cycles (FC), i.e. topologically independent loops.

Definition 1. The system of bodies and joints that corresponds to a connected component of Γ , which connects the ground vertex with the vertex of the moving platform, is called a *limb*. The subgraph corresponding to limb $l = 1, \dots, L$ is denoted with $\Gamma_{(l)}$, where L is the total number of limbs.

The number of independent kinematic loops of limb l , i.e. the number of FCs of $\Gamma_{(l)}$, is denoted with γ_l . The FCs corresponding to the kinematic loops of limb l are denoted with $\Lambda_{\lambda(l)}, \lambda = 1, \dots, \gamma_l$.

Definition 2. A limb is called *simple* if and only if it is a simple (i.e. serial) kinematic chain. It is called *complex* if and only if it comprises kinematic loops. If any two FCs of the topological graph $\Gamma_{(l)}$ have at most one common vertex (and are hence edge-disjoint), the limb is called *hybrid*. Hybrid limbs are also called serial-parallel limbs as the kinematic loops are arranged in series within the limb.

The following assumption 1 holds true for almost all PKM with complex limbs.

Assumption 1. It is assumed in the following that the PKM possess hybrid limbs only.

Example 1 (3RR[2RR]R Delta). The Delta robot is arguably the best-known and most successful PKM with complex limbs. The kinematic design of the Delta robot, as reported in the patent [22], contains revolute joints only, as shown in fig. 1a). The four revolute joints 3,4,5,7, forming the parallelogram loop within a limb, resemble a planar 4-bar linkage (see fig. 1b). The axes of joints 3 and 5 intersect the axis of joint 2, and the axes of joints 4 and 7 intersect the axis of joint 6. A similar design was reported in [55, 56] with the difference that the axes do not intersect. Both designs are denoted with 3RR[2RR]R, which indicates that each of the three limbs comprises an actuated R joint (joint 1) followed by a passive R joint (joint 2), which connects to the loop formed by parallel arrangement of two RR chains (joints 3 and 4 respectively 5 and 7), indicated by the bracket, that is connected to the platform by another R joint (joint 6). Frequently, this design is simply denoted 3RUU as the R joints with intersecting axes kinematically function as U joints (neglecting bodies 2 and 4). The topological graph is shown in fig. 2a). Each of the $L = 3$ limbs possesses $\gamma_l = 1$ FC, as shown in fig. 2b).

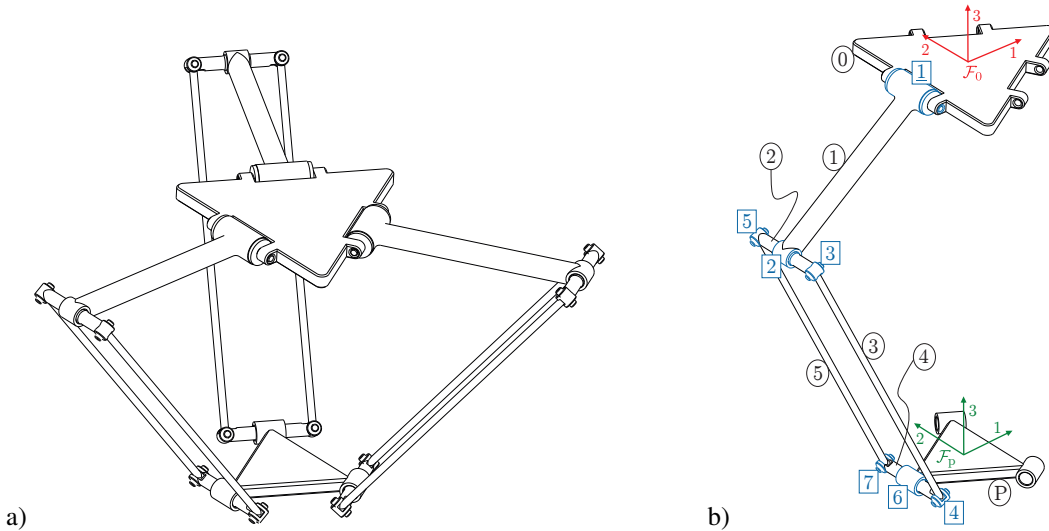


Fig. 1. a) Drawing of a 3RR[2RR]R Delta robot. b) Representative limb of this Delta robot

Example 2 (3R[2US] Delta). From a practical perspective, it is difficult to ensure that the axes of the R joints forming the 4-bar are parallel. Moreover, as a spatial mechanism, the parallelogram in the 3R[2SS] is overconstrained. In an alternative design, which is adopted in most commercial implementations of the Delta concept, spherical joints are used at both ends of the rods to connect them directly to platform and base, respectively. This is generally considered to be the original Delta design [1, 2]. It is referred to as 3R[2SS] design (often simply denoted as 3RSS). This kinematics would allow spinning of the rods about their longitudinal axes. In order to avoid this spinning (or rather slipping), most Delta robots are equipped with pinned braces (e.g. Yaskawa and Motoman Delta robot has braces at both ends), which restricts the S joints to function as U joints. Thus this Delta design becomes a 3R[2UU] kinematics (often simply denoted as 3RUU), where the axes of the two U joints that are fixed to the ground are parallel, and so are those fixed to the platform. The loop formed by the four U joints would again be overconstrained, but the braces are introduced to only restrain the bars rather than to geometrically

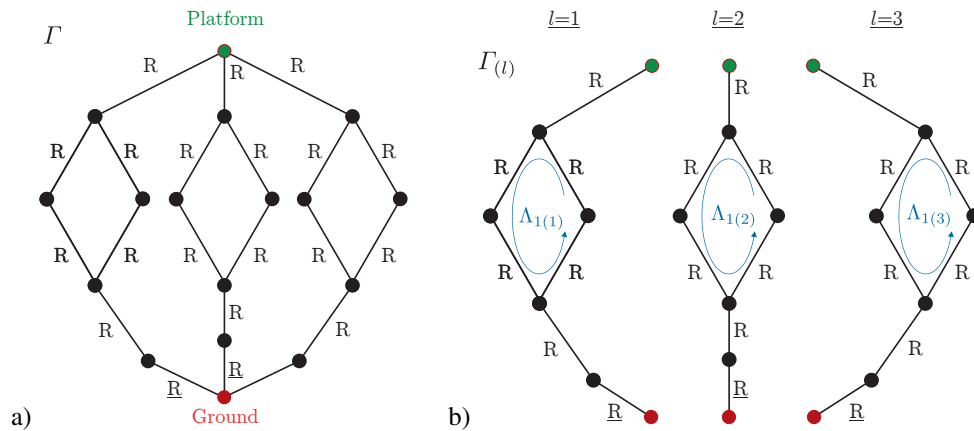


Fig. 2. a) Topological graph of the $3\overline{R}R[2\overline{R}R]R$ Delta. b) Subgraphs $\Gamma_{(l)}$ representing the $L = 3$ limbs of this Delta.

constraint them. A model that describes this kinematics is to use S joints at the platform and U joints to connect the rods to the articulated arm. This model will be referred to as $3\overline{R}[2US]$ design in the following. Its topological graph is shown in fig. 3. The parallelogram loop is now formed by the two U and the two S joints.

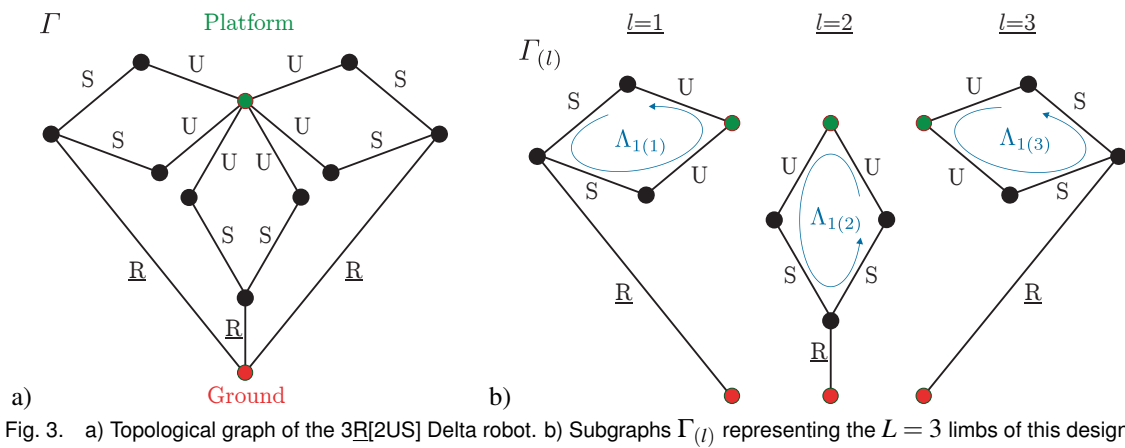


Fig. 3. a) Topological graph of the $3\overline{R}[2US]$ Delta robot. b) Subgraphs $\Gamma_{(l)}$ representing the $L = 3$ limbs of this design.

Example 3 (IRSBot-2). Fig. 4 shows a sketch of the IRSBot-2, which was presented in [23], and fig. 5 shows its topological graph. Each of the $L = 2$ limbs possesses $\gamma_l = 2$ kinematic loops, $\Lambda_{1(l)}$ and $\Lambda_{2(l)}$. Due to the serial arrangement of these FCs, the limbs possess a hybrid topology.

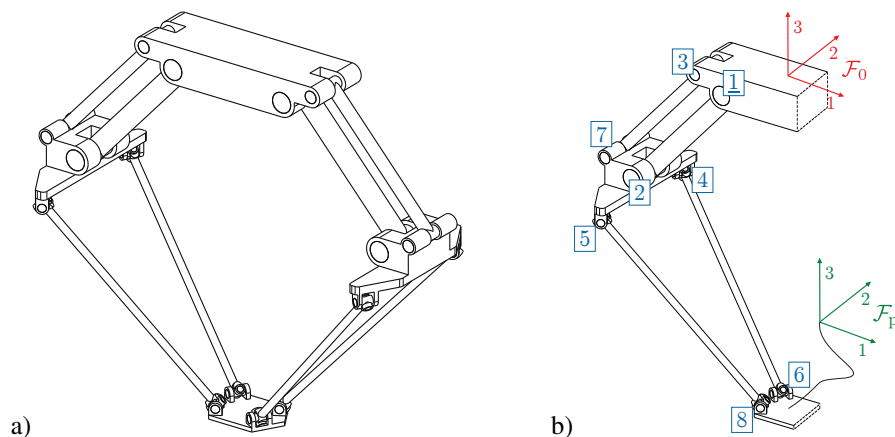


Fig. 4. a) Drawing of the IRSBot-2 presented in [23] (courtesy of Sébastien Briot, Laboratoire des Sciences du Numérique de Nantes). b) Representative limb comprising two loops.

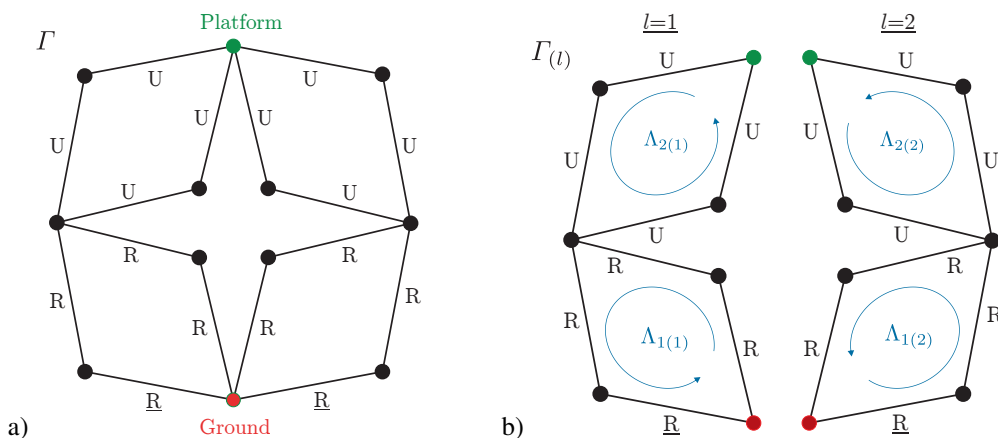


Fig. 5. a) Topological graph of the IRSBot-2. b) Subgraphs $\Gamma^{(l)}$ representing the $L = 2$ limbs. The hybrid topology of the limbs is clearly visible as $\Lambda_{1(l)}$ and $\Lambda_{2(l)}$ are arranged in series.

The topological graph $\Gamma^{(l)}$ of limb l possesses γ_l fundamental cycles itself. Further, any two limbs, being connected to the platform, form a FC. In total the PKM hence comprises $\gamma = L \cdot \gamma_l + L - 1 = L(\gamma_l + 1) - 1$ FCs (assuming identical limbs). Indeed, for PKM with simple limbs there are $L - 1$ FCs [49]. For structurally identical limbs, the subgraphs are congruent. Following the standard approach of modeling multibody systems in terms of relative coordinates (joint variable), a system of loop closure constraints would be introduced for each of these γ FCs. A tailored formulation for such PKM can be introduced exploiting the special topology as presented in this paper.

3 Forward Kinematics of a Complex Limb

The forward kinematics encompasses the determination of the motion of all bodies of the limb, including the platform, for given motion of a set of independent joints. For a simple limb, when separated from the PKM, all joints can move independently, whereas for a PKM with complex limbs, the joints must satisfy certain loop constraints. Explicit solution of the geometric loop constraints in closed form is possible for particular PKM only. This is therefore not assumed in the following. Instead, the solution of the velocity constraints will be used to formulate the differential kinematics limb, and for solving the geometric constraints.

3.1 Associated Tree-Topology System, Graph Labeling

Vertices (bodies) of the topological graph $\Gamma_{(l)}$ of limb l are numbered with $i = 0, 1, 2, \dots, n_l$, where index 0 refers to the ground, and the platform is labeled with P. Edges (joints) are indexed with $i = 1, \dots, \mathfrak{N}_l$. $\Gamma_{(l)}$ possesses γ_l fundamental cycles. A spanning tree $G_{(l)}$ on $\Gamma_{(l)}$ is obtained by removing exactly one edge (cut-edge) of each FC, which defines a tree-topology system comprising n_l moving bodies and n_l joints (tree-edges). There is a unique path in $G_{(l)}$ from any vertex (body) to the root (ground). A *ground-directed spanning tree* $\vec{G}_{(l)}$ is then introduced by directing all edges of $G_{(l)}$ so to point toward the ground within this path. In the so constructed $\vec{G}_{(l)}$, there is a unique directed path from any vertex (moving body) to the ground. In particular, there is a path from platform to ground, and the platform motion is determined by the motion of the corresponding kinematic chain. The latter must indeed respect the loop constraints imposed by the kinematic loops.

The root-directed tree $\vec{G}_{(l)}$ induces a partial order of bodies: Body j is a *predecessor* of i if j comes after i in the directed path from i to 0. This is denoted with $j \prec_l i$ (or simply with $j \prec i$ if it is clear that it refers to limb l). The direct predecessor j of i is indicated with $j = i - 1$ (or simply $j = i - 1$). The tree is *canonical* if $j \prec_l i$ implies $j < i$. For sake of simplicity, the n_l tree-edges are numbered with body indices $i = 1, \dots, n_l$, so that the tree-edge connecting vertex i with its predecessor is labeled with i . Cut-edges are thus indexed with $i = n_l + 1, \dots, \mathfrak{N}_l$.

Definition 3. Joints that correspond to edges in $G_{(l)}$ are called *tree-joints* of the limb. Joints that correspond to the cut-edges in the co-tree $\Gamma_{(l)} \setminus G_{(l)}$ are called *cut-joints*.

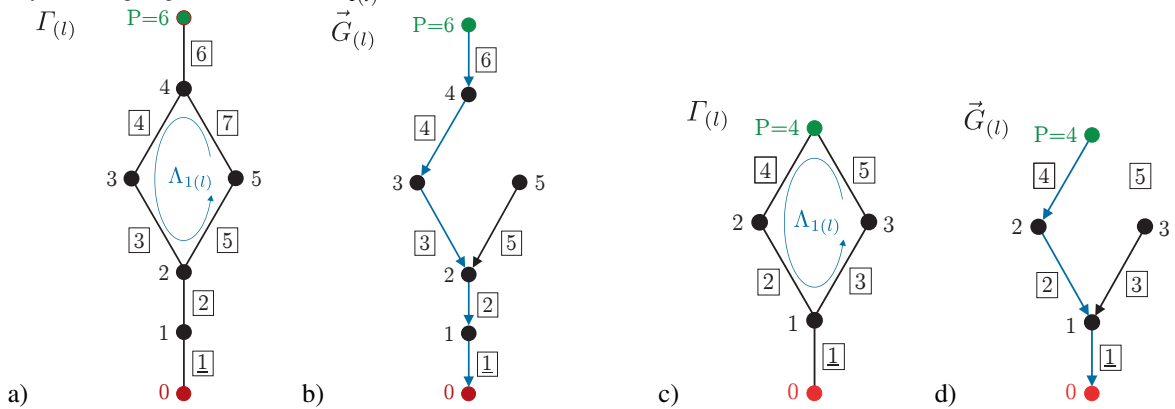
Body (and thus joint) indices can be taken arbitrarily from the index set $\{1, \dots, \mathfrak{N}_l\}$. However, to aid the matrix formulation of the kinematics and the EOM (appendix A), the following assumption is made.

Assumption 2. The body indices of each limb are assigned so that the spanning tree $\vec{G}_{(l)}$ is canonical [53, 4].

Denote with $\boldsymbol{\eta}_{(l)} := (\vartheta_{1(l)}, \dots, \vartheta_{N_l(l)})^T \in \mathbb{V}^{N_l}$ the overall vector of N_l joint variables of limb l , and with $\boldsymbol{\vartheta}_{(l)} := (\vartheta_{1(l)}, \dots, \vartheta_{n_l(l)}) \in \mathbb{V}^{n_l}$ the vector of n_l tree-joint variables (i.e. vector $\boldsymbol{\eta}_{(l)}$ with cut-joint variables removed). If the PKM comprises 1-DOF joints only, then $N_l = \mathfrak{N}_l$ and $n_l = n_l$. A general PKM comprises multi-DOF joints, so that $N_l \leq \mathfrak{N}_l$ and $n_l \leq n_l$.

Example 4 (3RR[2RR]R Delta –cont.). Fig. 6a) shows the labeled topological graph of limb l . Removing, for instance, edge 7 from the FC $\Lambda_{1(l)}$ yields the directed spanning tree shown in fig. 6b). Joint 7 is the cut-joint of this FC. The path from platform to ground is shown in blue color. The platform motion is thus determined by joints 1, 2, 3, 4, and 6. The seven 1-DOF R joints give rise to the vector of $N_l = 7$ joint variables $\boldsymbol{\eta}_{(l)} = (\vartheta_{1(l)}, \dots, \vartheta_{7(l)})^T$. The vector of $n_l = 6$ tree-joint variables is $\boldsymbol{\vartheta}_{(l)} = (\vartheta_{1(l)}, \dots, \vartheta_{6(l)})^T$.

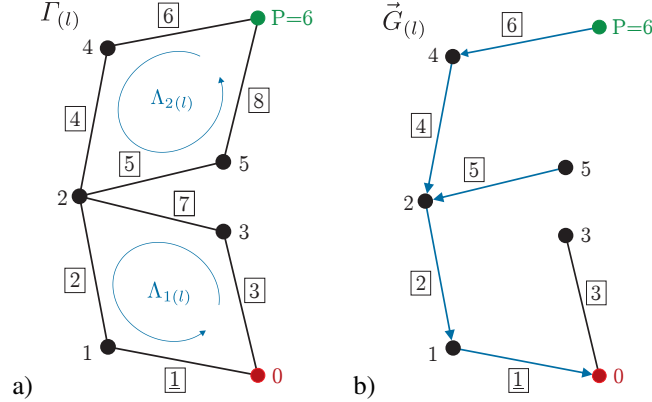
Fig. 6. a) Labeled subgraph $\Gamma_{(l)}$ of a limb of the 3RR[2RR]R Delta ($\mathfrak{N}_l = 7$), and b) directed spanning tree $\vec{G}_{(l)}$ ($n_l = 6$) obtained by removing edge 5 from the FC $\Lambda_{1(l)}$. c) Subgraph $\Gamma_{(l)}$ of a limb of the 3R[2US] Delta ($\mathfrak{N}_l = 5$), and d) directed spanning tree $\vec{G}_{(l)}$ ($n_l = 4$) obtained by removing edge 4 from the FC $\Lambda_{1(l)}$.



Example 5 (3R[2US] Delta –cont.). The labeled topological graph of limb l is shown in fig. 6c). Removing, for instance, edge 5 (representing a U joint) from the FC $\Lambda_{1(l)}$ yields the directed spanning tree, with $n_l = 4$ tree-joints shown in fig. 6d). The platform motion is determined by joints 1, 2, and 4. Using two angles as joint variables for a U joint and three angles for an S joint leads to the vector $\boldsymbol{\eta}_{(l)}$ of $N_l = 11$ joint variables, and the vector $\boldsymbol{\vartheta}_{(l)}$ of $n_l = 9$ tree-joint variables.

Example 6 (IRSBot-2 –cont.). For each of the two FCs of the IRSBot-2, one edge must be removed. Eliminating edge 7 from $\Lambda_{1(l)}$ and edge 8 from $\Lambda_{2(l)}$ yields the directed tree shown in fig. 7b). Joints 7 and 8 are the cut-joints. The platform motion is determined by joints 1,2,4, and 6. The system is parameterized by $N_l = 12$ joint variables in $\eta_{(l)}$, and the $n_l = 9$ tree-joint variables constitute the vector $\vartheta_{(l)}$.

Fig. 7. a) Labeled subgraph $\Gamma_{(l)}$ of a limb of the IRSBot-2 ($\mathfrak{N}_l = 8$). b) directed spanning tree $\vec{G}_{(l)}$ ($n_l = 6$) obtained by removing edge 3 from the FC $\Lambda_{1(l)}$ and edge 7 from $\Lambda_{2(l)}$.



3.2 Kinematics of the Associated Tree-Topology System

Once a spanning tree $G_{(l)}$ is introduced, the limb can be treated as a tree-topology system. The pose of body k of the limb is determined by the joints in the kinematic chain from that body toward the ground corresponding to the directed path from vertex k to 0 in $\vec{G}_{(l)}$. The direction of edges has a kinematic meaning. The joint represented by the directed edge is regarded as enabling the motion of a body relative to its predecessor (defined by the target vertex of the edge). This is important for interpreting the joint variables. For example, the angle of revolute joint 5 of the 3RR[2RR]R Delta describes the rotation of body 5 relative to body 2 (not that of body 2 relative to body 5), according to the directed tree in fig. 6b).

The absolute configuration (or pose) of body k w.r.t. the inertial frame (IFR) is denoted with $\mathbf{C}_k \in SE(3)$ in (117). For sake of simplicity, and without loss of generality, in the following, the kinematics is described assuming 1-DOF joints (so that $n_l = n_l$), which admits describing joint motions by a 1-parameter screw motion. Notice that any mechanism can be modeled with 1-DOF joints by modeling multi-DOF joints as series of 1-DOF joints. Denote with \underline{k} the index of the last body in the path from body k to the ground, i.e. $0 = \underline{k} - 1$. The pose of body k in limb l is determined by the product of exponentials (118) as

$$\mathbf{C}_{k(l)}(\vartheta_{(l)}) = f_{k(l)}(\vartheta_{(l)})\mathbf{A}_{k(l)} \quad (1)$$

with $\mathbf{A}_{k(l)} = \mathbf{C}_{k(l)}(\mathbf{0})$ being the zero reference configuration of the body, and (omitting index (l))

$$f_k(\vartheta) = \exp(\vartheta_{\underline{k}}\mathbf{Y}_{\underline{k}}) \cdots \exp(\vartheta_{\underline{k}-1}\mathbf{Y}_{\underline{k}-1}) \exp(\vartheta_k\mathbf{Y}_k) \quad (2)$$

where $\mathbf{Y}_{i(l)}$ denotes the screw coordinate vector of tree-joint i at the zero reference configuration $\eta_{(l)} = \mathbf{0}$ of the tree-topology system, represented in IFR. The relative configuration of body r w.r.t. body k is $\mathbf{C}_{k,r} := \mathbf{C}_k^{-1}\mathbf{C}_r$.

The twist of body k of limb l in body-fixed representation is determined by (125) in appendix A as

$$\mathbf{V}_k = \mathbf{J}_{k,\underline{k}}(\vartheta)\dot{\vartheta}_{\underline{k}} + \cdots + \mathbf{J}_{k,\underline{k}-1}(\vartheta)\dot{\vartheta}_{\underline{k}-1} + \mathbf{J}_{k,k}(\vartheta)\dot{\vartheta}_k \quad (3)$$

where the $6 \times n_l$ matrix

$$\mathbf{J}_k = (\mathbf{J}_{k,\underline{k}}, \cdots, \mathbf{J}_{k,\underline{k}-1}, \mathbf{J}_{k,k}, \mathbf{0}, \dots, \mathbf{0}) \quad (4)$$

is the *geometric Jacobian* of body k as part of the tree-topology system. The non-zero columns of \mathbf{J}_k are the instantaneous joint screw coordinates represented in \mathcal{F}_k as shown in (127) in appendix A. If tree-joint i is not contained in the directed path in \vec{G} from body k to ground, then $\mathbf{J}_{k,i} = \mathbf{0}$.

The platform pose and twist are determined by the tree-joint variables of limb l and their velocities as (Note that the reference configuration \mathbf{A}_p is the same for all limbs.)

$$\mathbf{C}_p(\boldsymbol{\vartheta}_{(l)}) = f_p(\boldsymbol{\vartheta}_{(l)})\mathbf{A}_p \quad (5)$$

$$\mathbf{V}_{p(l)} = \mathbf{J}_{p(l)}\dot{\boldsymbol{\vartheta}}_{(l)}. \quad (6)$$

The Jacobian $\mathbf{J}_{p(l)}(\boldsymbol{\vartheta}_{(l)})$ comprises the instantaneous screws of the joints in the path from platform to ground in $\vec{G}_{(l)}$.

The platform pose is usually parameterized in terms of *task-space coordinates* $\mathbf{x} \in \mathbb{V}^{\delta_p}$. With slight abuse of notation, the corresponding mapping is also denoted with f_p , so that $\mathbf{x} = f_p(\boldsymbol{\eta})$. The time derivatives of the taskspace coordinates are related to the platform twist by a relation of the form

$$\mathbf{V}_p = \mathbf{H}_p(\mathbf{x})\dot{\mathbf{x}}. \quad (7)$$

Typical choices for \mathbf{x} are components of the position vector vector \mathbf{r}_p of the platform in combination with three rotation parameters, e.g. Euler-/Cardan-angles or rotation axis/angle. In the latter case, the mapping \mathbf{H}_p is the left-trivialized differential of the exponential map on $SO(3)$. Another choice for canonical coordinates is the use of screw coordinates, in which case \mathbf{H}_p is the left-trivialized differential of the exponential map on $SE(3)$ [57].

The platform acceleration is determined by

$$\dot{\mathbf{V}}_{p(l)} = \mathbf{J}_{p(l)}\ddot{\boldsymbol{\vartheta}} + \dot{\mathbf{J}}_{p(l)}\dot{\boldsymbol{\vartheta}}. \quad (8)$$

The time derivative of the joint screw coordinates $\mathbf{J}_{k,a}$ are given in closed form as in (135).

Example 7 (3RR[2RR]R Delta –cont.). According to the directed path in $\vec{G}_{(l)}$ in fig. 6b), the platform pose is $\mathbf{C}_p = f_p(\boldsymbol{\vartheta})\mathbf{A}_p$ with ($k = 1, p = 6$)

$$f_p(\boldsymbol{\vartheta}) = \exp(\vartheta_1 \mathbf{Y}_1) \exp(\vartheta_2 \mathbf{Y}_2) \exp(\vartheta_3 \mathbf{Y}_3) \exp(\vartheta_4 \mathbf{Y}_4) \exp(\vartheta_6 \mathbf{Y}_6). \quad (9)$$

and its geometric Jacobian is, with tree-joint variables $\boldsymbol{\vartheta}_{(l)} = (\vartheta_1, \dots, \vartheta_6)^T$,

$$\mathbf{J}_p = \left(\mathbf{J}_{p,1}, \mathbf{J}_{p,2}, \mathbf{J}_{p,3}, \mathbf{J}_{p,4}, \mathbf{0}, \mathbf{J}_{p,6} \right). \quad (10)$$

The chain connecting body $k = 5$, for instance, to the ground contains joints 1,2, and 5. The body-fixed geometric Jacobian of body 5 is thus

$$\mathbf{J}_5 = \left(\mathbf{J}_{5,1}, \mathbf{J}_{5,2}, \mathbf{0}, \mathbf{0}, \mathbf{J}_{5,5}, \mathbf{0} \right). \quad (11)$$

The platform can only translate, and the platform position vector delivers the taskspace coordinates $\mathbf{x} := \mathbf{r}_p$. The explicit screw coordinate vectors \mathbf{Y}_i and reference configurations are presented in section 9.1.

Remark 1. The product of exponentials (118) is a powerful method that enables describing the motion of kinematic chain in terms of simple geometric parameters. The body poses can, of course, be determined using any other classical method. Using the Denavit-Hartenberg convention, for instance, it would be expressed as the product of homogenous transformation matrices, which take the place of the exponential maps [58, 59].

3.3 Cut-Joint Formulation of Loop Constraints

The kinematic loops for which constraints are introduced are defined by the FCs. Since the FCs are topologically independent and edge-disjoint (assumption 1), the loop constraints can be solved independently. The solution of the overall system of constraints in limb l is hence determined by the solution for the γ_l individual loops. A FC is defined by the cut-edge. There are two conceptually different approaches to formulate the loop constraints: the *cut-joint* formulation and the *cut-body* formulation. The first method involves constraints specific to the cut-joint, whereas the latter imposes a generic system of loop constraints.

3.3.1 Cut-Joint constraints

In the cut-joint formulation, the cut-joints, corresponding to the cut-edges of the FCs $\Lambda_{\lambda(l)}, \lambda = 1, \dots, \gamma_l$, are removed from the model. This yields a tree-topology system with n_l tree-joint variables whose topology is represented by the spanning tree $G(l)$. This tree-system is then subjected to a system of cut-joint constraints in order to satisfy loop closure.

The configuration of the tree-topology system associated to limb l is described by the n_l joint variables in $\vartheta(l)$. Denote with $\vartheta_{(\lambda,l)}$ the vector comprising the $n_{\lambda,l}$ joint variables of the joints in FC $\Lambda_{\lambda(l)}$ except those of the cut joint. The system of $m_{\lambda,l}$ geometric, velocity and acceleration constraints are respectively expressed as

$$g_{(\lambda,l)}(\vartheta_{(\lambda,l)}) = \mathbf{0} \quad (12)$$

$$\mathbf{G}_{(\lambda,l)} \dot{\vartheta}_{(\lambda,l)} = \mathbf{0} \quad (13)$$

$$\mathbf{G}_{(\lambda,l)} \ddot{\vartheta}_{(\lambda,l)} + \dot{\mathbf{G}}_{(\lambda,l)} \dot{\vartheta}_{(\lambda,l)} = \mathbf{0} \quad (14)$$

A joint with δ DOF imposes $6 - \delta$ constraints. If all constraints are independent, then $m_{\lambda,l} = 6 - \delta$, otherwise they are reduced to a set of $m_{\lambda,l} < 6 - \delta$ independent constraints, which is not a topic of this paper. It is assumed that the constraint Jacobian $\mathbf{G}_{(\lambda,l)}(\boldsymbol{\eta}(l))$ is a regular $m_{\lambda,l} \times n_{\lambda,l}$ matrix. The generic DOF of the separated limb l is then $\delta_l := n_l - (m_{1,l} + \dots + m_{\gamma_l,l})$.

The formulation of cut-joint constraints for various technical joints (lower and higher pairs) are well-known in the field of multibody system dynamics [60,61,62]. For completeness the formulation of *elementary cut-joint constraints*, which can be combined to the constraints for specific technical joints, is briefly presented next.

Assume the cut-joint of FC $\Lambda_{\lambda(l)}$ connects body k and body r . A cut-joint frame is introduced at either body, denoted with $\mathcal{J}_{k,\lambda(l)}$ and $\mathcal{J}_{r,\lambda(l)}$, respectively. These are usually located at the rotation center of a spherical or universal joint, or at the joint axis of a revolute or cylindrical joints, for instance. The configuration of the cut-joint frame on body k and r relative to \mathcal{F}_k and \mathcal{F}_r is respectively

$$\mathbf{S}_{k,\lambda(l)} = \begin{pmatrix} \mathbf{R}_{k,\lambda(l)} & {}^k \mathbf{d}_{k,\lambda(l)} \\ \mathbf{0} & \mathbf{1} \end{pmatrix}, \quad \mathbf{S}_{r,\lambda(l)} = \begin{pmatrix} \mathbf{R}_{r,\lambda(l)} & {}^r \mathbf{d}_{r,\lambda(l)} \\ \mathbf{0} & \mathbf{1} \end{pmatrix} \quad (15)$$

where ${}^k \mathbf{d}_{k,\lambda(l)} \in \mathbb{R}^3$ is the position vector from the body-fixed reference frame \mathcal{F}_k to the origin of joint frame $\mathcal{J}_{k,\lambda(l)}$, resolved in \mathcal{F}_k , and analogously ${}^r \mathbf{d}_{r,\lambda(l)} \in \mathbb{R}^3$ at body r . Further, $\mathbf{R}_{k,\lambda(l)}$ and $\mathbf{R}_{r,\lambda(l)}$ is the rotation matrix from $\mathcal{J}_{k,\lambda(l)}$ to \mathcal{F}_k , and from $\mathcal{J}_{r,\lambda(l)}$ to \mathcal{F}_r . Since in the following all derivations refer to limb l , the index (l) will be omitted.

Distance constraints: The distance vector of the origin of the two cut-joint frames resolved in $\mathcal{J}_{k,\lambda}$ is

$$\begin{aligned} {}^{k,\lambda} \Delta \mathbf{r}_\lambda &= \mathbf{R}_{k,\lambda}^T \left(\mathbf{R}_{k,r} {}^r \mathbf{d}_{r,\lambda} - {}^k \mathbf{d}_{k,\lambda} + \mathbf{R}_k^T (\mathbf{r}_r - \mathbf{r}_k) \right) \\ &= {}^{k,\lambda} \mathbf{r}_r - {}^{k,\lambda} \mathbf{r}_k + {}^{k,\lambda} \mathbf{d}_{r,\lambda} - {}^{k,\lambda} \mathbf{d}_{k,\lambda} \end{aligned} \quad (16)$$

with relative rotation matrix $\mathbf{R}_{k,r} := \mathbf{R}_k^T \mathbf{R}_r$ of body r relative body k . This relative translation is restricted according to the cut-joint motion. For most technical joints, the cut-joint frame \mathcal{J}_k can be introduced so that some components of ${}^{k,\lambda} \Delta \mathbf{r}_\lambda$ must vanish (or depend on the joint rotation, e.g. screw joints).

The relative velocity is readily found in terms of the body-fixed twists of the connected bodies k and r , and their geometric

Jacobians, as

$$\begin{aligned}
{}^{k,\lambda}\Delta\dot{\mathbf{r}}_\lambda &= \begin{pmatrix} \mathbf{R}_{k,\lambda}^T ({}^k\tilde{\mathbf{r}}_r - {}^k\tilde{\mathbf{r}}_k + {}^k\tilde{\mathbf{d}}_{r,\lambda}) & -\mathbf{R}_{k,\lambda}^T & -\mathbf{R}_{\lambda,r} {}^r\tilde{\mathbf{d}}_{r,\lambda} & \mathbf{R}_{\lambda,r} \end{pmatrix} \begin{pmatrix} \boldsymbol{\omega}_k \\ \mathbf{v}_k \\ \boldsymbol{\omega}_r \\ \mathbf{v}_r \end{pmatrix} \\
&= \begin{pmatrix} {}^{k,\lambda}\Delta\mathbf{r}_\lambda + {}^k\tilde{\mathbf{d}}_{r,\lambda} & -\mathbf{R}_{k,\lambda}^T & -\mathbf{R}_{\lambda,r} {}^r\tilde{\mathbf{d}}_{r,\lambda} & \mathbf{R}_{\lambda,r} \end{pmatrix} \begin{pmatrix} \boldsymbol{\omega}_k \\ \mathbf{v}_k \\ \boldsymbol{\omega}_r \\ \mathbf{v}_r \end{pmatrix} \\
&= \begin{pmatrix} {}^{k,\lambda}\Delta\mathbf{r}_\lambda + {}^k\tilde{\mathbf{d}}_{r,\lambda} & -\mathbf{R}_{k,\lambda}^T & -\mathbf{R}_{\lambda,r} {}^r\tilde{\mathbf{d}}_{r,\lambda} & \mathbf{R}_{\lambda,r} \end{pmatrix} \begin{pmatrix} \mathbf{J}_k \\ \mathbf{J}_r \end{pmatrix} \dot{\boldsymbol{\vartheta}}_{(l)} =: \mathbf{G}_{(\lambda,l)}^{\text{dist}} \dot{\boldsymbol{\vartheta}}_{(\lambda,l)} \quad (17)
\end{aligned}$$

with rotation matrix $\mathbf{R}_{\lambda,r} := \mathbf{R}_{k,\lambda}^T \mathbf{R}_{k,r}$ from body frame \mathcal{F}_r to cut-joint frame $\mathcal{J}_{k,\lambda(l)}$. The last term follows noting that the relative velocity only depends on motions of joints within the FC $\Lambda_{\lambda(l)}$. The velocity constraints are introduced by equating the relevant components of ${}^{k,\lambda}\Delta\dot{\mathbf{r}}_\lambda$ to zero.

Orientation constraints: Denote with ${}^{k,\lambda}\mathbf{e}_k$ a constant unit vector expressed in $\mathcal{J}_{k,\lambda}$, and with ${}^{r,\lambda}\mathbf{e}_r$ one expressed in $\mathcal{J}_{r,\lambda}$ (omitting subscript (l)). A constraint on the relative orientation of body k and r can be described by enforcing that these two vectors remain perpendicular, i.e.

$$0 = {}^{k,\lambda}\mathbf{e}_k^T \Delta\mathbf{R}_\lambda {}^{r,\lambda}\mathbf{e}_r \quad (18)$$

with $\Delta\mathbf{R}_\lambda := \mathbf{R}_{k,\lambda}^T \mathbf{R}_{k,r} \mathbf{R}_{r,\lambda}$. The velocity constraints are readily obtained with $\Delta\dot{\mathbf{R}}_\lambda = \mathbf{R}_{k,r}^T (\mathbf{R}_{k,r} \tilde{\boldsymbol{\omega}}_r - \tilde{\boldsymbol{\omega}}_k \mathbf{R}_{k,r}) \mathbf{R}_{r,\lambda}$ as

$$\begin{aligned}
0 &= {}^k\mathbf{e}_k^T \tilde{\boldsymbol{\omega}}_k - {}^r\mathbf{e}_r^T \tilde{\boldsymbol{\omega}}_r \\
&= \begin{pmatrix} {}^k\mathbf{e}_k^T \tilde{\boldsymbol{\omega}}_k & -{}^r\mathbf{e}_r^T \tilde{\boldsymbol{\omega}}_r \end{pmatrix} \begin{pmatrix} \boldsymbol{\omega}_k \\ \boldsymbol{\omega}_r \end{pmatrix} \\
&= \begin{pmatrix} {}^k\mathbf{e}_k^T \tilde{\boldsymbol{\omega}}_k & \mathbf{0} & -{}^r\mathbf{e}_r^T \tilde{\boldsymbol{\omega}}_r & \mathbf{0} \end{pmatrix} \begin{pmatrix} \mathbf{J}_k \\ \mathbf{J}_r \end{pmatrix} \dot{\boldsymbol{\vartheta}}_{(l)} =: \mathbf{G}_{(\lambda,l)}^{\text{ori}} \dot{\boldsymbol{\vartheta}}_{(\lambda,l)} \quad (19)
\end{aligned}$$

with the constant vectors ${}^k\mathbf{e}_k := \mathbf{R}_{k,\lambda} {}^{k,\lambda}\mathbf{e}_k$ and ${}^r\mathbf{e}_r := \mathbf{R}_{r,\lambda} {}^{r,\lambda}\mathbf{e}_r$ resolved in \mathcal{F}_k and \mathcal{F}_r , respectively. For a joint with δ^{rot} rotary DOFs, $6 - \delta^{\text{rot}}$ of such orientation constraints are introduced. The joint frames are usually introduced so that \mathbf{e}_k and \mathbf{e}_r are aligned with the coordinate axes. Then ${}^{r,\lambda}\mathbf{e}_r$ and ${}^{k,\lambda}\mathbf{e}_k$ are one of the unit vectors $\mathbf{u}_1 = (1, 0, 0)^T$ etc., and (18) simply requires that one component of the relative rotation matrix $\Delta\mathbf{R}_\lambda$ must be zero.

Constraints for technical joints: The above two types of elementary constraints can be combined to the constraint system of particular technical joints. Spherical and universal joints, for example, do not allow for relative translations so that the distance constraints are

$${}^{k,\lambda}\Delta\mathbf{r}_\lambda = \mathbf{0}, \quad {}^{k,\lambda}\Delta\dot{\mathbf{r}}_\lambda = \mathbf{0}. \quad (20)$$

A universal joint allows for independent rotations about two perpendicular axes, and thus imposes one orientation constraint. Introducing the joint frames so that one rotation axis is along the 1-axis of $\mathcal{J}_{k,\lambda}$, and the other rotation axis is along the 2-axis of $\mathcal{J}_{r,\lambda}$ (which is common practice [60,61,63]), the constant vectors in (18) are ${}^{r,\lambda}\mathbf{e}_r = \mathbf{u}_1 = (1, 0, 0)^T$ and ${}^{k,\lambda}\mathbf{e}_k = \mathbf{u}_2 = (0, 1, 0)^T$. The orientation constraint is that the $(1, 2)$ -element of $\Delta\mathbf{R}_\lambda$ must be zero.

A revolute joint imposes two rotation constraints. If the rotation axis of a revolute joint is aligned with the 3-axes of both joint frames (remaining parallel), then one constraint is defined by the vectors ${}^{r,\lambda}\mathbf{e}_r = \mathbf{u}_1 = (0, 0, 1)^T$ and ${}^{k,\lambda}\mathbf{e}_k = \mathbf{u}_2 = (1, 0, 0)^T$, and the second constrained by ${}^{r,\lambda}\mathbf{e}_r = \mathbf{u}_1 = (0, 0, 1)^T$ and ${}^{k,\lambda}\mathbf{e}_k = \mathbf{u}_2 = (0, 1, 0)^T$.

3.3.2 Resolution of velocity constraints via block partitioning of constraint Jacobian

It is assumed in the following that the $m_{\lambda,l}$ cut-joint constraints (12) are independent, so that $\mathbf{G}_{(\lambda,l)}$ is a full rank $m_{\lambda,l} \times n_{\lambda,l}$ matrix. The constraints (13) can be written as

$$\mathbf{G}_{\mathbf{y}(\lambda,l)}\dot{\mathbf{y}}_{(\lambda,l)} + \mathbf{G}_{\mathbf{q}(\lambda,l)}\dot{\mathbf{q}}_{(\lambda,l)} = \mathbf{0} \quad (21)$$

where $\dot{\mathbf{q}}_{(\lambda,l)}$ comprises $\delta_{\lambda,l} = n_{\lambda,l} - m_{\lambda,l}$ independent velocity coordinates, and $\dot{\mathbf{y}}_{(\lambda,l)}$ consists of $m_{\lambda,l}$ dependent joint rates. Accordingly, $\mathbf{G}_{\mathbf{y}(\lambda,l)}$ is a regular $m_l \times m_l$ submatrix, and $\mathbf{G}_{\mathbf{q}(\lambda,l)}$ is a $m_{\lambda,l} \times \delta_{\lambda,l}$ matrix. The solution of the velocity constraints (13) is then given in terms of the independent velocities as

$$\begin{pmatrix} \dot{\mathbf{y}}_{(\lambda,l)} \\ \dot{\mathbf{q}}_{(\lambda,l)} \end{pmatrix} = \mathbf{H}_{(\lambda,l)}\dot{\mathbf{q}}_{(\lambda,l)} \quad (22)$$

with the $n_{\lambda,l} \times \delta_{\lambda,l}$ matrix $\mathbf{H}_{(\lambda,l)}$ given explicitly as

$$\mathbf{H}_{(\lambda,l)} := \begin{pmatrix} -\mathbf{G}_{\mathbf{y}(\lambda,l)}^{-1}\mathbf{G}_{\mathbf{q}(\lambda,l)} \\ \mathbf{I} \end{pmatrix}_{(\lambda,l)}. \quad (23)$$

With the block partitioning in (21), a solution of the acceleration constraints (14) is

$$\begin{pmatrix} \ddot{\mathbf{y}}_{(\lambda,l)} \\ \ddot{\mathbf{q}}_{(\lambda,l)} \end{pmatrix} = \mathbf{H}_{(\lambda,l)}\ddot{\mathbf{q}}_{(\lambda,l)} + \dot{\mathbf{H}}_{(\lambda,l)}\dot{\mathbf{q}}_{(\lambda,l)} \quad (24)$$

with

$$\dot{\mathbf{H}}_{(\lambda,l)}(\boldsymbol{\eta}_{(\lambda,l)}, \dot{\boldsymbol{\eta}}_{(\lambda,l)}) = \begin{pmatrix} \mathbf{G}_{\mathbf{y}(\lambda,l)}^{-1}(\dot{\mathbf{G}}_{\mathbf{y}(\lambda,l)}\mathbf{G}_{\mathbf{y}(\lambda,l)}^{-1}\mathbf{G}_{\mathbf{q}(\lambda,l)} - \dot{\mathbf{G}}_{\mathbf{q}(\lambda,l)}) \\ \mathbf{0} \end{pmatrix}_{(\lambda,l)}. \quad (25)$$

It should be noticed, that the set of independent velocities can be determined numerically by computing the null-space of $\mathbf{G}_{(\lambda,l)}$ using SVD or QR decompositions. However, a predetermined set of independent coordinates $\mathbf{q}_{(\lambda,l)}$ is often available, which determined the block partitioning.

Example 8 (3RR[2RR]R Delta –cont.). Joint 7 is used as cut-joint of the 4-bar parallelogram forming the FC $\Lambda_{1(l)}$. The three remaining tree-joints are subjected to the revolute joint constraints. Selecting ϑ_4 as independent velocity coordinate for the 4-bar loop yields

$$\boldsymbol{\vartheta}_{(1,l)} = (\vartheta_3, \vartheta_4, \vartheta_5)^T, \quad \mathbf{y}_{(1,l)} = (\vartheta_3, \vartheta_5)^T, \quad \mathbf{q}_{(1,l)} = (\vartheta_4).$$

Joint frames \mathcal{J}_4 and \mathcal{J}_5 are defined at link 4 and 5, respectively, as shown in fig. 8. Then three rows of the constraint Jacobian $\mathbf{G}_{(\lambda,l)}$ are identically zero, and it can be reduced to a 3×4 matrix. As long as the 4-bar linkage remains a parallelogram, it is $\mathbf{G}_{\mathbf{y}(\lambda,l)}^{-1}\mathbf{G}_{\mathbf{q}(\lambda,l)} = (1, 1)^T$, and the solution of the velocity constraints is (22), with

$$\mathbf{H}_{(1,l)} = \begin{pmatrix} -\mathbf{G}_{\mathbf{y}(\lambda,l)}^{-1}\mathbf{G}_{\mathbf{q}(\lambda,l)} \\ \mathbf{I} \end{pmatrix} = \begin{pmatrix} -1 \\ -1 \\ 1 \end{pmatrix}. \quad (26)$$

Accordingly, the solution of the geometric loop constraints is $\vartheta_3 = \vartheta_5 = -\vartheta_4$, with $\boldsymbol{\vartheta} = \mathbf{0}$ corresponding to the reference in fig. 1.

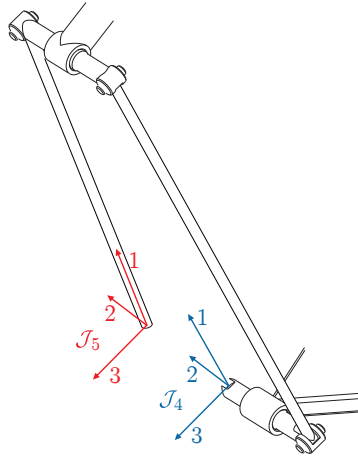


Fig. 8. Parallelogram loop of the Delta. Cut-joint constraints are introduced between joint frames \mathcal{J}_4 and \mathcal{J}_5 . The loop constraints are expressed in cut-joint frame \mathcal{J}_4 at link 4.

Example 9 (IRSBot-2 –cont.). The constraint resolution of the parallelogram loop $\Lambda_{1(l)}$ proceeds as for the Delta. The tree-joint velocities $\dot{\boldsymbol{\vartheta}}_{(1,l)} = (\dot{\vartheta}_1, \dot{\vartheta}_2, \dot{\vartheta}_3)^T$ are expressed in terms of the independent velocity $\dot{\mathbf{q}}_{(1,l)} = (\dot{\vartheta}_1)$, with $\mathbf{H}_{(1,l)}$ as in (26). The 4U loop $\Lambda_{2(l)}$ is cut open by removing joint 8 according to the spanning tree in fig. 7b). The remaining $n_{2,l} = 6$ joint variables of the three U-joints in $\boldsymbol{\vartheta}_{(2,l)} = (\vartheta_{4,1}, \vartheta_{4,2}, \vartheta_{5,1}, \vartheta_{5,2}, \vartheta_{6,1}, \vartheta_{6,2})^T$ are subjected to $m_{2,l} = 4$ constraints (three distance and one orientation constraint). The DOF of the loop is $\delta_{\lambda,l} = 2$, and the joint variables of joint 5 are selected as independent $\mathbf{q}_{(2,l)} = (\vartheta_{6,1}, \vartheta_{6,2})$, and $\mathbf{y}_{(2,l)} = (\vartheta_{4,1}, \vartheta_{4,2}, \vartheta_{5,1}, \vartheta_{5,2})^T$. The 4×6 constraint Jacobian \mathbf{G} has full rank and so has the submatrix \mathbf{G}_y , except at a kinematic singularity, which is not critical for the relevant range of motion. The solution (22) of the velocity constraints is obtained with

$$\mathbf{H}_{(2,l)} := \begin{pmatrix} -\mathbf{G}_y^{-1} \mathbf{G}_q \\ \mathbf{I}_{2,2} \end{pmatrix}$$

Remark 2 (Computational Aspects). The selection of independent coordinates, i.e. partitioning of the matrix $\mathbf{G}_{(\lambda,l)}$ is not unique, unless these $\mathbf{q}_{(\lambda,l)}$ correspond to the actuated joints. Moreover, the selection of a well-conditioned submatrix $\mathbf{G}_y(\lambda,l)$ is crucial for numerical stability. The partitioning can be carried out by means of numerical methods for matrix decomposition, such as QR or SVD, which would take into account the selection of a well-conditioned submatrix to be inverted. This is also addressed in connection with constraint stabilization of MBS models [64, 65]. Computational methods for optimal coordinate partitioning for multibody system models were reported in [66, 67, 68, 69, 70].

The assumption of a full rank constraint Jacobian may not be satisfied if the loop constraints are redundant, so that the $m_{\lambda,l} \times m_{\lambda,l}$ matrix $\mathbf{G}_y(\lambda,l)$ is singular. The treatment of redundant constraints in multibody system models has been a research for many years, and numerical approaches were proposed [71, 72]. Whether and how redundant constraints can be eliminated analytically depends on the particular mechanism. When the motion space of a loop is known explicitly, as in case of planar or spherical linkages, the elimination is straightforward. Clearly, then the choice of reference frame in which the constraints are expressed is crucial, as obvious from the above 4-bar parallelogram. A generally applicable semianalytic method based on analytic identification of motion spaces has been reported in [73, 74]. When modeling the Delta with universal joints at either end of the bars, the constraints are redundant, for example. Yet, in this case it is possible to remove redundant constraints. In the general case of overconstrained and so-called paradoxical [75, 76] mechanisms, this is not possible and numerical decomposition must be used.

Remark 3 (Selection of cut-joint). For a cut-joint with δ DOF, a system of $m_{\lambda,l} = 6 - \delta$ cut-joint constraints is imposed to the $n_l = N_l - \delta$ joint variables. Consequently, the system of constraints can be minimized by selecting a cut-joint with high DOF δ on the expense of a larger DOF of the tree-system. The latter implies a larger system of dynamic motion equations for the tree-topology system (see sec. 6.2).

3.4 Cut-Body Formulation of Loop Constraints

In the cut-body formulation, the cut-edge merely determines how a FC is traversed in order to formulate the loop closure constraints, while the number of constraints does not depend on the selection of cut-edge. The cut-body formulation does

not introduce a tree-topology system. This is clearly different from the cut-joint formulation, where the cut-edge determines the cut-joint to be removed, and thus the tree-topology system as well as the number of constraints.

3.4.1 Kinematic loop constraints

The N_l joint variables of limb l are subjected to the constraints due to the γ_l loops within the limb. Denote with $\boldsymbol{\eta}_{(\lambda,l)}$ the vector of $N_{\lambda,l}$ joint variables of all joints in FC $\Lambda_{\lambda(l)}$. The loop closure condition for $\Lambda_{\lambda(l)}$, $\lambda = 1, \dots, \gamma_l$ gives rise to a system of geometric constraints of the form [76, 77]

$$g_{(\lambda,l)}(\boldsymbol{\eta}_{(\lambda,l)}) = \mathbf{I} \quad (27)$$

and the corresponding velocity constraints

$$\mathbf{G}_{(\lambda,l)} \dot{\boldsymbol{\eta}}_{(\lambda,l)} = \mathbf{0}. \quad (28)$$

The constraints of the γ_l individual FCs are independent due to the loop-partitioned limbs. The generic DOF of the separated limb l is $\delta_l := N_l - (m_{1,l} + \dots + m_{\gamma_l,l})$, with $m_{\lambda,l}$ being the generic rank of $\mathbf{G}_{(\lambda,l)}$.

The constraints can be formulated as a POE, similarly to (2). In contrast to the forward kinematics of the tree-topology system, the interpretation of joint motions depends on the direction of the FC, so that orientation of edges must be taken into account. Denote with $\sigma_{(\lambda,l)}(i) \in \{-1, 0, 1\}$ the entries of the fundamental cycle matrix, which indicates whether a directed edge is part of a FC. If edge i is contained in Λ_l and has the same direction as $\Lambda_{\lambda(l)}$, then $\sigma_{(\lambda,l)}(i) = 1$; if it is directed opposite to the FC, then $\sigma_{(\lambda,l)}(i) = -1$; and $\sigma_{(\lambda,l)}(i) = 0$ if it is not part of the FC.

Denote with $\bar{\lambda}$ the cut-edge, i.e. the single edge of Λ_l not belonging to the spanning tree. This edge is used as start edge when traversing the FC. The last edge visited is denoted with $\underline{\lambda}$. The loop orientation thus induces an ordering within the FC. The geometric loop constraint can now be expressed as

$$g_{(\lambda,l)}(\boldsymbol{\eta}_{(\lambda,l)}) = \exp(\sigma_{(\lambda,l)}(\bar{\lambda}) \vartheta_{\bar{\lambda}} \mathbf{Y}_{\bar{\lambda}}) \cdot \dots \cdot \exp(\sigma_{(\lambda,l)}(\underline{\lambda}) \vartheta_{\underline{\lambda}} \mathbf{Y}_{\underline{\lambda}}). \quad (29)$$

By convention, the cut-joint has the same orientation as the FC, i.e. $\sigma_{(\lambda,l)}(\bar{\lambda}) = 1$.

The $6 \times N_{\lambda,l}$ Jacobian $\mathbf{G}_{(\lambda,l)}(\boldsymbol{\eta}_{(l)})$ is given in terms of the instantaneous screw coordinate vectors of all joints belonging to the kinematic loop according to FC $\Lambda_{\lambda(l)}$. Denote with $\mathbf{S}_i, i \in \Lambda_{\lambda(l)}$ the instantaneous joint screw coordinate vector of joint i in the FC λ of limb l represented in a general reference frame (when represented in the body-fixed frame at body k , for instance, then $\mathbf{S}_i := \mathbf{J}_{k,i}$ are the body-fixed screws (127)). Taking into account the orientation within the FC, the velocity constraints (28) are

$$\mathbf{0} = \sum_{i \in \Lambda_{\lambda(l)}} \sigma_{(\lambda,l)}(i) \mathbf{S}_i \dot{\vartheta}_i \quad (30)$$

which can be written in the form (28) with the constraint Jacobian

$$\mathbf{G}_{(\lambda,l)} = \left(\sigma_{(\lambda,l)}(1) \mathbf{S}_1, \dots, \sigma_{(\lambda,l)}(N_l) \mathbf{S}_{N_l} \right) \quad (31)$$

where column i not corresponding to a joint in $\Lambda_{\lambda(l)}$ is zero since then $\sigma_{(\lambda,l)}(i) = 0$.

Example 10 (3RR[2RR]R Delta –cont.). The one kinematic loop is formed by joints 3, 4, 5, 7 of the parallelogram linkage (fig. 1b), and represented by the FC $\Lambda_{1(l)}$. The corresponding joint coordinate vector is $\boldsymbol{\eta}_{(1,l)} = (\vartheta_3, \vartheta_4, \vartheta_5, \vartheta_7)$. Edge 7 is used as cut-edge. The orientation of $\Lambda_{1(l)}$ in fig. 6b) induces the ordering 5, 3, 4, 7. Edge 5 is directed opposite to the FC. The constraint mapping in (27) and the Jacobian in (31) are thus (omitting subscript (l) on the right-hand side)

$$\begin{aligned} \mathbf{g}_{(1,l)}(\boldsymbol{\eta}_{(1,l)}) &= \exp(-\vartheta_5 \mathbf{Y}_5) \exp(\vartheta_3 \mathbf{Y}_3) \exp(\vartheta_4 \mathbf{Y}_4) \exp(\vartheta_7 \mathbf{Y}_7) \\ \mathbf{G}_{(1,l)} &= \left(\mathbf{S}_3, \mathbf{S}_4, -\mathbf{S}_5, \mathbf{S}_7 \right). \end{aligned} \quad (32)$$

Example 11 (IRSBot-2 –cont.). According to the directed spanning tree in fig. 7b), the geometric loop constraints for the FCs $\Lambda_{1(l)}$ and $\Lambda_{2(l)}$ of the IRSBot-2 are determined by the constraint maps (omitting again subscript (l) on the right-hand side)

$$\begin{aligned}\mathbf{g}_{(1,l)}(\boldsymbol{\eta}_{(1,l)}) &= \exp(-\vartheta_3 \mathbf{Y}_3) \exp(\vartheta_1 \mathbf{Y}_1) \exp(\vartheta_2 \mathbf{Y}_2) \exp(\vartheta_7 \mathbf{Y}_7) \\ \mathbf{g}_{(2,l)}(\boldsymbol{\eta}_{(2,l)}) &= \exp(-\vartheta_5 \mathbf{Y}_5) \exp(\vartheta_4 \mathbf{Y}_4) \exp(\vartheta_6 \mathbf{Y}_6) \exp(\vartheta_8 \mathbf{Y}_8).\end{aligned}\quad (33)$$

The constraint Jacobian in (28) for the respective FC is (omitting subscript (l) on the right-hand side)

$$\mathbf{G}_{(1,l)} = \left(\mathbf{S}_1, \mathbf{S}_2, -\mathbf{S}_3, \mathbf{S}_7 \right) \quad (34)$$

$$\mathbf{G}_{(2,l)} = \left(\mathbf{S}_4, -\mathbf{S}_5, \mathbf{S}_6, \mathbf{S}_8 \right). \quad (35)$$

The corresponding joint coordinate vectors are $\boldsymbol{\eta}_{(1,l)} = (\vartheta_1, \vartheta_2, \vartheta_3, \vartheta_7)$ and $\boldsymbol{\eta}_{(2,l)} = (\vartheta_4, \vartheta_5, \vartheta_6, \vartheta_8)$.

3.4.2 Constraint resolution using reciprocal screws

The reciprocal screw approach is widely used for deriving the inverse kinematics Jacobian of a PKM [78, 56, 79, 80]. It also provides a means to analytically solve the velocity constraints. Although for general complex mechanisms this approach is difficult to pursue, it is described in the following as it offers inside into the PKM kinematics.

The rank of the $6 \times N_{\lambda,l}$ Jacobian $\mathbf{G}_{(\lambda,l)}$, denoted with $m_{\lambda,l}$, is the dimension of the screw system defined by the \mathbf{S}_i . A set of $m_{\lambda,l}$ linearly independent screws can be selected and used to form a $6 \times m_{\lambda,l}$ submatrix $\mathbf{G}_{\mathbf{z}(\lambda,l)}$. The remaining $\delta_{\lambda,l} := N_{\lambda,l} - m_{\lambda,l}$ screw coordinates, which are linearly dependent to the former, provide the columns of a $6 \times (N_{\lambda,l} - m_{\lambda,l})$ submatrix $\mathbf{G}_{\mathbf{q}(\lambda,l)}$. Here, $\delta_{\lambda,l}$ is the generic DOF of the FC $\Lambda_{\lambda(l)}$ when considered separated from the mechanism. With this partitioning of the constraint Jacobian, the constraint (28) can be written as

$$\mathbf{G}_{\mathbf{z}(\lambda,l)} \dot{\mathbf{z}}_{(\lambda,l)} + \mathbf{G}_{\mathbf{q}(\lambda,l)} \dot{\mathbf{q}}_{(\lambda,l)} = \mathbf{0} \quad (36)$$

where $\dot{\mathbf{z}}_{(\lambda,l)}$ is the vector of dependent, and $\dot{\mathbf{q}}_{(\lambda,l)}$ that of the $N_{\lambda,l} - m_{\lambda,l}$ independent joint velocity variable of the loop.

There is a screw that is reciprocal to all $m_{\lambda,l}$ screws forming the columns of $\mathbf{G}_{\mathbf{z}(\lambda,l)}$ but not to the screw forming its j th column and not to the screws forming $\mathbf{G}_{\mathbf{q}}$. There is one such screw for each of the $m_{\lambda,l}$ columns of $\mathbf{G}_{\mathbf{q}}$. A $m_{\lambda,l} \times 6$ matrix $\mathbf{W}_{(\lambda,l)}$ is constructed whose rows are the axes coordinate vectors of these reciprocal screws. Premultiplication of (36) with this matrix yields

$$\mathbf{W}_{(\lambda,l)} \mathbf{G}_{\mathbf{z}(\lambda,l)} \dot{\mathbf{z}}_{(\lambda,l)} + \mathbf{W}_{(\lambda,l)} \mathbf{G}_{\mathbf{q}(\lambda,l)} \dot{\mathbf{q}}_{(\lambda,l)} = \mathbf{0}. \quad (37)$$

The term $\mathbf{W}_{(\lambda,l)} \mathbf{G}_{\mathbf{z}(\lambda,l)}$ is a diagonal $m_{\lambda,l} \times m_{\lambda,l}$ matrix, and (37) can be solved as

$$\dot{\mathbf{z}}_{(\lambda,l)} = - \left(\mathbf{W}_{(\lambda,l)} \mathbf{G}_{\mathbf{z}(\lambda,l)} \right)^{-1} \mathbf{W}_{(\lambda,l)} \mathbf{G}_{\mathbf{q}(\lambda,l)} \dot{\mathbf{q}}_{(\lambda,l)}. \quad (38)$$

For hybrid limbs these solutions can be derived independently for all γ_l FCs giving rise to a solution of the overall velocity loop constraints of FC $\Lambda_{\lambda(l)}$ in terms of $\dot{\mathbf{q}}_{(l)}$. The main task, and principle challenge, of this approach is the determination of the reciprocal screws. They can be constructed geometrically for specific linkages, but this becomes cumbersome for more complex robots. The method for constructing reciprocal screws presented in [81] may alleviate this difficulty.

Example 12 (3RR[2RR]R Delta –cont.). Joints 3, 4, 5, 7 of the 3RR[2RR]R Delta constitute a planar 4-bar parallelogram linkage (fig. 1b), which defines the only FC $\Lambda_{\lambda(l)}$ of limb $l = 1, 2, 3$. The subscript $(1, l)$ is omitted in the following. Denote with \mathbf{p}_i the position vector of a point on the axis of joint i relative to an arbitrary reference frame, and with the \mathbf{e}_i the unit vector along this joint axis, as shown in fig. 9. The joint screws are then $\mathbf{S}_i = (\mathbf{e}_i, \mathbf{p}_i \times \mathbf{e}_i)^T$. The velocity loop constraints (28) are

$$\mathbf{S}_3 \dot{\vartheta}_3 + \mathbf{S}_4 \dot{\vartheta}_4 - \mathbf{S}_5 \dot{\vartheta}_5 + \mathbf{S}_7 \dot{\vartheta}_7 = \mathbf{0}. \quad (39)$$

Since all \mathbf{e}_i are identical, the dimension of the screw system is $\text{rank}(\mathbf{S}_3, \mathbf{S}_4, -\mathbf{S}_5, \mathbf{S}_7) = 3$. The screws of joints 3,5,7 are used as independent columns, and the constraints (39) are written as in (36) with

$$\mathbf{G}_z = (\mathbf{S}_3, -\mathbf{S}_5, \mathbf{S}_7), \quad \mathbf{G}_q = (\mathbf{S}_4) \quad (40)$$

where $\mathbf{z} = (\vartheta_3, \vartheta_5, \vartheta_7)^T$ and $\mathbf{q} = (\vartheta_4)$. The 4-bar motion is thus parameterized by the angle of joint 4, as in example 8. The axis coordinates of the (unit) screws that are reciprocal all joint screws, but not to the screw of joint j and joint 4, can be introduced as

$$\mathbf{W}_3 = \begin{pmatrix} \mathbf{p}_5 \times \mathbf{u}_{5,7} \\ \mathbf{u}_{5,7} \end{pmatrix}, \quad \mathbf{W}_5 = \begin{pmatrix} \mathbf{p}_3 \times \mathbf{u}_{3,7} \\ \mathbf{u}_{3,7} \end{pmatrix}, \quad \mathbf{W}_7 = \begin{pmatrix} \mathbf{p}_3 \times \mathbf{u}_{3,5} \\ \mathbf{u}_{3,5} \end{pmatrix} \quad (41)$$

where $\mathbf{u}_{i,j} := (\mathbf{p}_i - \mathbf{p}_j) / \|\mathbf{p}_i - \mathbf{p}_j\|$ is the unit vector along the line passing through joints i and j . \mathbf{W}_3 and \mathbf{W}_7 represent a force along link 5 and 2, respectively, while \mathbf{W}_5 represents a force along the line through points \mathbf{p}_7 and \mathbf{p}_3 . Notice that, $\|\mathbf{p}_7 - \mathbf{p}_4\| = L_4$, $\|\mathbf{p}_3 - \mathbf{p}_4\| = L_3$, $\|\mathbf{p}_5 - \mathbf{p}_7\| = L_5$, $\|\mathbf{p}_5 - \mathbf{p}_3\| = L_2$, where L_i is the length of link i . Denote with $[\mathbf{a}, \mathbf{b}, \mathbf{c}] = \mathbf{a}^T (\mathbf{b} \times \mathbf{c})$ the wedge product. Premultiplication of \mathbf{G}_z and \mathbf{G}_q with $\mathbf{W} = (\mathbf{W}_3, \mathbf{W}_5, \mathbf{W}_7)^T$ yields

$$\mathbf{W}\mathbf{G}_z = \text{diag}(\mathbf{W}_3^T \mathbf{S}_3, -\mathbf{W}_5^T \mathbf{S}_5, \mathbf{W}_7^T \mathbf{S}_7) = \text{diag}(L_2 [\mathbf{e}_3, \mathbf{u}_{5,3}, \mathbf{u}_{5,7}], -L_2 [\mathbf{e}_5, \mathbf{u}_{3,5}, \mathbf{u}_{3,7}], L_5 [\mathbf{e}_7, \mathbf{u}_{5,7}, \mathbf{u}_{3,5}]) \quad (42)$$

$$\mathbf{W}\mathbf{G}_q = \begin{pmatrix} \mathbf{W}_3^T \mathbf{S}_4 \\ \mathbf{W}_5^T \mathbf{S}_4 \\ \mathbf{W}_7^T \mathbf{S}_4 \end{pmatrix} = \begin{pmatrix} L_4 [\mathbf{e}_4, \mathbf{u}_{7,4}, \mathbf{u}_{5,7}] \\ L_3 [\mathbf{e}_4, \mathbf{u}_{3,4}, \mathbf{u}_{3,7}] \\ L_3 [\mathbf{e}_4, \mathbf{u}_{3,4}, \mathbf{u}_{3,5}] \end{pmatrix} \quad (43)$$

and thus

$$(\mathbf{W}\mathbf{G}_z)^{-1} \mathbf{W}\mathbf{G}_q = \begin{pmatrix} \frac{L_4}{L_2} [\mathbf{e}_4, \mathbf{u}_{7,4}, \mathbf{u}_{5,7}] \\ \frac{L_3}{L_2} [\mathbf{e}_3, \mathbf{u}_{5,3}, \mathbf{u}_{5,7}] \\ -\frac{L_3}{L_2} [\mathbf{e}_4, \mathbf{u}_{3,4}, \mathbf{u}_{3,7}] \\ \frac{L_3}{L_2} [\mathbf{e}_5, \mathbf{u}_{3,5}, \mathbf{u}_{3,7}] \\ \frac{L_3}{L_5} [\mathbf{e}_4, \mathbf{u}_{3,4}, \mathbf{u}_{3,5}] \\ \frac{L_3}{L_5} [\mathbf{e}_7, \mathbf{u}_{5,7}, \mathbf{u}_{3,5}] \end{pmatrix} = \begin{pmatrix} 1 \\ 1 \\ 1 \\ 1 \\ 1 \\ 1 \end{pmatrix}. \quad (44)$$

The last term is obtained with the special geometry, according to which $\mathbf{e}_3 = \mathbf{e}_4 = \mathbf{e}_5 = \mathbf{e}_6$, $\mathbf{u}_{5,3} = \mathbf{u}_{7,4}$, $\mathbf{u}_{3,4} = \mathbf{u}_{5,7}$, and $L_2 = L_4$, $L_3 = L_5$, and with $L_3 [\mathbf{e}_4, \mathbf{u}_{3,4}, \mathbf{u}_{3,7}] = -L_2 [\mathbf{e}_5, \mathbf{u}_{3,5}, \mathbf{u}_{3,7}]$. Thus (38) yields the obvious 4-bar relations $\dot{\vartheta}_3 = \dot{\vartheta}_5 = \dot{\vartheta}_7 = -\dot{\vartheta}_4$ (ref. example 8).

Example 13 (IRSBot-2 –cont.). The kinematics of the parallelogram loop $\Lambda_{1(l)}$ and the 4U loop $\Lambda_{2(l)}$ of the IRSBot-2 were investigated in [23] using the method of reciprocal screws. In this publication, the loop constraints were not resolved, rather the representative screw system (which is a system of screws describing the motion of a loop, i.e. the constraint solution) was determined in order to solve the velocity forward kinematics. The parallelogram loop can be treated as for the 3RR[2RR]R Delta. The 4U loop becomes rather complicated, however, and is not presented here.

3.4.3 Resolution of velocity constraints via block partitioning of constraint Jacobian

In contrast to the above reciprocal screw approach, the constraints (28) be solved via block partitioning of $\mathbf{G}_{(\lambda,l)}$, as for the cut-joint formulation, which provides a generally applicable numerical approach. It is assumed that all $m_{\lambda,l} \leq 6$ constraints are independent, i.e. $\mathbf{G}_{(\lambda,l)}$ is a full rank $m_{\lambda,l} \times N_{\lambda,l}$ matrix. The coordinate vector $\boldsymbol{\eta}$ is split into a vector of $\delta_{\lambda,l} = N_{\lambda,l} - m_{\lambda,l}$ independent coordinates $\mathbf{q}_{(\lambda,l)}$, and a vector $\mathbf{z}_{(\lambda,l)}$ consists of the remaining dependent coordinates of the FC. The velocity constraints are then written as in (36) with a regular square $m_{\lambda,l} \times m_{\lambda,l}$ submatrix $\mathbf{G}_{z(\lambda,l)}$, and a $m_{\lambda,l} \times \delta_{\lambda,l}$ submatrix $\mathbf{G}_{q(\lambda,l)}$. The solution of (28) is then

$$\begin{pmatrix} \dot{\mathbf{z}}_{(\lambda,l)} \\ \dot{\mathbf{q}}_{(\lambda,l)} \end{pmatrix} = \mathbf{H}_{(\lambda,l)} \dot{\mathbf{q}}_{(\lambda,l)} \quad (45)$$

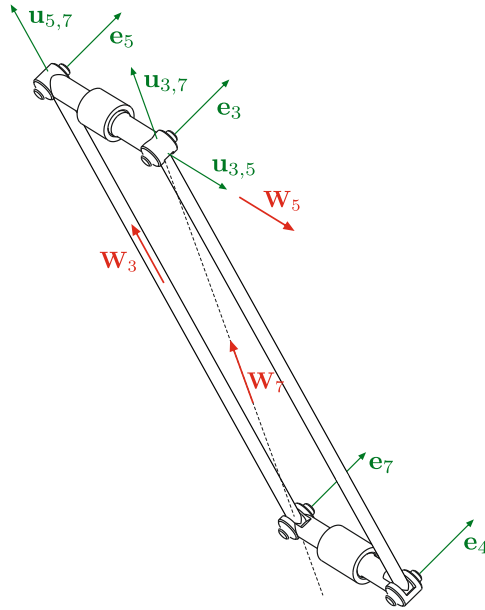


Fig. 9. Screw geometry of the 4-bar parallelogram loop of the Delta. For joint and body numbering refer to fig. 1b).

with

$$\mathbf{H}_{(\lambda,l)} := \begin{pmatrix} -\mathbf{G}_z^{-1}\mathbf{G}_q \\ \mathbf{I} \end{pmatrix}_{(\lambda,l)}. \quad (46)$$

Notice that the same independent coordinates $\mathbf{q}_{(\lambda,l)}$ may be selected as in the cut-joint formulation since the DOF $\delta_{\lambda,l}$ of the FC is indeed the same for both formulations. Then $\mathbf{y}_{(\lambda,l)}$ is the vector $\mathbf{z}_{(\lambda,l)}$ with the cut-joint variables removed.

Remark 4 (Cut-Body vs. cut-joint formulation). *The cut-joint formulation has a two-fold advantage over the cut-body formulation. Firstly, it leads to a smaller system of $m_{\lambda,l} < 6$ constraints for the FC, and a smaller dimension of the matrix to be inverted in (23). Secondly, the number n_l of tree-joint variables, i.e. the DOF of the tree-topology system of limb l , is smaller than the total number N_l of joint variables. On the other hand, the cut-joint formulation may introduce artificial singularities.*

Example 14 (3RR[2RR]R Delta –cont.). *The 4-bar parallelogram forms the only FC $\Lambda_{1(l)}$. The constraints are expressed in a body-fixed frame \mathcal{F}_4 that is arbitrarily located at link 4 but oriented as \mathcal{J}_4 in fig. 8. Then the rows 1,2, and 6 are identically zero, and $\mathbf{G}_{(1,l)}$ can be reduced to a 3×4 matrix. Again, ϑ_4 is selected as independent velocity coordinate for the 4-bar loop so that*

$$\boldsymbol{\eta}_{(1,l)} = (\vartheta_3, \vartheta_4, \vartheta_5, \vartheta_7)^T, \quad \mathbf{z}_{(1,l)} = (\vartheta_3, \vartheta_5, \vartheta_7)^T, \quad \mathbf{q}_{(1,l)} = (\vartheta_4)$$

where the coordinates have been rearranged in accordance with (46). As long as the 4-bar linkage remains a parallelogram, it is $\mathbf{G}_z^{-1}\mathbf{G}_q = (1, 1, 1)^T$, and the solution of the velocity constraints is (22), with

$$\mathbf{H}_{(1,l)} := \begin{pmatrix} -\mathbf{G}_z^{-1}\mathbf{G}_q \\ 1 \end{pmatrix} = \begin{pmatrix} -1 \\ -1 \\ -1 \\ 1 \end{pmatrix}.$$

3.5 Velocity Forward Kinematics of Limb Mechanism

The motion of the FC $\Lambda_{\lambda(l)}$ of limb l is determined by the $\delta_{\lambda,l}$ independent joint variables $\mathbf{q}_{(\lambda,l)}$. In general, some joints of the limb are not part of a FC. The corresponding $\delta_{0,l}$ joint variables are $\vartheta_i, i \in G_l \setminus \Lambda_{\lambda(l)}, l = 1, \dots, \gamma_l$. Since the γ_l FCs are

serially arranged within the limb (assumption 1), the motion of the separated limb l (including the platform) is determined by the $\delta_l := \delta_{0,l} + \delta_{1,l} + \dots + \delta_{\gamma_l,l}$ joint variables, which are summarized in the vector

$$\mathbf{q}^{(l)} := (\mathbf{q}_{(1,l)}, \dots, \mathbf{q}_{(\gamma_l,l)}, \vartheta_{n+1}, \dots, \vartheta_N)^T \quad (47)$$

which consists of the elements of $\mathbf{q}_{(\lambda,l)}$, $\lambda = 1, \dots, \gamma_l$ followed by variables of the remaining tree-joint that are not contained in a FC. Elements of $\mathbf{q}^{(l)}$ represent generalized coordinates, and δ_l is the DOF of the separated limb including the platform. In the following, the cut-joint formulation is employed as this can be immediately exploited for the dynamics modeling. The tree-joint velocities of limb l are determined by the generalized velocities of the limb as

$$\dot{\boldsymbol{\vartheta}}^{(l)} = \mathbf{H}^{(l)} \dot{\mathbf{q}}^{(l)} \quad (48)$$

where the $n_l \times \delta_l$ matrix is

$$\mathbf{H}^{(l)} := \mathbf{P}^{(l)} \begin{pmatrix} \mathbf{H}_{(1,l)} & \mathbf{0} & \dots & \mathbf{0} \\ \mathbf{0} & \mathbf{H}_{(2,l)} & & \mathbf{0} \\ & & \ddots & \vdots \\ \vdots & & & \mathbf{H}_{(\gamma_l,l)} & \mathbf{0} \\ \mathbf{0} & \mathbf{0} & \dots & \mathbf{0} & \mathbf{I} \end{pmatrix} \quad (49)$$

constructed from the matrices in (22), and $\mathbf{P}^{(l)}$ is a permutation matrix that assigns the rows of $\mathbf{H}_{(\lambda,l)}$ to the corresponding joint variables in $\boldsymbol{\vartheta}^{(l)}$.

The body-fixed twist of body k of the separated limb l is determined in terms of the generalized velocities, by the Jacobian (4) along with the solution (48) as

$$\mathbf{V}_{k^{(l)}} = \mathbf{L}_{k^{(l)}} \dot{\mathbf{q}}^{(l)}. \quad (50)$$

with the *compound geometric Jacobian* of body k in limb l

$$\mathbf{L}_{k^{(l)}} := \mathbf{J}_{k^{(l)}} \mathbf{H}^{(l)}. \quad (51)$$

In particular,

$$\mathbf{L}_{p^{(l)}} := \mathbf{J}_{p^{(l)}} \mathbf{H}^{(l)} \quad (52)$$

is the *compound forward kinematics Jacobian* of limb l .

Remark 5. To construct the compound Jacobian, instead of using the permutation matrix $\mathbf{P}^{(l)}$ in (49), the joint variables in $\boldsymbol{\eta}^{(l)}$, and accordingly the columns of $\mathbf{J}_{k^{(l)}}$, could simply be rearranged.

Example 15 (3RR[2RR]R Delta –cont.). In the separated limb, the $\delta_{0,l} = 3$ joints 1,2, and 5 are unconstrained (see tree topology in fig. 6b). The vector $\boldsymbol{\vartheta}_{1^{(l)}} = (\vartheta_3, \vartheta_4, \vartheta_5)^T$ comprises the joint variables of joints forming the FC $\Lambda_{1^{(l)}}$, and $\dot{\boldsymbol{\vartheta}}_{1^{(l)}}$ is subjected to the loop constraints. Their solution is expressed in terms of $\dot{\vartheta}_4$, with matrix $\mathbf{H}_{(1,l)}$ in (26). The velocity of the limb l is thus determined by $\dot{\mathbf{q}}^{(l)} = (\dot{\vartheta}_4, \dot{\vartheta}_1, \dot{\vartheta}_2, \dot{\vartheta}_6)^T$ as

$$(\dot{\vartheta}_3, \dot{\vartheta}_5, \dot{\vartheta}_4, \dot{\vartheta}_1, \dot{\vartheta}_2, \dot{\vartheta}_6)^T = \begin{pmatrix} \mathbf{H}_{(1,l)} & \mathbf{0}_{3,3} \\ \mathbf{0}_{3,1} & \mathbf{I}_{3,3} \end{pmatrix} \dot{\mathbf{q}}^{(l)}.$$

The DOF of the limb is $\delta_l = 4$. The velocity vector $\dot{\boldsymbol{\vartheta}}_{(l)} = (\dot{\vartheta}_1, \dots, \dot{\vartheta}_6)^T$ is then obtained by reordering the elements of the vector on the left-hand side using the permutation matrix

$$\mathbf{P}_{(l)} = \begin{pmatrix} 0 & 0 & 0 & 1 & 0 & 0 \\ 0 & 0 & 0 & 0 & 1 & 0 \\ 1 & 0 & 0 & 0 & 0 & 0 \\ 0 & 0 & 1 & 0 & 0 & 0 \\ 0 & 1 & 0 & 0 & 0 & 0 \\ 0 & 0 & 0 & 0 & 0 & 1 \end{pmatrix}.$$

Along with (26), the matrix in (49) is thus

$$\mathbf{H}_{(l)} = \mathbf{P}_{(l)} \begin{pmatrix} \mathbf{H}_{(1,l)} & \mathbf{0}_{3,3} \\ \mathbf{0}_{3,1} & \mathbf{I}_{3,3} \end{pmatrix} = \begin{pmatrix} 0 & 1 & 0 & 0 \\ 0 & 0 & 1 & 0 \\ -1 & 0 & 0 & 0 \\ 1 & 0 & 0 & 0 \\ -1 & 0 & 0 & 0 \\ 0 & 0 & 0 & 1 \end{pmatrix}. \quad (53)$$

The solution of velocity constraints is determined by the constant matrix $\mathbf{H}_{(l)}$ due to the special parallelogram geometry so that the joint variables in the FC are linearly related. The compound Jacobian $\mathbf{L}_{k(l)}$ of body k is then obtained with (51). In particular, the forward kinematics Jacobian $\mathbf{L}_{p(l)}$ is obtained by premultiplication of $\mathbf{J}_{p(l)}$ in (10) with $\mathbf{H}_{(l)}$. The rank of this matrix 4.

Example 16 (IRSBot-2 –cont.). With the joint coordinate vectors $\boldsymbol{\vartheta}_{1(l)} = (\vartheta_1, \vartheta_2, \vartheta_3)^T$ and $\boldsymbol{\vartheta}_{2(l)} = (\vartheta_{4,1}, \vartheta_{4,2}, \vartheta_{5,1}, \vartheta_{5,2}, \vartheta_{6,1}, \vartheta_{6,2})^T$, and independent coordinates $\mathbf{q}_{(l)} = (\vartheta_1, \vartheta_{6,1}, \vartheta_{6,2})^T$ (see example 9), the velocity constraints of limb l are resolved as

$$(\dot{\vartheta}_1, \dot{\vartheta}_2, \dot{\vartheta}_3, \dot{\vartheta}_{4,1}, \dot{\vartheta}_{4,2}, \dot{\vartheta}_{5,1}, \dot{\vartheta}_{5,2}, \dot{\vartheta}_{6,1}, \dot{\vartheta}_{6,2})^T = \begin{pmatrix} \mathbf{H}_{(1,l)} & \mathbf{0}_{3,2} \\ \mathbf{0}_{6,1} & \mathbf{H}_{(2,l)} \end{pmatrix} \dot{\mathbf{q}}_{(l)} = \mathbf{H}_{(l)} \dot{\mathbf{q}}_{(l)}.$$

3.6 Taskspace Velocity

Consider the complete PKM with all limbs assembled. The platform of the PKM has a DOF $\delta_p \leq 6$, and δ_p 'components' of the platform motion are regarded as kinematic output of the PKM. The corresponding components of the platform twist (usually represented in the platform frame \mathcal{F}_p) form the *task space velocity* \mathbf{V}_t vector, i.e. the velocity output. The task space velocity is formally related to the platform twist via

$$\mathbf{V}_p = \mathbf{P}_p \mathbf{V}_t \quad (54)$$

where \mathbf{P}_p is a unimodular $6 \times \delta_p$ velocity distribution matrix, which assigns the δ_p components of the task space velocity to the components of the platform twist. Assuming appropriately attached platform (end-effector) frame \mathcal{F}_p , typical choices are

$$\mathbf{P}_p^{\text{trans}} = \begin{pmatrix} \mathbf{0}_{3,3} \\ \mathbf{I}_3 \end{pmatrix}, \mathbf{P}_p^{\text{rot}} = \begin{pmatrix} \mathbf{I}_{3,3} \\ \mathbf{0}_3 \end{pmatrix}, \mathbf{P}_p^{\text{planar}} = \begin{pmatrix} 0 & 0 & 0 \\ 0 & 0 & 0 \\ 0 & 0 & 1 \\ 1 & 0 & 0 \\ 0 & 1 & 0 \\ 0 & 0 & 0 \end{pmatrix}, \mathbf{P}_p^{\text{SCARA}} = \begin{pmatrix} 0 & 0 & 0 \\ 0 & 0 & 0 \\ 0 & 0 & 1 \\ 1 & 0 & 0 \\ 0 & 1 & 0 \\ 0 & 0 & 1 \end{pmatrix}. \quad (55)$$

Here, $\mathbf{P}_p^{\text{trans}}$, $\mathbf{P}_p^{\text{rot}}$, and $\mathbf{P}_p^{\text{planar}}$ account for spatial translations and rotations, and for planar motions ($\delta_p = 3$), while $\mathbf{P}_p^{\text{SCARA}}$ is used for Schönflies/SCARA motion ($\delta_p = 4$). The corresponding task space velocities are $\mathbf{V}_t^{\text{trans}} = (\mathbf{v})^T$, $\mathbf{V}_t^{\text{rot}} = (\boldsymbol{\omega})^T$, and $\mathbf{V}_t^{\text{planar}} = (\boldsymbol{\omega}_3, v_1, v_2)^T$, $\mathbf{V}_t^{\text{SCARA}} = (\boldsymbol{\omega}_3, \mathbf{v})^T$.

Now consider the separated limb l , including the platform. The twist of the platform is determined with (52) in terms of the independent joint velocities as $\mathbf{V}_{p(l)} = \mathbf{L}_{p(l)}\dot{\mathbf{q}}(l)$. The instantaneous mobility of the platform is $\text{rank } \mathbf{L}_{p(l)}(\boldsymbol{\eta}(l))$. The rank in general depends on the configuration. It may change in singular configurations of the limb. Moreover, $\mathbf{L}_{p(l)}$ may exhibit a permanent drop of rank when the PKM is assembled. The following assumption is made throughout the paper. Denote with $r_l \leq \delta_l$ the maximal rank of $\mathbf{L}_{p(l)}$, i.e. its rank at a generic configuration $\boldsymbol{\eta}(l)$.

Assumption 3. *It is assumed that in a regular configuration $\boldsymbol{\eta} \in V$ of the PKM, the forward kinematics Jacobian $\mathbf{L}_{p(l)}$ has maximal rank r_l .*

Remark 6. *This assumption does not exclude overconstrained mechanisms per se, but rather allows for exceptionally overconstrained mechanisms, of which the Delta is a good example. The platform motion of the latter is generated by the intersection of the motion spaces of the platform in the separated limbs. The compound Jacobian of each limb has maximal rank 4.*

3.7 Geometric Forward Kinematics of Limb Mechanism

Corresponding to the velocity relation (48), there is a solution of the geometric constraints of the form $\boldsymbol{\vartheta}(l) = \boldsymbol{\Psi}_{k(l)}(\mathbf{q}(l))$, with a mapping $\boldsymbol{\Psi}_{k(l)} : \mathbb{V}^{\delta_l} \rightarrow \mathbb{V}^m$. The geometric forward kinematics problem of the limb is then solved by inserting this into (5) to provide $\mathbf{C}_p(\mathbf{q}(l))$, respectively $\mathbf{x}(\mathbf{q}(l))$. If a closed form solution is available, it provides a solution of the velocity constraints, instead of (12). However, such an explicit solutions can be determined in closed form only in special cases, such as the 3RR[2RR]R Delta, for instance, and this is usually rather involved. In the general situation, the solution of the velocity constraints (48) gives rise to a numerical solution of the geometric constraints. A simple and efficient way is to use the Newton step

$$\Delta\boldsymbol{\vartheta}(l) = \mathbf{H}(l)(\boldsymbol{\vartheta}(l))\Delta\mathbf{q}(l). \quad (56)$$

A solution is found as $\boldsymbol{\vartheta}(l) := \boldsymbol{\vartheta}(l) + \Delta\boldsymbol{\vartheta}(l)$ after only a few iteration steps (except near singularities, where $\mathbf{G}_{y(l)}$ or $\mathbf{G}_{q(l)}$ in (21) become ill conditioned). Alternatively, the velocity relation (48) can be numerically integrated for given $\mathbf{q}(l)(t)$.

4 Inverse Kinematics of PKM Mechanism

The (standard) velocity inverse kinematics problem of the PKM is to determine the actuator velocity for a given task space velocity. The kinematics and dynamics modeling necessitates to determine the motion of all bodies of the PKM, however. This amounts to solving the velocity *inverse kinematics problem of the mechanism*, which consists in finding the independent velocities $\dot{\mathbf{q}}(l)$ of all limbs in terms of the task space velocity. The latter allow to compute the motion of all bodies and joints via the solutions (22) for the individual FCs.

The platform DOF δ_p of the PKM and the maximal rank r_l of limb Jacobian need not be equal. The subsequent formulation for the inverse kinematics must distinguish these two cases.

Definition 4. *If the platform DOF of the PKM is the same as the DOF of the platform when it is connected to the separated limb only, i.e. $\delta_p = r_l$, then the PKM is called equimobile.*

Definition 5. *If $r_l < \delta_l$, then limb l is kinematically redundant. A PKM is kinematically redundant if it contains a kinematically redundant limb.*

The limb of an equimobile PKM admits the same platform mobility when it is separated and when the PKM is assembled, whereas a limb of a non-equimobile PKM is subjected to additional constraints when the limbs are assembled to the PKM. The compound platform Jacobian of a kinematically non-redundant limb is a regular $\delta_l \times \delta_l$ -matrix. In the following, only non-redundant PKM are considered. The formulation is straightforwardly extended to kinematically redundant PKM [49].

4.1 Velocity and Acceleration Inverse Kinematics of Equimobile PKM

A task space Jacobian $\mathbf{L}_{t(l)}$ of limb l is constructed by selecting the relevant $\delta_p = r_l$ rows of the forward kinematics Jacobian $\mathbf{L}_{p(l)}$ in (52). The task space velocity is then determined as

$$\mathbf{V}_t = \mathbf{L}_{t(l)}\dot{\mathbf{q}}(l), \quad l = 1, \dots, L. \quad (57)$$

When the PKM is non-redundant, $\mathbf{L}_{t(l)}$ is a $\delta_p \times \delta_p$ -matrix, and (57) can be solved to obtain the velocity inverse kinematics solution for limb l as

$$\dot{\mathbf{q}}_{(l)} = \mathbf{F}_{(l)} \mathbf{V}_t, \quad \text{with } \mathbf{F}_{(l)} := \mathbf{L}_{t(l)}^{-1}. \quad (58)$$

The complete inverse kinematics for limb l is then obtained with (48) as

$$\dot{\boldsymbol{\vartheta}}_{(l)} = \mathbf{H}_{(l)} \mathbf{F}_{(l)} \mathbf{V}_t \quad (59)$$

where $\mathbf{H}_{(l)} \mathbf{F}_{(l)}$ serves as inverse kinematics Jacobian of the limb mechanism. The latter can be replaced by a closed form expression if a closed form solution of the inverse kinematics is known.

Time derivative of (59) yields a solution to the acceleration inverse kinematics problem

$$\begin{aligned} \ddot{\boldsymbol{\vartheta}}_{(l)} &= \mathbf{H}_{(l)} \mathbf{F}_{(l)} \dot{\mathbf{V}}_t + (\dot{\mathbf{H}}_{(l)} - \mathbf{H}_{(l)} \mathbf{F}_{(l)} \dot{\mathbf{L}}_{t(l)}) \mathbf{F}_{(l)} \mathbf{V}_t \\ &= \mathbf{H}_{(l)} \mathbf{F}_{(l)} \dot{\mathbf{V}}_t + (\dot{\mathbf{H}}_{(l)} - \mathbf{H}_{(l)} \mathbf{F}_{(l)} \dot{\mathbf{L}}_{t(l)}) \dot{\mathbf{q}}_{(l)} \end{aligned} \quad (60)$$

with $\dot{\mathbf{H}}_{(l)}$ in (25), and $\dot{\mathbf{L}}_{t(l)}$ is found with (52) as

$$\dot{\mathbf{L}}_{p(l)}(\boldsymbol{\vartheta}_{(l)}, \dot{\boldsymbol{\vartheta}}_{(l)}) = \dot{\mathbf{J}}_{p(l)} \mathbf{H}_{(l)} + \mathbf{J}_{p(l)} \dot{\mathbf{H}}_{(l)}. \quad (61)$$

4.2 Velocity and Acceleration Inverse Kinematics of Non-Equimobile PKM

The rank r_l of the compound forward kinematics Jacobian $\mathbf{L}_{p(l)}$ of limb l of a non-equimobile PKM exceeds the platform DOF δ_p . The task space Jacobian $\mathbf{L}_{t(l)}$ of limb l is constructed by selecting r_l rows of $\mathbf{L}_{p(l)}$. Then, only δ_p components of $\mathbf{L}_{t(l)} \dot{\mathbf{q}}_{(l)}$ correspond to the components of \mathbf{V}_t , while the remaining $r_l - \delta_p$ equations represent constraints on the platform twist. The latter correspond to constraints imposed on the motion of limb l . This is formalized with help of a $r_l \times \delta_p$ velocity distribution matrix $\mathbf{D}_{t(l)}$, which assigns the components of the task space velocity \mathbf{V}_t to the relevant rows of the task space Jacobian of limb l . The equation

$$\mathbf{D}_{t(l)} \mathbf{V}_t = \mathbf{L}_{t(l)} \dot{\mathbf{q}}_{(l)}, \quad l = 1, \dots, L \quad (62)$$

then summarizes the forward kinematics of the limb as well as the imposed constraints.

The task space Jacobian $\mathbf{L}_{t(l)}$ of a kinematically non-redundant limb (i.e. $r_l = \delta_l$) is an invertible $r_l \times r_l$ matrix, and the solution of the velocity inverse kinematics is

$$\dot{\mathbf{q}}_{(l)} = \mathbf{F}_l \mathbf{V}_t, \quad \text{with } \mathbf{F}_l = \mathbf{L}_{t(l)}^{-1} \mathbf{D}_{t(l)}. \quad (63)$$

The overall solution for the velocity inverse kinematics of the limb mechanism is as in (59).

Example 17 (3RR[2RR]R Delta –cont.). *The platform of the 3-DOF 3RR[2RR]R Delta can only translate, and its DOF is $\delta_p = 3$. The task space velocity vector $\mathbf{V}_t = (\mathbf{v}_p) \in \mathbb{R}^3$ consists of the three components of the EE velocity \mathbf{v}_p . The forward kinematics Jacobian of a limb has rank $r_l = 4$, which is equal to the DOF δ_l of the separated limb, and the PKM is not equimobile. The platform of a separated limb can perform Schönflies motion, i.e. spatial translations plus an independent rotation about an axis parallel to the axis of joint 1 (which is parallel to axes of joint 2 and 6). Expressed in the platform frame \mathcal{F}_p shown in fig. 1b), the 2-component of the angular velocity is non-zero, and thus rows 2,4,5, and 6 are non-zero and are used to construct the 4×4 task space Jacobian $\mathbf{L}_{t(l)}$. The selection matrix extracting the translation part of the platform twist is (the zero row enforces the angular velocity be zero)*

$$\mathbf{D}_{t(l)} = \begin{pmatrix} \mathbf{0}_{1,3} \\ \mathbf{I}_3 \end{pmatrix}, \quad l = 1, 2, 3. \quad (64)$$

Example 18 (IRSBot-2 –cont.). The DOF of a separated limb is $\delta_l = 3$, and its motion is parameterized with $\mathbf{q}_{(l)} = (\vartheta_1, \vartheta_{5,1}, \vartheta_{5,2})^T$. The platform motion is due to the translation of the parallelogram loop in the 1-3-plane of the platform frame \mathcal{F}_p shown in fig. 4b) combined with the rotation about the normal to the plane defined by the 4 U-joints and the translation along this normal. The 3-component of the angular velocity vector ${}^P\boldsymbol{\omega}$ is used to represent the platform rotation. The task space Jacobian of the limb is accordingly constructed from columns 3,4 and 6. When the limbs are assembled, the platform of the 2-DOF IRSBot-2 can only perform planar translations ($\delta_p = 2$) in the 1-3-plane of the platform frame. The task space velocity vector is $\mathbf{V}_t = (v_1, v_3)^T$. The selection matrix assigning the two translation components is (the zero row enforces the angular velocity be zero)

$$\mathbf{D}_{t(l)} = \begin{pmatrix} \mathbf{0}_{1,2} \\ \mathbf{I}_2 \end{pmatrix}, l = 1, 2. \quad (65)$$

4.3 Velocity Inverse Kinematics of general PKM

In the preceding example 18, it must be noted that the selection of ω_3 fails to represent the angular motion when the 4U loop is aligned vertical. This may not be relevant for practical applications, but is a good example for the fact that, when the forward kinematics Jacobian (51) represented in platform frame does not comprise exactly r_l non-zero components, the selection of r_l rows may introduce singularities. In such cases the pseudoinverse solution can always be used without preselection of a taskspace Jacobian. The unique solution of $\mathbf{V}_p = \mathbf{L}_{p(l)}\dot{\mathbf{q}}_{(l)}$ is the inverse kinematics solution for limb l in terms of the left pseudoinverse $\mathbf{L}^+ = (\mathbf{L}^T\mathbf{L})^{-1}\mathbf{L}$

$$\dot{\mathbf{q}}_{(l)} = \mathbf{L}_{p(l)}^+ \mathbf{V}_p \quad (66)$$

which is then used in (59).

4.4 Geometric Inverse Kinematics of the Limb Mechanism

The geometric inverse kinematics problem of the limb mechanism is to determine the joint variables $\boldsymbol{\vartheta}_{(l)}$ for given taskspace coordinates \mathbf{x} , i.e. evaluation of the inverse kinematics mapping

$$\Psi_{\text{IK}(l)} : \mathbb{V}^{\delta_p} \rightarrow \mathbb{V}^{n_l}, \quad \boldsymbol{\vartheta}_{(l)} = \Psi_{\text{IK}(l)}(\mathbf{x}). \quad (67)$$

For certain PKM, the inverse kinematics map Ψ_{IK} can be derived in closed form, as for the 3RR[2RR]R Delta and the IRSBot-2, for instance. In the general case, when this cannot (or is too complicated to) be expressed in closed form, a solution can be obtained numerically. The Jacobian of $\Psi_{\text{IK}(l)}$ is given by $\mathbf{F}_{(l)}\mathbf{H}_{(l)}$ in (59). The inverse kinematics map (56) can be evaluated by means of the simple iteration scheme,

$$\Delta\boldsymbol{\vartheta}_{(l)} = \mathbf{H}_{(l)}(\boldsymbol{\vartheta}_{(l)})\mathbf{F}_{(l)}(\boldsymbol{\vartheta}_{(l)})\Delta\mathbf{x} \quad (68)$$

which yields the update $\boldsymbol{\vartheta}_{(l)} := \boldsymbol{\vartheta}_{(l)} + \Delta\boldsymbol{\vartheta}_{(l)}$. This iteration step is repeated until a solution with the desired precision is obtained. When using (68), the taskspace coordinates \mathbf{x} are the canonical coordinates according to the representation of \mathbf{V}_t in \mathcal{F}_p .

5 Inverse Kinematics of PKM

The velocity inverse kinematics problem is to determine the velocity of the actuated joints for given task space velocity. Assuming a fully actuated PKM, the number of actuator variables n_{act} is equal to or greater than the DOF δ of the PKM. A subset $\boldsymbol{\vartheta}_{(l)\text{act}}$ of $n_{\text{act}(l)}$ variables of the independent coordinates $\mathbf{q}_{(l)}, l = 1, \dots, L$ of the limbs corresponds to the actuated joints. The tree-topology system can always be introduced so that the variables of actuated joints are contained in $\mathbf{q}_{(l)}$. Denote the overall vector of actuated joint coordinates with $\boldsymbol{\vartheta}_{\text{act}} \in \mathbb{V}^{n_{\text{act}}}$. If $n_{\text{act}} > \delta$, the PKM is called *redundantly actuated* [82]. For a non-redundantly actuated PKM, the actuator coordinates represent generalized coordinates, which are usually denoted with $\mathbf{q} := \boldsymbol{\vartheta}_{\text{act}} \in \mathbb{V}^{\delta}$.

The actuator velocities of limb l are readily obtained as

$$\dot{\boldsymbol{\vartheta}}_{(l)\text{act}} = \mathbf{J}_{\text{IK}(l)}(\boldsymbol{\vartheta}_{(l)})\mathbf{V}_t \quad (69)$$

where $\mathbf{J}_{\text{IK}(l)}$ consists of the $n_{\text{act}(l)}$ rows of matrix $\mathbf{F}_{(l)}$ in (58), (63) or (66). The velocity inverse kinematics solution of the PKM is then $\dot{\boldsymbol{\vartheta}}_{\text{act}} = \mathbf{J}_{\text{IK}} \mathbf{V}_t$, with the $n_{\text{act}} \times \delta_p$ *inverse kinematics Jacobian of the manipulator*

$$\mathbf{J}_{\text{IK}}(\boldsymbol{\vartheta}) := \begin{pmatrix} \mathbf{J}_{\text{IK}(1)}(\boldsymbol{\vartheta}_{(1)}) \\ \vdots \\ \mathbf{J}_{\text{IK}(L)}(\boldsymbol{\vartheta}_{(L)}) \end{pmatrix}. \quad (70)$$

The geometric inverse kinematics problem of the PKM consists in finding the actuator coordinates $\boldsymbol{\vartheta}_{(l)\text{act}}$ for given taskspace coordinates \mathbf{x} , or platform pose \mathbf{C}_p . This boils down to determine the closed form expression of the inverse kinematics map $f_{\text{IK}} : \mathbb{V}^{\delta_p} \rightarrow \mathbb{V}^{n_{\text{act}}}$, which satisfies $\boldsymbol{\vartheta}_{\text{act}} = f_{\text{IK}}(\mathbf{x})$. Such explicit expressions are available if the inverse kinematics of the limb mechanism can be solved as $\mathbf{q}_{(l)} = \mathbf{q}_{(l)}(\mathbf{x})$, e.g. for the $\underline{3RR}[2RR]R$ Delta. If no closed form relations are available, the numerical solution is already known with (68).

Remark 7. *The DOF of the PKM and/or the assignment of actuators may be different in different motion modes. If a PKM is operated with different motion modes, it must be switched between the corresponding kinematic models.*

6 Dynamic Equations of Motion (EOM)

In this section a task space formulation of the EOM for a PKM with complex limbs is derived, i.e. EOM in terms of the task space velocity \mathbf{V}_t and acceleration. To this end, the platform is removed so to obtain a tree-topology system with separated complex limbs not containing the platform. For these limbs, the dynamic EOM are formulated. To this end, the EOM of an associated tree-topology system is formulated and the loop closure constraints are subsequently enforced employing the inverse kinematics solution of the mechanism. These EOM along with the EOM of the platform body give rise to the overall system of EOM for the PKM. This approach gives rise to a systematic method for deriving EOM of PKM with complex limbs that is easily implemented and is computationally efficient. It facilitates flexible use of the dynamic formulation of the EOM of tree-topology systems that is deemed most appropriate. It further admits using recursive $O(n)$ evaluation and parallel/distributed computation.

6.1 Kinematics of a complex limb without platform

A tree-topology system is obtained from the tree-topology according to \bar{G} by eliminating the platform and all joints connecting it to the limbs. This is shown in fig. 10 for the $\underline{3RR}[2RR]R$ Delta and the IRSBot-2. Each limb gives rise to a tree-topology system where the last joint connecting the limb to the platform removed. The remaining $\bar{n}_l < n_l$ joint variables, summarized in $\bar{\boldsymbol{\vartheta}}_{(l)} \in \mathbb{V}^{\bar{n}_l}$, determine the configuration of this tree-topology system. The vector of the remaining independent joint variables is denoted with $\bar{\mathbf{q}}$ (possibly the same as \mathbf{q}). The joint velocities $\dot{\boldsymbol{\vartheta}}_{(l)}$ are determined in terms of $\dot{\mathbf{q}}_{(l)}$ by the solution (48) of the loop constraints. Denoting with $\bar{\mathbf{H}}_{(l)}$ the submatrix of $\mathbf{H}_{(l)}$ with the rows corresponding to the remaining \bar{n}_l joint variables, then

$$\dot{\boldsymbol{\vartheta}}_{(l)} = \bar{\mathbf{H}}_{(l)} \dot{\mathbf{q}}_{(l)}. \quad (71)$$

6.2 EOM of the tree-topology system of a separated limb

The dynamic EOM of the tree-topology system of limb l without platform can be written in terms of the coordinates $\bar{\boldsymbol{\vartheta}}_{(l)}$ as

$$\bar{\mathbf{M}}_{(l)} \ddot{\bar{\boldsymbol{\vartheta}}}_{(l)} + \bar{\mathbf{C}}_{(l)} \dot{\bar{\boldsymbol{\vartheta}}}_{(l)} + \bar{\mathbf{Q}}_{(l)}^{\text{grav}} + \bar{\mathbf{Q}}_{(l)} = \bar{\mathbf{Q}}_{(l)}^{\text{act}} \quad (72)$$

where $\bar{\mathbf{M}}_{(l)}(\bar{\boldsymbol{\vartheta}}_{(l)})$ is the generalized mass matrix, $\bar{\mathbf{C}}_{(l)}(\dot{\bar{\boldsymbol{\vartheta}}}_{(l)}, \bar{\boldsymbol{\vartheta}}_{(l)})$ is the generalized Coriolis/centrifugal matrix, and $\bar{\mathbf{Q}}_{(l)}^{\text{grav}}(\bar{\boldsymbol{\vartheta}}_{(l)})$ are the generalized forces due to gravity. The vector of generalized forced $\bar{\mathbf{Q}}_{(l)}(\dot{\bar{\boldsymbol{\vartheta}}}_{(l)}, \bar{\boldsymbol{\vartheta}}_{(l)})$ accounts for joint friction, elastic forces, and all other effects, and the non-zero entries in $\bar{\mathbf{Q}}_{(l)}^{\text{act}}(t)$ are the drive forces/torques collocated to the n_{act} variables of actuated joints. In appendix B, the Lie group formulation from [83, 84] is summarized, which allows deriving (72) without resorting to specific parameterization of joint geometries.

There are various ways to derive the EOM of multibody systems, such as the limb of a PKM, in terms of relative coordinates (joint variables). So-called matrix methods [59], in particular, provide systematic formulations that can be easily implemented and are computationally efficient at the same time. This was formalized by the spatial operator algebra approach (SOA) [85, 86, 4], which gave rise to efficient $O(n)$ -algorithms [87]. Taking into account the geometric nature of the EOM, Lie group methods for MBS dynamics have been proposed in [88], which represent a geometric version of the SOA formulation. Lie group formulations for general MBS with tree-topology were reported in [89, 83, 84], where the closed form EOM are determined on system level in terms of simple matrix operations. Also recursive $O(n)$ -algorithms were reported [88, 90, 91]. They are already an established approach for robotic systems [92]. Lie group methods provide powerful tools which not only allow computationally efficient evaluation of the EOM but also enable efficient formulations of the linearized equations (for stability analysis), parameter sensitivity, as well as higher-order derivatives, which are crucial for model-based control and optimization [90, 91]. In this context, the conceptual similarity of the natural orthogonal complement (NOC) approach [93, 3] and the Lie group method should be mentioned.

In order to account for general formulations, and to allow for using recursive algorithms to evaluate the equations (72), the left hand side of the ODE system is written as

$$\varphi_{(l)}(\bar{\vartheta}_{(l)}, \dot{\bar{\vartheta}}_{(l)}, \ddot{\bar{\vartheta}}_{(l)}) := \bar{\mathbf{M}}_{(l)} \ddot{\bar{\vartheta}}_{(l)} + \bar{\mathbf{C}}_{(l)} \dot{\bar{\vartheta}}_{(l)} + \bar{\mathbf{Q}}_{(l)}^{\text{grav}} + \bar{\mathbf{Q}}_{(l)}. \quad (73)$$

This admits flexible use of alternative formulations or algorithms to evaluate the dynamics of the L limbs. The EOM of the limbs are occasionally simplified, and then the term $\varphi_{(l)}(\bar{\vartheta}_{(l)}, \dot{\bar{\vartheta}}_{(l)}, \ddot{\bar{\vartheta}}_{(l)})$ is substituted accordingly. In [2, 45], for instance, the lower arm segments (forming the parallelogram) of Delta-like PKM were split into two halves, and their mass was added to the upper arm and the platform, respectively.

6.3 EOM of a complex limb

The coordinates $\bar{\vartheta}_{(l)}$ are subjected to the loop closure constraints due to the γ_l FCs of limb l . The relation (71) provides an explicit solution of the velocity constraints in terms of δ_l independent velocities $\dot{\bar{\mathbf{q}}}_{(l)}$. The coordinates $\bar{\mathbf{q}}_{(l)}$ serve as generalized coordinates of limb l (without platform). Jourdain's principle of virtual power applied to (72) along with the variations $\delta \dot{\bar{\vartheta}}_{(l)} = \bar{\mathbf{H}}_{(l)} \delta \dot{\bar{\mathbf{q}}}_{(l)}$ yields

$$\bar{\mathbf{M}}_{(l)} \ddot{\bar{\mathbf{q}}}_{(l)} + \bar{\mathbf{C}}_{(l)} \dot{\bar{\mathbf{q}}}_{(l)} + \bar{\mathbf{Q}}_{(l)}^{\text{grav}} + \bar{\mathbf{Q}}_{(l)} = \bar{\mathbf{Q}}_{(l)}^{\text{act}} \quad (74)$$

where

$$\begin{aligned} \bar{\mathbf{M}}_{(l)}(\bar{\vartheta}_{(l)}) &:= \bar{\mathbf{H}}_{(l)}^T \bar{\mathbf{M}}_{(l)} \bar{\mathbf{H}}_{(l)} \\ \bar{\mathbf{C}}_{(l)}(\bar{\vartheta}_{(l)}, \dot{\bar{\vartheta}}_{(l)}) &:= \bar{\mathbf{H}}_{(l)}^T (\bar{\mathbf{M}}_{(l)} \dot{\bar{\mathbf{H}}}_{(l)} + \bar{\mathbf{C}}_{(l)} \bar{\mathbf{H}}_{(l)}) \\ \bar{\mathbf{Q}}_{(l)}(\bar{\vartheta}_{(l)}) &:= \bar{\mathbf{H}}_{(l)}^T \bar{\mathbf{Q}}_{(l)}, \quad \bar{\mathbf{Q}}_{(l)}^{\text{act}}(\bar{\vartheta}_{(l)}) := \bar{\mathbf{H}}_{(l)}^T \bar{\mathbf{Q}}_{(l)}^{\text{act}}, \quad \bar{\mathbf{Q}}_{(l)}^{\text{grav}}(\bar{\vartheta}) := \bar{\mathbf{H}}_{(l)}^T \bar{\mathbf{Q}}_{(l)}^{\text{grav}}. \end{aligned} \quad (75)$$

The matrices (75) depend on the coordinates $\bar{\vartheta}_{(l)}$ and velocity of the tree-system. The velocity $\dot{\bar{\vartheta}}_{(l)}$ can be replaced with $\dot{\bar{\mathbf{q}}}_{(l)}$ using (48), and $\bar{\vartheta}_{(l)}$ can be replaced with a (closed form or numerical) solution on terms of $\bar{\mathbf{q}}_{(l)}$. The equations (75) are also referred to as the Woronets equations [94] as a similar form first appeared in [95, 96].

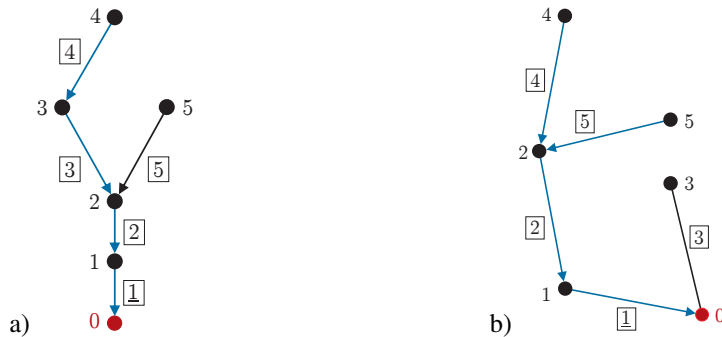


Fig. 10. Directed graph of the tree-topology system for a limb of a) the 3RR[2RR]R Delta and b) the IRSBot-2, obtained after removing the platform.

6.4 EOM of the Platform

The platform twist $\mathbf{V}_p = (\boldsymbol{\omega}_p, \mathbf{v}_p)^T$ in body-fixed representation consists of the linear velocity \mathbf{v}_p and angular velocity $\boldsymbol{\omega}_p$ of the platform frame \mathcal{F}_p , relative to the world frame \mathcal{F}_0 . The dynamics of the platform body is governed by the Newton-Euler equations, which can be summarized as (see appendix B)

$$\mathbf{M}_p \dot{\mathbf{V}}_p + \mathbf{G}_p \mathbf{M}_p \mathbf{V}_p + \mathbf{W}_p^{\text{grav}} = \mathbf{W}_p^{\text{EE}} \quad (76)$$

where the constant 6×6 inertia matrix \mathbf{M}_p and matrix \mathbf{G}_p is, respectively,

$$\mathbf{M}_p = \begin{pmatrix} \boldsymbol{\Theta} & m\tilde{\mathbf{d}} \\ -m\tilde{\mathbf{d}} & m\mathbf{I} \end{pmatrix}, \quad \mathbf{G}_p(\mathbf{V}_p) = \begin{pmatrix} \tilde{\boldsymbol{\omega}}_p \tilde{\mathbf{v}}_p \\ \mathbf{0} \tilde{\boldsymbol{\omega}}_p \end{pmatrix} \quad (77)$$

with the body-fixed inertia tensor $\boldsymbol{\Theta}$ w.r.t. \mathcal{F}_p , and \mathbf{d} is the position vector of the COM represented in \mathcal{F}_p . Acting at the platform are the wrench $\mathbf{W}_p^{\text{grav}}(\mathbf{x})$ due to gravity and the EE-wrench $\mathbf{W}_p^{\text{EE}}(t)$ (due to interaction of the PKM), where a wrench $\mathbf{W}_p = (\mathbf{m}_p^T, \mathbf{f}_p^T)$, represented in \mathcal{F}_p , consists of a torque \mathbf{m}_p and a force \mathbf{f}_p . The gyroscopic matrix is related to the matrix of the coadjoint action on $se(3)$ by $\mathbf{G}_p(\mathbf{V}_p) = -\mathbf{ad}_{\mathbf{V}_p}^T$. Moreover, the left-hand side of (76) are the Euler-Poincaré equations of the rigid body on $SE(3)$ [97, 98, 94]. The equation (76) holds true for an arbitrary body-fixed reference frame. The gravity wrench is

$$\mathbf{W}_p^{\text{grav}} = -\mathbf{M}_p \mathbf{Ad}_{\mathbf{C}_p}^{-1} \begin{pmatrix} \mathbf{0} \\ \mathbf{g} \end{pmatrix} \quad (78)$$

where ${}^0\mathbf{g}$ is the vector of gravitational acceleration expressed in the inertial frame.

6.5 Task Space Formulation of the EOM for PKM with Complex Limbs

The dynamics of the disconnected platform and of the L separated limbs are governed by the EOM (76) and (74), respectively. When assembled their motion is constrained. The task space velocity determines the platform twists via (54) and the velocity of the limbs via (58), (63) or (66). Denote with $\bar{\mathbf{F}}_{(l)}$ the submatrix of $\mathbf{F}_{(l)}$ with rows corresponding to the generalized coordinates $\bar{\mathbf{q}}_{(l)}$, so that $\dot{\bar{\mathbf{q}}}_{(l)} = \bar{\mathbf{F}}_{(l)} \mathbf{V}_t$ and hence $\dot{\boldsymbol{\vartheta}}_{(l)} = \bar{\mathbf{H}}_{(l)} \bar{\mathbf{F}}_{(l)} \mathbf{V}_t$.

The principle of virtual power finally yields the dynamic EOM in task space velocity coordinates

$$\mathbf{M}_t \dot{\mathbf{V}}_t + \mathbf{C}_t \mathbf{V}_t + \mathbf{W}_t^{\text{grav}} + \mathbf{W}_t = \mathbf{W}_t^{\text{EE}} + \mathbf{J}_{\text{IK}}^T \mathbf{u}(t) \quad (79)$$

with the $\delta \times \delta$ generalized mass matrix and Coriolis matrix

$$\begin{aligned} \mathbf{M}_t(\boldsymbol{\vartheta}) &:= \sum_{l=1}^L \bar{\mathbf{F}}_{(l)}^T \bar{\bar{\mathbf{M}}}_{(l)} \bar{\mathbf{F}}_{(l)} + \mathbf{P}_p^T \mathbf{M}_p \mathbf{P}_p \\ &= \sum_{l=1}^L \bar{\mathbf{F}}_{(l)}^T \bar{\mathbf{H}}_{(l)}^T \bar{\bar{\mathbf{M}}}_{(l)} \bar{\mathbf{H}}_{(l)} \bar{\mathbf{F}}_{(l)} + \mathbf{P}_p^T \mathbf{M}_p \mathbf{P}_p \end{aligned} \quad (80)$$

$$\begin{aligned} \mathbf{C}_t(\boldsymbol{\vartheta}, \dot{\boldsymbol{\vartheta}}) &:= \sum_{l=1}^L \bar{\mathbf{F}}_{(l)}^T (\bar{\mathbf{C}}_{(l)} \bar{\mathbf{F}}_{(l)} + \bar{\bar{\mathbf{M}}}_{(l)} \dot{\bar{\mathbf{F}}}_{(l)}) + \mathbf{P}_p^T \mathbf{G}_p \mathbf{M}_p \mathbf{P}_p \\ &= \sum_{l=1}^L \bar{\mathbf{F}}_{(l)}^T \bar{\mathbf{H}}_{(l)}^T (\bar{\mathbf{C}}_{(l)} \bar{\mathbf{H}}_{(l)} \bar{\mathbf{F}}_{(l)} + \bar{\bar{\mathbf{M}}}_{(l)} (\dot{\bar{\mathbf{H}}}_{(l)} \bar{\mathbf{F}}_{(l)} + \bar{\mathbf{H}}_{(l)} \dot{\bar{\mathbf{F}}}_{(l)})) + \mathbf{P}_p^T \mathbf{G}_p \mathbf{M}_p \mathbf{P}_p, \end{aligned} \quad (81)$$

the inverse kinematics Jacobian $\mathbf{J}_{\text{IK}}(\boldsymbol{\vartheta})$ in (70), and the vector $\mathbf{u} \in \mathbb{R}^{N_{\text{act}}}$ of $N_{\text{act}} \geq \delta$ actuator forces/torques. The vector of

generalized forces

$$\mathbf{W}_t^{\text{EE}}(t) := \mathbf{P}_p^T \mathbf{W}_p^{\text{EE}}(t) \quad (82)$$

$$\mathbf{W}_t(\vartheta, \dot{\vartheta}, t) := \sum_{l=1}^L \bar{\mathbf{F}}_{(l)}^T \bar{\mathbf{Q}}_{(l)} = \sum_{l=1}^L \bar{\mathbf{F}}_{(l)}^T \bar{\mathbf{H}}_{(l)}^T \bar{\mathbf{Q}}_{(l)} \quad (83)$$

$$\mathbf{W}_t^{\text{grav}}(\vartheta, \mathbf{x}) := \sum_{l=1}^L \bar{\mathbf{F}}_{(l)}^T \bar{\mathbf{Q}}_{(l)}^{\text{grav}} + \mathbf{P}_p^T \mathbf{W}_p^{\text{grav}} = \sum_{l=1}^L \bar{\mathbf{F}}_{(l)}^T \bar{\mathbf{H}}_{(l)}^T \bar{\mathbf{Q}}_{(l)}^{\text{grav}} + \mathbf{P}_p^T \mathbf{W}_p^{\text{grav}} \quad (84)$$

accounts for EE-loads and all other loads. The gyroscopic matrix in (77) is evaluated with the task space velocity: $\mathbf{G}_p = \mathbf{G}_p(\mathbf{P}_p \mathbf{V}_t)$. The dependency of the terms in (79) on ϑ is kept as all expressions in (75) depend on $\bar{\vartheta}$, and further $\bar{\mathbf{F}}_{(l)}$ depends on $\vartheta_{(l)}$ (the complete set of tree-joint variables including the joint connecting limb l to the platform).

The above equations in terms of ϑ are derived making use of the relations (71) and (59). If the inverse kinematics map ψ_{IK} of the mechanism can be expressed in closed form, the dynamic equations (79) can be derived solely in terms of the task space coordinates \mathbf{x} and velocity \mathbf{V}_t . Then, $\bar{\mathbf{H}}_{(l)} \bar{\mathbf{F}}_{(l)}$ is replaced by the (inverse kinematics) Jacobian of ψ_{IK} . Yet, this usually leads to very complex expressions.

The EOM (79) can be expressed in terms of the general form of the EOM (73), and introducing $\varphi_p(\mathbf{x}, \mathbf{V}_t, \dot{\mathbf{V}}_t) := \mathbf{M}_p \mathbf{P}_p \dot{\mathbf{V}}_t + \mathbf{G}_p \mathbf{M}_p \mathbf{P}_p \mathbf{V}_t + \mathbf{W}_p^{\text{grav}}$, as

$$\sum_{l=1}^L \bar{\mathbf{H}}_{(l)}^T \bar{\mathbf{F}}_{(l)}^T \varphi_{(l)}(\bar{\vartheta}_{(l)}, \dot{\bar{\vartheta}}_{(l)}, \ddot{\bar{\vartheta}}_{(l)}) + \mathbf{P}_p^T \varphi_p(\mathbf{x}, \mathbf{V}_t, \dot{\mathbf{V}}_t) = \mathbf{W}_t^{\text{EE}} + \mathbf{J}_{\text{IK}}^T \mathbf{u} \quad (85)$$

with the kinematic relations (59) and (60).

6.6 Formulation of the EOM for non-redundant PKM in terms of actuator coordinates

The solution of the velocity forward kinematics problem of a non-redundant PKM (not kinematically redundant nor redundantly actuated) is obtain from (69) as

$$\mathbf{V}_t = \mathbf{J}_{\text{FK}} \dot{\vartheta}_{\text{act}} \quad (86)$$

where $\mathbf{J}_{\text{FK}} := \mathbf{J}_{\text{IK}}^{-1}$ is the forward kinematics Jacobian. Combined with (59), this yields a solution of the velocity forward kinematics problem of the mechanism as

$$\dot{\vartheta}_{(l)} = \mathbf{H}_{(l)} \mathbf{F}_{(l)} \mathbf{J}_{\text{FK}} \dot{\vartheta}_{\text{act}}. \quad (87)$$

With this relation, the principle of virtual power applied to (79) yields the dynamic equation in actuator coordinates

$$\mathbf{M}_a \ddot{\vartheta}_a + \mathbf{C}_a \dot{\vartheta}_a + \mathbf{Q}_a^{\text{grav}} + \mathbf{Q}_a = \mathbf{Q}_a^{\text{EE}} + \mathbf{u} \quad (88)$$

with the $\delta \times \delta$ generalized mass and Coriolis matrix

$$\mathbf{M}_a(\boldsymbol{\eta}) := \mathbf{J}_{\text{FK}}^T \mathbf{M}_t \mathbf{J}_{\text{FK}} \quad (89)$$

$$\mathbf{C}_a(\bar{\vartheta}, \dot{\vartheta}) := \mathbf{J}_{\text{FK}}^T (\mathbf{C}_t \mathbf{J}_{\text{FK}} + \mathbf{M}_t \dot{\mathbf{J}}_{\text{FK}}) = \mathbf{J}_{\text{FK}}^T (\mathbf{C}_t - \mathbf{M}_t \mathbf{J}_{\text{FK}} \dot{\mathbf{J}}_{\text{IK}}) \mathbf{J}_{\text{FK}}. \quad (90)$$

The vector \mathbf{u} of actuator forces/torques appears explicitly, while the generalized EE forces and the vector of all remaining forces are

$$\mathbf{Q}_a(\vartheta, \dot{\vartheta}, t) := \mathbf{J}_{\text{FK}}^T \mathbf{W}_t, \quad \mathbf{Q}_a^{\text{grav}}(\vartheta) := \mathbf{J}_{\text{FK}}^T \mathbf{W}_t^{\text{grav}} \quad (91)$$

$$\mathbf{Q}_a^{\text{EE}}(\vartheta, t) := \mathbf{J}_{\text{FK}}^T \mathbf{W}_t^{\text{EE}}. \quad (92)$$

By construction, (88) depends on the joint coordinates ϑ . It can be transformed to actuator coordinated by solving the geometric forward kinematics problem of the mechanism, which is to find the joint coordinates $\vartheta(t)$ for given actuator coordinates $\vartheta_{\text{act}}(t)$. The solution is given by the forward kinematics map $\Psi_{\text{FK}} : \mathbb{V}^{n_{\text{act}}} \rightarrow \mathbb{V}^n$, so that $\vartheta = \Psi_{\text{FK}}(\vartheta_{\text{act}})$. For PKM in general, Ψ_{FK} cannot be expressed in closed form. Again, in special cases, such as the $3\text{RR}[2\text{RR}]R$ Delta, a closed form expression is available (and the non-uniqueness problem can be tackled). In more complicated situations, such as the active ankle PKM module reported in [99], explicit solutions can be obtained by means of an algebraic description of the constraints, and their solution using algorithms from computational algebraic geometry. Then, ϑ and its time derivatives can be substituted by the actuator coordinates ϑ_{act} and their derivatives. The term $\bar{\mathbf{H}}_{(l)} \bar{\mathbf{F}}_{(l)} \mathbf{J}_{\text{FK}}$ is then replaced by the Jacobian of Ψ_{FK} . For a non-redundantly actuated PKM, the actuator variables serve as generalized coordinates: $\mathbf{q}(t) := \vartheta_{\text{act}}$.

7 Modular Modeling

Almost all PKM are built from structurally identical limbs. Consequently, the PKM can be regarded as being assembled from L instances of a *representative limb* (RL), which implies that the topological graph Γ is the union of L congruent subgraphs Γ_l . This allows reusing the kinematics and dynamics equations of a single RL for deriving the overall PKM model. To this end, L instances of the RL are mounted at the base and platform, respectively.

To account for the different locations of the limbs, the IFR \mathcal{F}_0 and the platform frame \mathcal{F}_p in the model for the RL are replaced by an arbitrarily located *construction frame* at the base, denoted \mathcal{F}'_0 , and at the platform, denoted \mathcal{F}'_p , respectively. This is shown in Fig. 11 for the RL of the $3\text{RR}[2\text{RR}]R$ Delta. In order to locate the L instances of the RL within the PKM model, a *mount frame* is defined at the ground and the platform, denoted with $\mathcal{F}_{0(l)}$ and $\mathcal{F}_{p(l)}$, respectively. Fig. 12 shows this for the Delta example. The l th instance of the RL is inserted between these two frames. That is, the overall PKM is assembled by identifying the mount frame $\mathcal{F}_{0(l)}$ for limb l at the base with the construction frame \mathcal{F}'_0 , and the mount frame at the platform $\mathcal{F}_{p(l)}$ with the construction frame \mathcal{F}'_p of the l th instance of the RL.

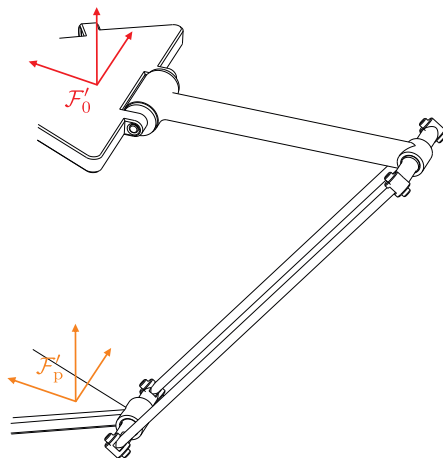


Fig. 11. Representative limb of the $3\text{RR}[2\text{RR}]R$ Delta robot. The construction frames \mathcal{F}'_0 and \mathcal{F}'_p are arbitrarily located.

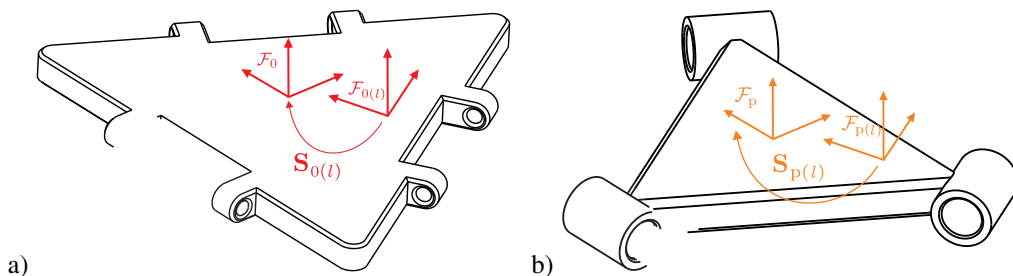


Fig. 12. Mount frames $\mathcal{F}_{0(l)}$ and $\mathcal{F}_{p(l)}$ at the ground a) and platform b) for the $3\text{RR}[2\text{RR}]R$ Delta. Instances of the representative limb are inserted between these mount frames, which means that \mathcal{F}'_0 (fig. 11) of the l th instance is identified with $\mathcal{F}_{0(l)}$ at the ground, and \mathcal{F}'_p is identified with $\mathcal{F}_{p(l)}$ at the platform.

The kinematic and dynamic model of the particular limb l are derived from the models of the RL as follows.

Kinematics: A change of IFR affects the body configurations (1), while a change of platform frame affects the forward kinematics and task space Jacobian of the limb in (52) and (57), respectively, and hence the inverse kinematics Jacobian $\mathbf{F}_{(l)}$ in (58). The geometric Jacobians of bodies $i = 1, \dots, n_l$ in (4) are unaffected, as they are represented in the body-fixed frames, which are identically located at all limbs, and the same applies to the compound Jacobians (51).

Denote with $\mathbf{C}'_i \in SE(3)$ the configuration of body i of the RL relative to the construction frame \mathcal{F}'_0 . Using (1), this is given by $\mathbf{C}'_i(\boldsymbol{\vartheta}') = f'_i(\boldsymbol{\vartheta}')\mathbf{A}'_i$ with

$$f'_i(\boldsymbol{\vartheta}') = \exp(\boldsymbol{\vartheta}'_i \mathbf{Y}'_i) \cdots \exp(\boldsymbol{\vartheta}'_{i-1} \mathbf{Y}'_{i-1}) \exp(\boldsymbol{\vartheta}'_1 \mathbf{Y}'_1) \quad (93)$$

where \mathbf{A}'_i is the zero reference configuration relative to \mathcal{F}'_0 , \mathbf{Y}'_i are the screw coordinate vectors represented in the construction frame \mathcal{F}'_0 , and $\boldsymbol{\eta}'$ is the joint coordinate vector of the RL.

The configuration of limb l is obtained by transforming (93) to \mathcal{F}_0 . The transformation from mount frame $\mathcal{F}_{0(l)}$ (which is identical to \mathcal{F}'_0 when the limb is mounted) to the global IFR \mathcal{F}_0 is denoted with $\mathbf{S}_{0(l)} \in SE(3)$. Thus, the configuration of body i of limb l relative to the IFR \mathcal{F}_0 is

$$\mathbf{C}_{i(l)} = \mathbf{S}_{0(l)} \mathbf{C}'_{i(l)} = \mathbf{S}_{0(l)} f'_{i(l)}(\boldsymbol{\vartheta}_{(l)}) \mathbf{A}'_{i(l)} = f_{i(l)}(\boldsymbol{\vartheta}_{(l)}) \mathbf{A}_{i(l)}. \quad (94)$$

The last term is of form (2) where the joint screw coordinates and the reference configuration are

$$\mathbf{Y}_{i(l)} = \mathbf{Ad}_{\mathbf{S}_{0(l)}} \mathbf{Y}'_i, \quad \mathbf{A}_{i(l)} = \mathbf{S}_{0(l)} \mathbf{A}'_i. \quad (95)$$

Denote with $\mathbf{S}_{p(l)} \in SE(3)$ the transformation from mount frame $\mathcal{F}_{p(l)}$ to the platform frame \mathcal{F}_p of the PKM. The reference configuration of \mathcal{F}'_p relative to \mathcal{F}'_0 of the RL is \mathbf{A}'_p . When the limb is mounted, \mathcal{F}'_p is identical to $\mathcal{F}_{p(l)}$, and \mathcal{F}'_0 is identical to $\mathcal{F}_{0(l)}$. The platform pose of the PKM is then, with (5), determined by limb l as $\mathbf{C}_p = \mathbf{S}_{0(l)} \mathbf{C}'_p \mathbf{S}_{p(l)}^{-1} = f_{p(l)}(\boldsymbol{\vartheta}_{(l)}) \mathbf{A}_{p(l)}$, where $\mathbf{A}_p = \mathbf{S}_{0(l)} \mathbf{A}'_p \mathbf{S}_{p(l)}^{-1}$.

The twist \mathbf{V}'_p of frame \mathcal{F}'_p of the RL is determined by the forward kinematics Jacobian \mathbf{J}'_p of the RL, and is related to the platform twist as $\mathbf{V}_{p(l)} = \mathbf{Ad}_{\mathbf{S}_{p(l)}} \mathbf{V}'_p$. The forward kinematics Jacobian of the tree-topology system of limb l is thus

$$\mathbf{J}_{p(l)} = \mathbf{Ad}_{\mathbf{S}_{p(l)}} \mathbf{J}'_p \quad (96)$$

and hence the compound forward kinematics Jacobian in (52) is

$$\mathbf{L}_{p(l)} = \mathbf{Ad}_{\mathbf{S}_{p(l)}} \mathbf{L}'_p \quad (97)$$

which gives rise to the task space Jacobian (57) and the inverse kinematics Jacobian $\mathbf{F}_{(l)}$.

Dynamics: The generalized mass and centrifugal/Coriolis matrix in the EOM (72) of the tree-topology system are invariant w.r.t. to a change of IFR (i.e. they are left-invariant under $SE(3)$ actions). They can be derived and implemented for the RL using (143) and (144). The only term in the EOM (72) that depends on the IFR is the vector of generalized gravity forces, which is determined by the relation (146) in appendix B. Let \mathbf{J}' be the system Jacobian of the RL defined in (132). Introducing the transformation $\mathbf{S}_{0(l)}$ from $\mathcal{F}_{0(l)}$ to \mathcal{F}_0 yields the generalized gravity forces of limb l

$$\mathbf{Q}_{(l)}^{\text{grav}} = -\mathbf{J}'^T \begin{pmatrix} \mathbf{M}_1 \mathbf{Ad}_{\mathbf{C}'_1}^{-1} \\ \mathbf{M}_2 \mathbf{Ad}_{\mathbf{C}'_2}^{-1} \\ \vdots \\ \mathbf{M}_{n_l} \mathbf{Ad}_{\mathbf{C}'_{n_l}}^{-1} \end{pmatrix} \mathbf{Ad}_{\mathbf{S}_{0(l)}}^{-1} \begin{pmatrix} \mathbf{0} \\ {}^0 \mathbf{g} \end{pmatrix} = -\mathbf{J}'^T \begin{pmatrix} \mathbf{M}_1 \mathbf{Ad}_{\mathbf{C}'_1}^{-1} \\ \mathbf{M}_2 \mathbf{Ad}_{\mathbf{C}'_2}^{-1} \\ \vdots \\ \mathbf{M}_{n_l} \mathbf{Ad}_{\mathbf{C}'_{n_l}}^{-1} \end{pmatrix}_{(l)} \begin{pmatrix} \mathbf{0} \\ \mathbf{R}_{0(l)}^T {}^0 \mathbf{g} \end{pmatrix}. \quad (98)$$

Obviously, the generalized gravity forces are obtained from the model for the RL by using the gravity vector $\mathbf{R}_{0(l)}^T {}^0 \mathbf{g}$ (instead of ${}^0 \mathbf{g}$) where $\mathbf{R}_{0(l)}$ is the rotation matrix in $\mathbf{S}_{0(l)}$.

8 Applications of the Dynamic Equations

The dynamic model can be employed to various means, in particular for solving the forward and inverse dynamics problem. By construction, (79) depends on ϑ , $\dot{\vartheta}$, as well as on \mathbf{V}_t , $\dot{\mathbf{V}}_t$, which must be taken into account when applying the model. In the following this is discussed in detail.

8.1 Forward Dynamics –Time Integration of the EOM

8.1.1 EOM in terms of taskspace coordinates and velocity

If the inverse kinematics map ψ_{IK} of the mechanism in (67) is available in closed form, ϑ can be replaced with \mathbf{x} . The joint velocity $\dot{\vartheta}$ can be replaced with \mathbf{V}_t using one of the relations (58), (63) or (66), or using the closed form relation for the particular PKM. Complementing (79) with the kinematic equations (7) leads to the EOM in terms of taskspace coordinates and velocity

$$\mathbf{M}_t(\mathbf{x})\dot{\mathbf{V}}_t + \mathbf{C}_t(\mathbf{x}, \mathbf{V}_t)\mathbf{V}_t + \mathbf{W}_t^{\text{grav}}(\mathbf{x}) + \mathbf{W}_t(\mathbf{x}, \mathbf{V}_t, t) = \mathbf{W}_t^{\text{EE}}(t) + \mathbf{J}_{IK}^T(\mathbf{x})\mathbf{u}(t) \quad (99)$$

$$\mathbf{V}_t = \mathbf{H}_t(\mathbf{x})\dot{\mathbf{x}}. \quad (100)$$

This is a system of $2\delta_p$ first-order ODEs in terms of the taskspace coordinates \mathbf{x} and velocities \mathbf{V}_t , which is linear in $\dot{\mathbf{x}}$ and $\dot{\mathbf{V}}_t$. It can be reformulated as the explicit ODE system

$$\dot{\mathbf{V}}_t = \mathbf{M}_t^{-1}(\mathbf{x}) (\mathbf{W}_t^{\text{EE}}(t) + \mathbf{J}_{IK}^T(\mathbf{x})\mathbf{u}(t) - \mathbf{C}_t(\mathbf{x}, \mathbf{V}_t)\mathbf{V}_t - \mathbf{W}_t^{\text{grav}}(\mathbf{x}) - \mathbf{W}_t(\mathbf{x}, \mathbf{V}_t, t)) \quad (101)$$

$$\dot{\mathbf{x}} = \mathbf{H}_t^{-1}(\mathbf{x})\mathbf{V}_t. \quad (102)$$

The parameterization of the platform motion with coordinates \mathbf{x} may introduce parameterization singularities, which happens when a three-parametric description of the platform orientation used. In such singularities, the inverse in (102) does not exist. The kinematic equations (100) could be inserted into (99) to yield a system of $\delta_p = \delta$ second-order ODEs in $\mathbf{x}(t)$. This, however, usually leads to very complicated expressions, and it is advisable to use the platform twist as velocity variables in (99). The singularity problem remains.

8.1.2 EOM in terms of joint coordinates and taskspace velocity

In general there is no closed form expression of the inverse kinematics map ψ_{IK} . Moreover, inserting it into (79) often yields equations (99) with very complicated terms. Instead, the dynamic equations (79) are complemented with the kinematic equations (59). This yields the EOM of the PKM with complex limbs

$$\mathbf{M}_t(\vartheta)\dot{\mathbf{V}}_t + \mathbf{C}_t(\vartheta, \dot{\vartheta})\mathbf{V}_t + \mathbf{W}_t^{\text{grav}}(\vartheta) + \mathbf{W}_t(\vartheta, \dot{\vartheta}, t) = \mathbf{W}_t^{\text{EE}}(t) + \mathbf{J}_{IK}^T(\vartheta)\mathbf{u}(t) \quad (103)$$

$$\dot{\vartheta}_{(l)} = \mathbf{H}_{(l)}(\vartheta)\mathbf{F}_{(l)}(\vartheta)\mathbf{J}_{FK}(\vartheta)\mathbf{V}_t \quad (104)$$

which is a system of $\delta_p + n$ first-order ODEs in terms of joint variables ϑ of the tree-topology system and the taskspace velocity \mathbf{V}_t that can be regarded as non-located state variables. It can be written as explicit ODE system

$$\dot{\mathbf{V}}_t = \mathbf{M}_t^{-1}(\vartheta) (\mathbf{W}_t^{\text{EE}}(t) + \mathbf{J}_{IK}^T(\vartheta)\mathbf{u}(t) - \mathbf{C}_t(\vartheta, \mathbf{V}_t)\mathbf{V}_t - \mathbf{W}_t^{\text{grav}}(\vartheta) - \mathbf{W}_t(\vartheta, \mathbf{V}_t, t)) \quad (105)$$

$$\dot{\vartheta}_{(l)} = \mathbf{H}_{(l)}(\vartheta)\mathbf{F}_{(l)}(\vartheta)\mathbf{V}_t \quad (106)$$

where $\mathbf{C}_t(\vartheta, \dot{\vartheta})$ and $\mathbf{W}_t(\vartheta, \dot{\vartheta}, t)$ in (105) are evaluated with (106) for given state vector $(\mathbf{V}_t, \vartheta)$.

The joint velocities $\dot{\vartheta}$ can be replaced with \mathbf{V}_t using (58), (63) or (66). Moreover, if the inverse kinematics of the mechanism can be solved explicitly ϑ can be replaced by \mathbf{x} , so that all terms in (79) depend on the state $(\mathbf{x}, \mathbf{V}_t)$ of the platform. This often leads to very complex expressions, and it may be computationally more efficient to separately evaluate the inverse kinematics and to insert the result into the dynamic EOM (see sec. 8.2).

8.1.3 EOM in terms of actuator coordinates

The dynamic equations (88) are complemented with the kinematic relation (87)

$$\mathbf{M}_a(\vartheta)\ddot{\vartheta}_{\text{act}} + \mathbf{C}_a(\vartheta, \dot{\vartheta})\dot{\vartheta}_{\text{act}} + \mathbf{Q}_a^{\text{grav}}(\vartheta) + \mathbf{Q}_a(\vartheta, \dot{\vartheta}, t) = \mathbf{Q}_a^{\text{EE}}(\vartheta) + \mathbf{u} \quad (107)$$

$$\dot{\vartheta}_{(l)} = \mathbf{H}_{(l)}(\vartheta)\mathbf{F}_{(l)}(\vartheta)\dot{\vartheta}_{\text{act}}. \quad (108)$$

This is a system of $\delta + n$ ODEs. The dynamic equations (107) form a second-order ODE system in ϑ_{act} , while the kinematic equations (108) form a first-order system. Remember that ϑ_{act} is a subset of $\dot{\vartheta}$.

8.2 Inverse Dynamics Formulation in Taskspace

For model-based control, the inverse dynamics in task space coordinates is most relevant since task space control schemes directly regulate the EE motion and achieves better tracking performance. Therefore, in the following, the inverse dynamics in task space is discussed. A joint space formulation is obtained from (88) if desired.

Inverse dynamics solution: The inverse dynamics amounts to determine the actuator forces/torques $\mathbf{u}(t)$ for a given motion of the PKM. In the following, the dynamics model (79) is used. The PKM motion is then represented by the joint trajectory $\boldsymbol{\eta}(t)$. The inverse dynamics solution for a non-redundantly actuated PKM ($\delta_p = n_{\text{act}}$) is

$$\mathbf{u}(t) = \mathbf{J}_{\text{IK}}^{-T}(\boldsymbol{\vartheta}) (\mathbf{M}_t(\boldsymbol{\vartheta})\dot{\mathbf{V}}_t + \mathbf{C}_t(\boldsymbol{\vartheta}, \dot{\boldsymbol{\vartheta}})\mathbf{V}_t + \mathbf{W}_t^{\text{grav}}(\boldsymbol{\vartheta}) + \mathbf{W}_t(\boldsymbol{\vartheta}, \dot{\boldsymbol{\vartheta}}, t) - \mathbf{W}_t^{\text{EE}}(t)) \quad (109)$$

$$= \mathbf{J}_{\text{IK}}^{-T}(\boldsymbol{\varphi}_t(\boldsymbol{\vartheta}, \dot{\boldsymbol{\vartheta}}, \ddot{\boldsymbol{\vartheta}}, \mathbf{x}, \mathbf{V}_t, \dot{\mathbf{V}}_t, t) - \mathbf{W}_t^{\text{EE}}(t)) \quad (110)$$

with

$$\boldsymbol{\varphi}_t(\boldsymbol{\vartheta}, \dot{\boldsymbol{\vartheta}}, \ddot{\boldsymbol{\vartheta}}, \mathbf{x}, \mathbf{V}_t, \dot{\mathbf{V}}_t, t) := \mathbf{M}_t\dot{\mathbf{V}}_t + \mathbf{C}_t\mathbf{V}_t + \mathbf{W}_t^{\text{grav}} + \mathbf{W}_t. \quad (111)$$

If the PKM is redundantly actuated ($\delta_p < n_{\text{act}}$), a (weighted) pseudoinverse of \mathbf{J}_{IK}^T is used [35].

The joint trajectory $\boldsymbol{\vartheta}(t)$ is determined from the taskspace motion, i.e. from $\mathbf{x}(t)$ and \mathbf{V}_t , by evaluating the inverse kinematics map (67) and inverse kinematics Jacobian (59) of the mechanism. If the joint motion can be expressed explicitly in terms of task space coordinates \mathbf{x} and velocities \mathbf{V}_t , then the dynamics model (99) is used, and the PKM motion is deduced from taskspace motion via the inverse kinematics map f_{IK} and Jacobian (70) of the PKM.

Parallel computation: The inherent parallel kinematic structure of PKM can be exploited for separate evaluation of the kinematics and dynamics of the complex limbs in parallel. To this end, the taskspace formulation (79) is expressed without substituting the joint velocity and acceleration into (72) using (71), as in (74), to obtain

$$\begin{aligned} \mathbf{J}_{\text{IK}}^T \mathbf{u}(t) &= \sum_{l=1}^L \bar{\mathbf{F}}_{(l)}^T \bar{\mathbf{H}}_{(l)}^T (\bar{\mathbf{M}}_{(l)} \ddot{\boldsymbol{\vartheta}}_{(l)} + \bar{\mathbf{C}}_{(l)} \dot{\boldsymbol{\vartheta}}_{(l)} + \bar{\mathbf{Q}}_{(l)}) + \mathbf{W}_t^{\text{grav}} + \mathbf{P}_p^T (\mathbf{M}_p \mathbf{P}_p \dot{\mathbf{V}}_t + \mathbf{G}_p \mathbf{M}_p \mathbf{P}_p \mathbf{V}_t + \mathbf{W}_p^{\text{grav}}) - \mathbf{W}_t^{\text{EE}} \quad (112) \\ &= \sum_{l=1}^L \bar{\mathbf{F}}_{(l)}^T \bar{\mathbf{H}}_{(l)}^T \boldsymbol{\varphi}_{(l)}(\boldsymbol{\vartheta}_{(l)}, \dot{\boldsymbol{\vartheta}}_{(l)}, \ddot{\boldsymbol{\vartheta}}_{(l)}) + \mathbf{P}_p^T \boldsymbol{\varphi}_p(\mathbf{x}, \mathbf{V}_t, \dot{\mathbf{V}}_t) - \mathbf{W}_t^{\text{EE}} \end{aligned}$$

denoting $\boldsymbol{\varphi}_p(\mathbf{x}, \mathbf{V}_t, \dot{\mathbf{V}}_t) := \mathbf{M}_p \mathbf{P}_p \dot{\mathbf{V}}_t + \mathbf{G}_p \mathbf{M}_p \mathbf{P}_p \mathbf{V}_t + \mathbf{W}_p^{\text{grav}}$. The crucial observation is that the term $\boldsymbol{\varphi}_{(l)}$, accounting for the dynamics of limb l , as well as $\bar{\mathbf{F}}_{(l)}$ and $\bar{\mathbf{H}}_{(l)}$ solely depend on the joint variables $\boldsymbol{\vartheta}_{(l)}$ and its time derivatives, and can thus be evaluated independently. Also the remaining term $\boldsymbol{\varphi}_p$ (NE equations of platform) depends on \mathbf{x} and on \mathbf{V}_t and its derivative only. Consequently, instead of evaluating the monolithic system (79), the individual terms in (112) can be evaluated in parallel by means of distributed computing. The same holds true for the inverse kinematics of the limbs.

A parallel/distributed evaluation scheme is summarized in fig. 13. There are $L + 1$ parallel computation threads/nodes. The first L computation nodes are allocated for computing the inverse kinematics and dynamics of the separated complex limbs. In the l th thread, the geometric inverse kinematics (67), and the velocity and acceleration inverse kinematics, (59) and (60), of limb l are solved in subsequent steps 1)–3). If the inverse kinematics map $\boldsymbol{\psi}_{\text{IK}(l)}$ (67) is available in closed form, these steps can be simplified, and $\bar{\mathbf{H}}_{(l)} \bar{\mathbf{F}}_{(l)}$ are replaced by the corresponding Jacobians. The dynamics equations of the limbs are evaluated in step 4). The $L + 1$ -st computation node evaluates the dynamic equations (76) of the platform. Results of these $L + 1$ computation runs are the auxiliary wrenches $\bar{\mathbf{W}}_{(l)}$ and $\bar{\mathbf{W}}_p$, but also the inverse kinematics Jacobians $\mathbf{F}_{(l)}$ of the limbs, which deliver the rows of the inverse kinematics Jacobian \mathbf{J}_{IK} of the PKM. The latter is inverted in the final computation step to compute the actuations \mathbf{u} . The overall inverse kinematics output are $\boldsymbol{\vartheta}, \dot{\boldsymbol{\vartheta}}$, and $\ddot{\boldsymbol{\vartheta}}$.

The equations (72) of the tree-topology system without platform (in step 4 of the L evaluation blocks) can be evaluated with an $O(n)$ inverse dynamics algorithm, thus replacing evaluation of $\boldsymbol{\varphi}_{(l)}$. There are various such algorithms using classical 3D vector formulations and DH-parameterization [100, 87], but also such using Lie group formulations [88, 92, 84, 90, 91].

The critical aspect deciding about the efficacy of a parallel implementation is the data exchange between the $N_l + 1$ compute nodes. Moreover, a massive parallel computing hardware with minimal communication overhead and latency is crucial.

9 Example: Inverse Dynamics of a 3RR[2RR]R Delta

In this section, the complete kinematic and dynamic model of a 3RR[2RR]R Delta robot is derived. To this end, the Lie group formulation summarized in appendix B is used. This formulation and the example model have been implemented in Mathematica, [which available as e-Component to this paper and at \[101\]](#). For numerical evaluation, the geometric and dynamic parameters are used that shall roughly resemble a MOTOMAN-MPP3H Delta robot.

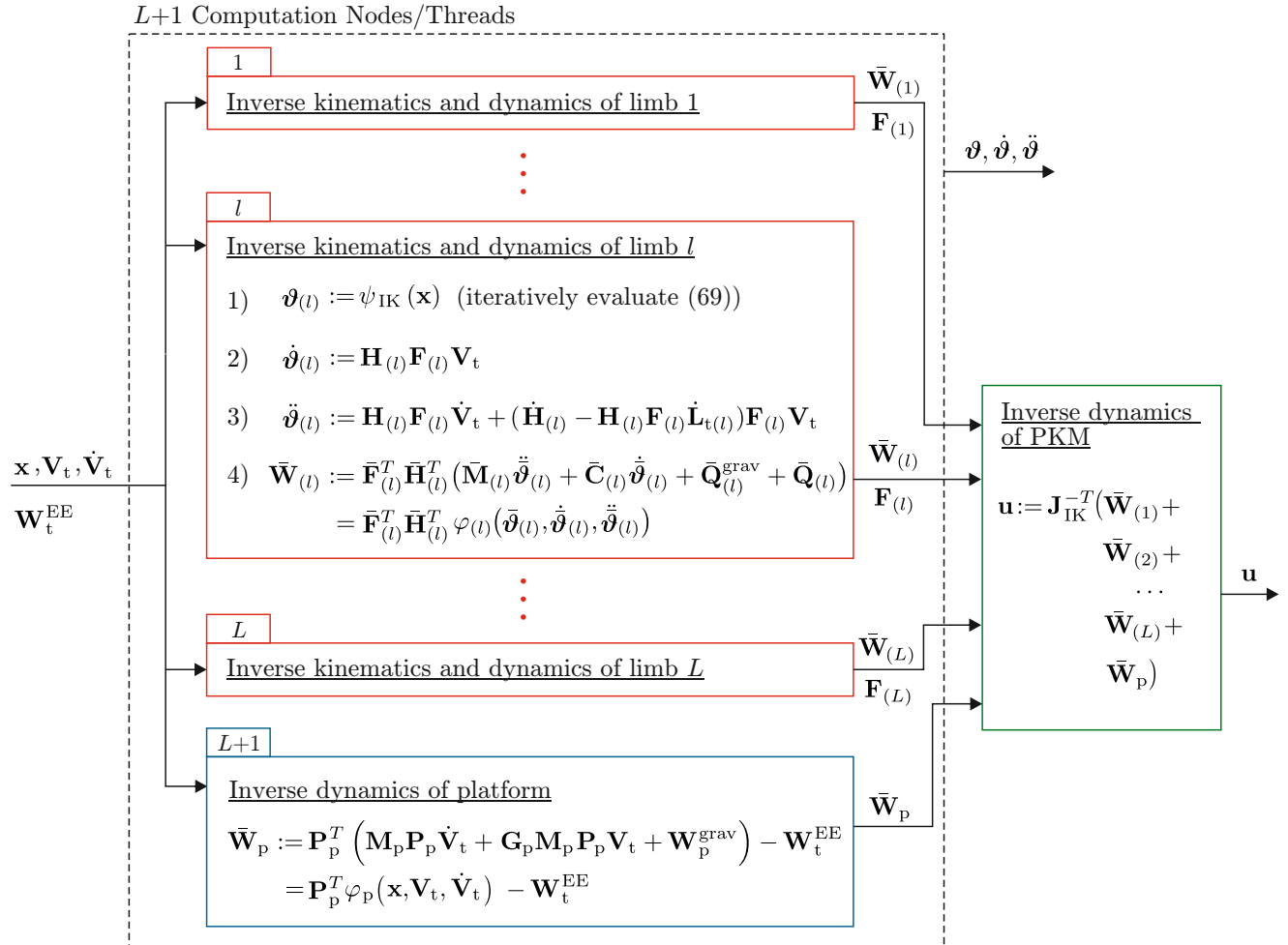
9.1 Kinematics of representative limb

The model of the 3RR[2RR]R Delta robot possesses $N = 3 \times 6$ revolute joints. The components of the platform position vector serve as task space coordinates, $\mathbf{x} := \mathbf{r}_p$. The joint angles of the three actuated revolute joints at the base serve as actuator coordinates, $\boldsymbol{\vartheta}_{\text{act}} := (\vartheta_{1(1)}, \vartheta_{1(2)}, \vartheta_{1(3)})^T$. For the Delta robot, the solutions to the inverse and forward kinematics problem can be expressed in closed form. This is not used here, but an iterative solution is pursued in order to capture the general situation. Bodies and joints are numbered as in Fig. 1b), the PKM topology is represented by the graph in Fig. 6a), and the tree-topology system is defined as in Fig. 6b).

Joint screws and reference configurations Fig. 14 shows the RL in the reference configuration, where the upper arms of all limbs are aligned horizontally. The construction frames \mathcal{F}'_0 and \mathcal{F}'_p are located at the center of the base and platform, respectively. The length of the upper arm (body 1) is denoted with a , the length of each of the rods (bodies 3 and 5) with c , and b denotes the length of the links (bodies 2 and 4) connecting the two rods. The R-joints at the base and platform are located at a distance of R_0 and R_p from the respective center, mutually aligned with 120° .

In order to simplify the expressions, the abbreviations $d := a + R_0 - R_p$ and $h := \sqrt{c^2 - d^2}$ (the height of the platform in reference configuration) are introduced. The position vectors \mathbf{y}'_i to the joint axes and the unit vectors \mathbf{e}'_i along the joint axes

Fig. 13. Computational scheme for parallel evaluation of inverse kinematics and dynamics. Input: taskspace coordinates \mathbf{x} , velocity \mathbf{V}_t , and acceleration $\dot{\mathbf{V}}_t$, and EE-loads \mathbf{W}_t^{EE} . Output: joint variables $\boldsymbol{\vartheta}$, velocities $\dot{\boldsymbol{\vartheta}}$, acceleration $\ddot{\boldsymbol{\vartheta}}$, and actuation forces/torques \mathbf{u} .



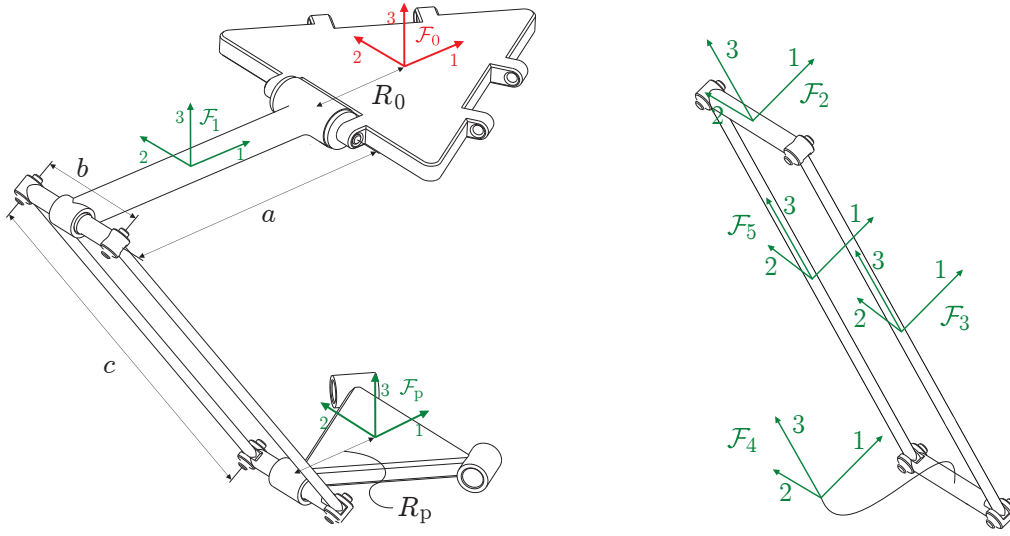


Fig. 14. Geometric parameters, and location of construction frames and body-frames of the representative limb of the $3RR[2RR]R$ Delta robot. The construction frames \mathcal{F}'_0 and \mathcal{F}'_p are located at center of the base and platform, respectively. In the reference configuration, the upper arm is aligned horizontally.

expressed in \mathcal{F}'_0 are

$$\begin{aligned} \mathbf{y}'_1 &= (-R_0, 0, 0)^T, \mathbf{y}'_2 = (-R_0 - a, 0, 0)^T, \mathbf{y}'_3 = (-R_0 - a, -b/2, 0)^T, \\ \mathbf{y}'_4 &= (-R_p, -b/2, -h)^T, \mathbf{y}'_5 = (-R_0 - a, b/2, 0)^T, \mathbf{y}'_6 = (-R_p, 0, -h)^T \\ \mathbf{e}'_i &= (0, -1, 0)^T, i = 1, 2, 6; \quad \mathbf{e}'_i = (h/c, 0, d/c)^T, i = 3, 4 \end{aligned}$$

which, according to (120), give rise to the screw coordinate vectors represented in \mathcal{F}'_0

$$\mathbf{Y}'_1 = \begin{pmatrix} 0 \\ -1 \\ 0 \\ 0 \\ 0 \\ R_0 \end{pmatrix}, \mathbf{Y}'_2 = \begin{pmatrix} 0 \\ -1 \\ 0 \\ 0 \\ 0 \\ a + R_0 \end{pmatrix}, \mathbf{Y}'_3 = \frac{1}{c} \begin{pmatrix} h \\ 0 \\ d \\ -bd/2 \\ d(a + R_0) \\ bh/2 \end{pmatrix}, \mathbf{Y}'_4 = \frac{1}{c} \begin{pmatrix} h \\ 0 \\ d \\ -bd/2 \\ h^2 + R_p d \\ bh/2 \end{pmatrix}, \mathbf{Y}'_5 = \frac{1}{c} \begin{pmatrix} h \\ 0 \\ d \\ bd/2 \\ d(a + R_0) \\ -bh/2 \end{pmatrix}, \mathbf{Y}'_6 = \begin{pmatrix} 0 \\ -1 \\ 0 \\ -h \\ 0 \\ R_p \end{pmatrix}.$$

The body-fixed frames are shown in fig. 14. The rotation matrices \mathbf{R}'_i and position vectors \mathbf{p}'_i , which determine the reference configurations \mathbf{A}'_i of the bodies, are

$$\mathbf{R}'_1 = \mathbf{R}'_6 = \mathbf{I}, \quad \mathbf{R}'_i = \frac{1}{c} \begin{pmatrix} h & 0 & -d \\ 0 & 1 & 0 \\ d & 0 & h \end{pmatrix}, \quad i = 2, \dots, 5$$

$$\mathbf{p}'_1 = \begin{pmatrix} -a/2 - R_0 \\ 0 \\ 0 \end{pmatrix}, \mathbf{p}'_2 = \begin{pmatrix} -a - R_0 \\ 0 \\ 0 \end{pmatrix}, \mathbf{p}'_3 = \begin{pmatrix} -d/2 - R_p \\ -b/2 \\ -h/2 \end{pmatrix}, \mathbf{p}'_4 = \begin{pmatrix} -R_p \\ 0 \\ -h \end{pmatrix}, \mathbf{p}'_5 = \begin{pmatrix} -d/2 - R_p \\ b/2 \\ -h/2 \end{pmatrix}, \mathbf{p}'_6 = \begin{pmatrix} 0 \\ 0 \\ -h \end{pmatrix}.$$

The joint screw coordinates in body-fixed representation are then found with (123) as

$${}^1\mathbf{X}'_1 = \begin{pmatrix} 0 \\ -1 \\ 0 \\ 0 \\ 0 \\ -a/2 \end{pmatrix}, {}^2\mathbf{X}'_2 = \begin{pmatrix} 0 \\ -1 \\ 0 \\ 0 \\ 0 \\ 0 \end{pmatrix}, {}^3\mathbf{X}'_3 = {}^5\mathbf{X}'_5 = \begin{pmatrix} (d^2 + h^2)/c^2 \\ 0 \\ 0 \\ 0 \\ 2ad + h^2 - d(d - 2R_0 + 2R_p) \\ 0 \end{pmatrix}, {}^4\mathbf{X}'_4 = \begin{pmatrix} (d^2 + h^2)/c^2 \\ 0 \\ 0 \\ 0 \\ 0 \\ b(d^2 + h^2)/(2c^2) \end{pmatrix}, {}^6\mathbf{X}'_6 = \begin{pmatrix} 0 \\ -1 \\ 0 \\ 0 \\ 0 \\ R_p \end{pmatrix}$$

A separated limb without platform comprises $\bar{n}_l = 5$ bodies. The kinematics model is expressed in terms of the matrices A' and X' in (133). According to the ordering and predecessor relation induced by the graph in fig. 10a), these are

$$A' = \begin{pmatrix} \mathbf{I} & \mathbf{0} & \mathbf{0} & \mathbf{0} & \mathbf{0} \\ \text{Ad}_{\mathbf{C}'_{2,1}} & \mathbf{I} & \mathbf{0} & \mathbf{0} & \mathbf{0} \\ \text{Ad}_{\mathbf{C}'_{3,1}} & \text{Ad}_{\mathbf{C}'_{3,2}} & \mathbf{I} & \mathbf{0} & \mathbf{0} \\ \text{Ad}_{\mathbf{C}'_{4,1}} & \text{Ad}_{\mathbf{C}'_{4,2}} & \text{Ad}_{\mathbf{C}'_{4,3}} & \mathbf{I} & \mathbf{0} \\ \text{Ad}_{\mathbf{C}'_{5,1}} & \text{Ad}_{\mathbf{C}'_{5,2}} & \mathbf{0} & \mathbf{0} & \mathbf{I} \end{pmatrix}, X' = \text{diag} ({}^1\mathbf{X}'_1, \dots, {}^5\mathbf{X}'_5). \quad (113)$$

Particular geometry parameter The geometric parameters are chosen so to roughly resemble a MOTOMAN-MPP3H Delta robot. All moving parts are approximated by geometric primitives for which the inertia parameters are determined. The principal dimensions are set to

$$R_0 = 150 \text{ mm}, R_p = 70 \text{ mm}, a = 250 \text{ mm}, b = 80 \text{ mm}, c = 1000 \text{ mm}.$$

Then the body-fixed joint coordinate vectors are

$${}^1\mathbf{X}'_1 = \begin{pmatrix} 0 \\ -1 \\ 0 \\ 0 \\ 0 \\ -1/8 \end{pmatrix}, {}^2\mathbf{X}'_2 = \begin{pmatrix} 0 \\ -1 \\ 0 \\ 0 \\ 0 \\ 0 \end{pmatrix}, {}^3\mathbf{X}'_3 = {}^5\mathbf{X}'_5 = \begin{pmatrix} 1 \\ 0 \\ 0 \\ 0 \\ 1/2 \\ 0 \end{pmatrix}, {}^4\mathbf{X}'_4 = \begin{pmatrix} 1 \\ 0 \\ 0 \\ 0 \\ 0 \\ 1/25 \end{pmatrix}, {}^6\mathbf{X}'_6 = \begin{pmatrix} 0 \\ -1 \\ 0 \\ 0 \\ 0 \\ 7/100 \end{pmatrix}$$

which are particularly simple since the joint axes are aligned with the body-fixed reference frames and could be readily deduced from the model, which is one advantage of the geometric Lie group formulation.

The platform configuration \mathbf{C}'_p is expressed in terms of the joint angles $\vartheta'_1, \vartheta'_2, \vartheta'_3, \vartheta'_4, \vartheta'_6$ via the POE (5). In the following, the closed form solution $\vartheta'_3 = \vartheta'_5 = -\vartheta'_4$ of the loop constraints will be used (see example 8), so that the vector of generalized coordinates is $\mathbf{q}_{(l)} = (\vartheta'_4, \vartheta'_1, \vartheta'_2, \vartheta'_6)^T$ (see example 15). The platform pose is then

$$\mathbf{C}'_p(\mathbf{q}_{(l)}) = \begin{pmatrix} c_{1+2+6} & 0 & -s_{1+2+6} & \frac{1}{200} (33(c_{1+2+4} + c_{1+2-4}) + 14c_{1+2+6} - 50c_1 + 2\xi s_{1+2} c_4 - 30) \\ 0 & 1 & 0 & -s_4 \\ s_{1+2+6} & 0 & c_{1+2+6} & \frac{1}{200} (14s_{1+2+6} + 66s_{1+2} c_4 - 50s_1 - \xi(c_{1+2+4} + c_{1+2-4})) \\ 0 & 0 & 0 & 1 \end{pmatrix}$$

with $s_i := \sin \vartheta'_i, c_i := \cos \vartheta'_i, s_{i \pm j \pm k} := \sin(\vartheta'_i \pm \vartheta'_j \pm \vartheta'_k), c_{i \pm j \pm k} := \cos(\vartheta'_i \pm \vartheta'_j \pm \vartheta'_k)$, and $\xi := \sqrt{8911}$.

The system Jacobian (131) is readily found with the above joint screw coordinates and the matrix (113) according to (132). The last block row in (132) is the geometric Jacobian of the platform $\mathbf{J}'_p := \mathbf{J}'_{n_l=6}$. Along with $\mathbf{H}'_{(l)}$ in (53), this yields the compound forward kinematics Jacobian $\mathbf{L}'_{p(l)}$ in (52). Rows 2,4,5,6 are used to construct $\mathbf{L}'_{(l)}$ in (57). The Jacobian in the velocity inverse kinematics solution of the mechanism (58) is finally obtained with (63), using the selection matrix in (64), as

$$\mathbf{F}'_{(l)}(\boldsymbol{\vartheta}_{(l)}) = \frac{1}{w_2} \begin{pmatrix} 0 & -w_2 \sec \vartheta'_4 & 0 \\ 4w_6 & -400 \tan \vartheta'_4 & -4u_6 \\ -4(w_6 - 25 \sec \vartheta'_4 \cos(\vartheta'_2 + \vartheta'_6)) \tan \vartheta'_4 (400 - u_2 \sec \vartheta'_4) & 4(u_6 - 25 \sec \vartheta'_4 \sin(\vartheta'_2 + \vartheta'_6)) & \\ -100 \sec \vartheta'_4 \cos(\vartheta'_2 + \vartheta'_6) & u_2 \tan \vartheta'_4 \sec \vartheta'_4 & 100 \sec \vartheta'_4 \sin(\vartheta'_2 + \vartheta'_6) \end{pmatrix} \quad (114)$$

where

$$\begin{aligned} u_2 &:= \xi \sin \vartheta'_2 + 33 \cos \vartheta'_2, & w_2 &:= \xi \cos \vartheta'_2 - 33 \sin \vartheta'_2 \\ u_6 &:= 33 \sin \vartheta'_6 + \xi \cos \vartheta'_6, & w_6 &:= 33 \cos \vartheta'_6 - \xi \sin \vartheta'_6 \end{aligned}$$

The compound inverse kinematics Jacobian in (59) is obtained with $\mathbf{H}'_{(l)}$ in (53).

9.2 Kinematics of the $L = 3$ limbs

The construction and mount frames of the limbs are all located the center of the base and platform, respectively. They are only rotated by $\pm 2/3\pi$. The respective transformations are

$$\mathbf{S}_{0(1)} = \mathbf{S}_{p(1)} = \mathbf{I}, \mathbf{S}_{0(2)} = \mathbf{S}_{p(2)} = \begin{pmatrix} -1/2 & -\sqrt{3}/2 & 0 & 0 \\ \sqrt{3}/2 & -1/2 & 0 & 0 \\ 0 & 0 & 1 & 0 \\ 0 & 0 & 0 & 1 \end{pmatrix}, \mathbf{S}_{0(3)} = \mathbf{S}_{p(3)} = \begin{pmatrix} -1/2 & -\sqrt{3}/2 & 0 & 0 \\ \sqrt{3}/2 & -1/2 & 0 & 0 \\ 0 & 0 & 1 & 0 \\ 0 & 0 & 0 & 1 \end{pmatrix}. \quad (115)$$

The configuration of body i is thus determined by (94), and the forward and inverse Jacobian by (96) and (97), respectively. Therewith, according to (70), the inverse kinematics Jacobian \mathbf{J}_{IK} is constructed from the second row of $\mathbf{F}'_{(l)}, l = 1, 2, 3$ in (114).

9.3 Dynamic parameters

The upper arm is represented by a solid cylinder with length $a = 250$ mm and 30 mm diameter. The bars forming the parallelogram are modeled as cylindrical rods with length $c = 1$ m and diameter of 10 mm. The link connecting the rods is a cylinder with length $b = 80$ mm and diameter 20 mm. The T-axis flange (which allows mounting a 4th rotary axis at the platform) is regarded as the dominant element contributing to the inertia of the moving platform. It is modeled as a solid cylinder with 90 mm diameter and 100 mm height. As the platform cannot rotate, with $\mathbf{P}_p := \mathbf{P}_p^{\text{trans}}$ in (55), the contribution of the platform inertia to the mass matrix in (80) reduced to $\mathbf{P}_p^T \mathbf{M}_p \mathbf{P}_p = m_p \mathbf{I}$, and the Coriolis/centrifugal term in (81) vanishes since $\mathbf{P}_p^T \mathbf{G}_p \mathbf{M}_p \mathbf{P}_p = \mathbf{0}$. This is clear, as the NE-equations (76) reduce to the balance of linear momentum. Thus only the mass of the platform must be determined.

All links are assumed to be made of aluminum. The inertia parameter are indeed not those of a real Delta robot, but serve the purpose of a numerical example.

9.4 Implementation and Results

Code Generation and Numerical Results The dynamic EOM (79) were generated symbolically in closed form using a Mathematica implementation of the Lie group formulation. The kinematic relations (59) and (60) were incorporated to obtain (79) solely in terms of $\vartheta, \mathbf{V}_t, \dot{\mathbf{V}}_t$. Further, the transposed inverse \mathbf{J}_{IK}^{-T} of the inverse kinematics Jacobian was generated symbolically. All equations were exported in C language, and implemented as C-mex function in Matlab compiled with the standard MinGW64 compiler.

For the mere purpose of checking the correctness of the model and code implementation, the inverse dynamics solution is computed for the straight-line motion of the platform prescribed by $\mathbf{r}(t) = (0, 0, -h)^T + (0.3, 0.4, 0.1)^T \sin(2\pi t/T), t = 0, \dots, T = 10$ s, with time step size of $\Delta t = 0.01$ s. The time evolution of actuator joint coordinates ϑ_{act} and the actuation torques \mathbf{u} are shown in fig. 16. The trajectories of all $N = 18$ joints and the actuation torques were validated against the commercial MBS dynamics simulation software Alaska. The numerical results match up to the prescribed accuracy. Figure 15 shows the 3D-view of the model with the geometric primitives. The results are identical up to the computational accuracy.

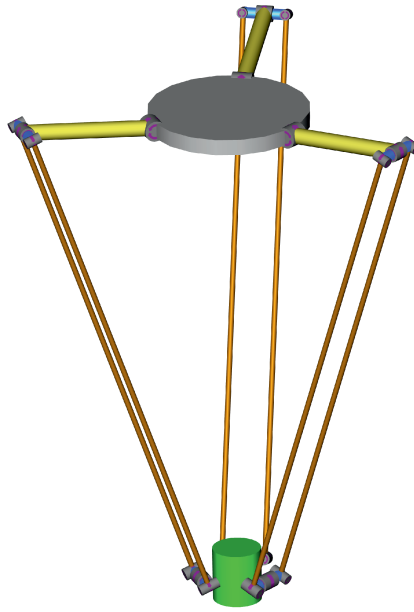


Fig. 15. Alaska model resembling the MOTOMAN-MPP3H Delta robot.

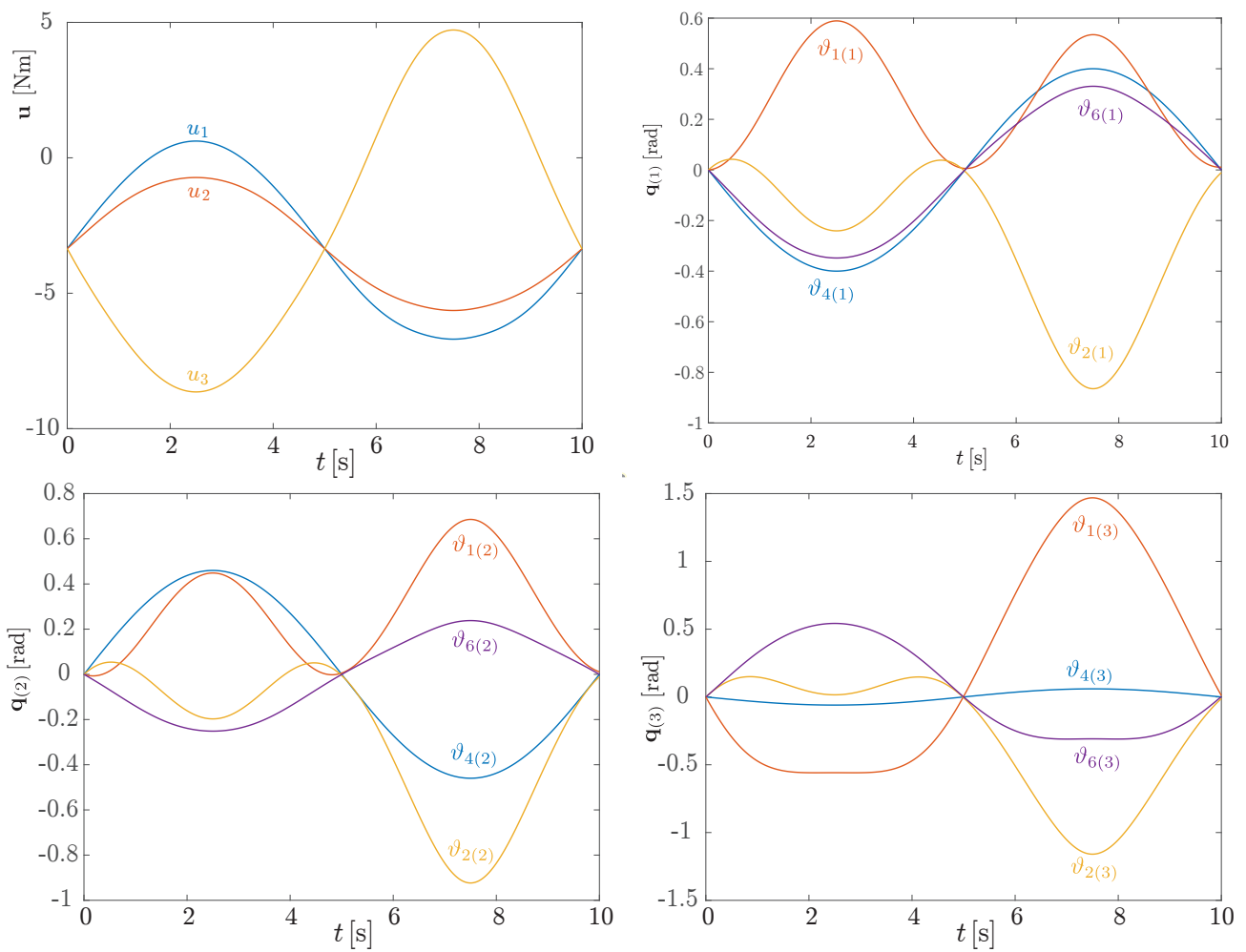


Fig. 16. Time evolution of actuation torques $\mathbf{u} = (u_1, u_2, u_3)^T$ and generalized coordinates $\mathbf{q}_{(l)} = (\vartheta_{4(l)}, \vartheta_{1(l)}, \vartheta_{2(l)}, \vartheta_{6(l)})^T$, $l = 1, 2, 3$ for the straight-line platform motion of the Delta model.

Performance Assessment The overall performance of an inverse dynamics evaluation is dictated by the time required for solving the geometric inverse kinematics problems for the L limbs and for the subsequent evaluation of the inverse dynamics model. This was determined for the closed form inverse dynamics model (109) and the parallel implementation. The following numerical experiments were conducted on a standard PC with an Intel i7-8700 CPU with 6 cores clocked at 3.2 GHz running MS-Windows 10 operating system. The following results, which are listed in table 1, were obtained by averaging over 10^6 evaluation runs. For parallel computation the Matlab Parallel Computing Toolbox is used.

1. Computation times for computing the inverse dynamics solution, i.e. for evaluating the symbolic expression of the monolithic form of (109), were determined. The geometric inverse kinematics is solved by executing two iterations of (67) for all limbs. The average time needed for solving the IK and computing the inverse dynamics solution was $2.74\mu\text{s}$ as listed in the first row of table 1.
2. Evaluating the inverse dynamics solution (109) involves evaluation of the EOM (79) and the subsequent multiplication with $\mathbf{J}_{\text{IK}}^{-T}$, which is known symbolically. It is instructive to quantify the time spent for evaluating (79) alone. The left-hand side of (79) was evaluated, which delivers the term $\phi_t - \mathbf{W}_t^{\text{EE}}$ in (110). The average time needed for (79) along with the IK solution is shown in table 1 as $2.75\mu\text{s}$. This confirms that the time for evaluating $\mathbf{J}_{\text{IK}}^{-T}$ is negligible. Moreover, the closed form (109), with $\phi_t - \mathbf{W}_t^{\text{EE}}$ being premultiplied with $\mathbf{J}_{\text{IK}}^{-T}$, allows the compiler to optimize the code.
3. To investigate the potential of a distributed computation of the EOM, the computation times spent for separate evaluation of the EOM of the limbs is determined. The equations for an individual limb l are evaluated at one computation node: The geometric inverse kinematics problems $\vartheta_{(l)} = \psi_{\text{IK}(l)}(\mathbf{x})$ is solved performing two iterations of (68), and the contribution of limb l to the sum in (112), i.e. the expression

$$\bar{\mathbf{W}}_{(l)} = \bar{\mathbf{F}}_{(l)}^T \bar{\mathbf{H}}_{(l)}^T \phi_{(l)}(\bar{\vartheta}_{(l)}, \dot{\bar{\vartheta}}_{(l)}, \ddot{\bar{\vartheta}}_{(l)}), \quad (116)$$

is evaluated on one computation node, while $L = 3$ computation nodes are running in parallel. This corresponds to the dashed box in fig. 13, except that the platform EOM are not investigated as they are computationally trivial. Table 1 shows the average necessary computation time. Notice that the reported times only account for the evaluations of the EOM in order to compute the auxiliary wrenches $\bar{\mathbf{W}}_{(l)}$ and Jacobians $\bar{\mathbf{F}}_{(l)}$, but they do not include the time needed for exchanging these quantities. Thus, these results are indicative only as the communication overhead to send them to the block on the right-hand side in fig. 13 strongly depends on the parallel computing framework. For instance, the communication overhead of the used Matlab Parallel Computing Toolbox (which is not intended for massive parallel computation) by far exceeds the computation time for the models. Therefore no timing is reported here. A parallel implementation will have to ensure minimal communication overhead, which is not the topic of this paper.

- 3./ It is also interesting to break down the overall time to that needed for parallel evaluation of the individual limbs. The time spent for evaluating the inverse kinematics and EOM for limb l (running on node l) is reported as experiment 3./ in table 1. The different mathematical expressions for the different limbs leads to slightly different times. Clearly, the overall time is dictated by the maximal time spent for a limb.

It should be mentioned that the parallel implementation may further benefit from employing a recursive $O(n)$ formulation for the inverse dynamic evaluation of the EOM of the limbs. A Lie group formulation of a recursive $O(n)$ inverse dynamics algorithm, using the same geometric description as in appendix B, was reported in [90,91]. The Matlab implementation can be found as media attachment to [91] and in the GitHub repository `shivesh1210/nth_order_eom_time_derivatives`.

Exp.	# Nodes	Equations	Computation Results	Eval. time in μs
1	1	IK (68) & ID (109)	$\boldsymbol{\vartheta}(t), \mathbf{u}(t)$	2.74
2	1	IK (68) for all limbs & EOM (79)	$\boldsymbol{\vartheta}(t), \mathbf{F}_{(l)}, l = 1, 2, 3, \boldsymbol{\varphi}_t - \mathbf{W}_t^{EE}$ in (109)	2.75
3	3	IK (68) & (116) of all limbs in parallel	$\boldsymbol{\vartheta}(t), \mathbf{F}_{(l)}, \bar{\mathbf{F}}_{(l)}^T \bar{\mathbf{H}}_{(l)}^T \boldsymbol{\varphi}_{(l)}, l = 1, 2, 3$	0.97
3.1	3	IK (68) & (116) for limb $l = 1$	$\boldsymbol{\vartheta}_{(1)}(t), \mathbf{F}_{(1)}, \bar{\mathbf{F}}_{(1)}^T \bar{\mathbf{H}}_{(1)}^T \boldsymbol{\varphi}_{(1)}$	0.97
3.2	3	IK (68) & (116) for limb $l = 2$	$\boldsymbol{\vartheta}_{(2)}(t), \mathbf{F}_{(2)}, \bar{\mathbf{F}}_{(2)}^T \bar{\mathbf{H}}_{(2)}^T \boldsymbol{\varphi}_{(2)}$	0.83
3.3	3	IK (68) & (116) for limb $l = 3$	$\boldsymbol{\vartheta}_{(3)}(t), \mathbf{F}_{(3)}, \bar{\mathbf{F}}_{(3)}^T \bar{\mathbf{H}}_{(3)}^T \boldsymbol{\varphi}_{(3)}$	0.83

Table 1. Experimentally determined computation times for serial and parallel evaluation of different expressions. Exp. 1: Total time for solving the inverse kinematics (IK) problem and for evaluating the inverse dynamics (ID) solution (109) on a single processing node. Exp. 2: Time elapsed for solving the IK problem and for evaluating the overall EOM (79), which yields the term $\boldsymbol{\varphi}_t - \mathbf{W}_t^{EE}$ in (109), on a single computation node. Exp. 3: Computation time needed for solving the IK problem and the term $\bar{\mathbf{F}}_{(l)}^T \boldsymbol{\varphi}_{(l)}$ in (116) for all limbs $l = 1, 2, 3$ in parallel (three parallel computation nodes are used). Exp. 3. l shows the time consumed by node l for evaluating limb l .

10 Conclusion

Utilizing the dynamic capabilities of PKM to their full extend necessitates appropriately accurate dynamics models. Such dynamics models have been reported in the past for PKM with simple limbs. In this paper a systematic modeling approach for rigid body PKM with complex hybrid limbs and ideal joints is presented so that now modular modeling approaches are available for the full spectrum of practically relevant types of PKM. The method is also general in terms of the formulation used for dynamics modeling the limbs. A Lie group formulation, respectively the geometric formulation in terms of joint screw coordinates, is used in this paper. Since PKM with simple limbs are included as special case, the paper can also be read as a guide to the modeling of PKM in general. The approach rests on the concept of constraint embedding, where the loop constraints within the limbs are resolved, so that the aggregated submechanism of a FC functions kinematically as a compound joint contributing its own dynamics. The method is demonstrated in detail for the 3RR[2RR]R Delta robot. For this example initial results on the computational performance of the presented parallel implementation are reported, which are indicative only as the actual performance gained by a distributed computation highly depends on the implementation.

Any dynamics modeling starts with an appropriate kinematic model, and shall hence account for the particular kinematic topology of PKM, which will especially exploit the modularity of PKM. 'Classical PKM', i.e. those that are currently used in industry, can be regarded as rigid body system interconnected either by ideal kinematic joints or by elastic elements giving rise to 'lumped parameter' models. This is contrasted by the recent trend of continuum robots consisting of inherently flexible elements. These flexible elements are usually rods or slender beams, which allows for a application of Cosserat beam models giving rise to closed form quasistatic inverse kinematics solutions [102]. The presented modular modeling approach will be adopted to continuum parallel robots by replacing the representative limb with a continuum model.

Acknowledgment

The author acknowledges support by the LCM-K2 Center within the framework of the Austrian COMET-K2 program.

A Kinematics of Lower-Pair Mechanisms with Tree-Topology

A body-fixed reference frame \mathcal{F}_k is attached at body k . The pose of body k relative to the IFR \mathcal{F}_0 is represented by the homogenous transformation matrix

$$\mathbf{C}_k = \begin{pmatrix} \mathbf{R}_k & \mathbf{r}_k \\ \mathbf{0} & 1 \end{pmatrix} \in SE(3) \quad (117)$$

which describes the transformation from \mathcal{F}_k to \mathcal{F}_0 , where $\mathbf{R}_k \in SO(3)$ is the corresponding rotation matrix, and $\mathbf{r}_k \in \mathbb{R}^3$ is the position vector of the origin of \mathcal{F}_k measured in \mathcal{F}_0 . Coordinate vectors resolved in frame \mathcal{F}_k are denoted with ${}^k\mathbf{p}$, where the superscript is omitted when it refers to the IFR ($k = 0$). In particular, the platform pose is described by the transformation \mathbf{C}_p from platform frame \mathcal{F}_p to inertia frame \mathcal{F}_0 .

The fact that frame transformations form the Lie group $SE(3)$ gives rise to Lie group formulations of kinematics and dynamics of MBS, which have become an established approach in robotics [92] and are increasingly used for MBS dynamics

noticing its algorithmic equivalence to the matrix and operator algebra methods [4, 87]. In this paper the Lie group formulation and notation from [83, 84] is used. One important feature of these methods is the compact and flexible description of the kinematic of kinematic chains by means of the so-called product of exponentials (POE). In the following, it is assumed again, for the sake of simplicity, that all joints are 1-DOF joints, so that $n_l = n_l$ and $\mathfrak{N}_l = N_l$.

First consider a single kinematic chain with n 1-DOF lower pair joints, with joint variables $\vartheta = (\vartheta_1, \dots, \vartheta_n)^T$ (rotation angles or translation coordinates). The configuration $\mathbf{C}_k \in SE(3)$ of body k of this chain is determined as

$$\mathbf{C}_k(\vartheta) = f_k(\vartheta_1, \dots, \vartheta_k) \mathbf{A}_k \quad (118)$$

with the product of exponentials

$$f_k(\vartheta) = \exp(\mathbf{Y}_1 \vartheta_1) \exp(\mathbf{Y}_2 \vartheta_2) \dots \exp(\mathbf{Y}_k \vartheta_k) \quad (119)$$

where $\mathbf{A}_k := \mathbf{C}_k(\mathbf{0})$ is the zero reference configuration, and \mathbf{Y}_i is the screw coordinate vector of joint i in spatial representation. The latter is determined as

$$\mathbf{Y}_i = \begin{pmatrix} \mathbf{e}_i \\ \mathbf{y}_i \times \mathbf{e}_i + h_i \mathbf{e}_i \end{pmatrix} \quad (120)$$

where $\mathbf{e}_i \in \mathbb{R}^3$ is a unit vector along the joint axis, and $\mathbf{y}_i \in \mathbb{R}^3$ is the vector to a point on the axis, both resolved in IFR \mathcal{F}_0 . The scalar $h_i \in \mathbb{R}$ is the pitch of the joint. For the particular case of revolute ($h = 0$) and prismatic joints ($h = \infty$), the screw coordinates are

$$\text{Revolute : } \mathbf{Y}_i = \begin{pmatrix} \mathbf{e}_i \\ \mathbf{y}_i \times \mathbf{e}_i \end{pmatrix}, \quad \text{Prismatic : } \mathbf{Y}_i = \begin{pmatrix} \mathbf{0} \\ \mathbf{e}_i \end{pmatrix}. \quad (121)$$

It is at times beneficial to represent the screw coordinates of joint i in the body-fixed frame \mathcal{F}_i at body i . This is then denoted with ${}^i\mathbf{X}_i$, and determined as

$${}^i\mathbf{X}_i = \begin{pmatrix} {}^i\mathbf{e}_i \\ {}^i\mathbf{x}_i \times {}^i\mathbf{e}_i + {}^i\mathbf{e}_i h_i \end{pmatrix} \quad (122)$$

with a unit vector ${}^i\mathbf{e}_i \in \mathbb{R}^3$ along the joint axis, and ${}^i\mathbf{x}_i \in \mathbb{R}^3$ being the vector to a point on this axis, where now both are represented in \mathcal{F}_i . The body-fixed and spatial representation are related by

$$\mathbf{Y}_i = \mathbf{Ad}_{\mathbf{C}_i} {}^i\mathbf{X}_i, \quad {}^i\mathbf{X}_i = \mathbf{Ad}_{\mathbf{A}_i}^{-1} \mathbf{Y}_i. \quad (123)$$

Now for a general tree-topology system, the ordering is defined by the spanning tree and the configuration of body k is determined by (1) in terms of the tree-joint variables $\boldsymbol{\eta}$.

The twist of body k represented in the body-fixed frame \mathcal{F}_k is

$$\mathbf{V}_k = \begin{pmatrix} {}^k\boldsymbol{\omega}_k \\ {}^k\mathbf{v}_k \end{pmatrix} \quad (124)$$

consists of the translation velocity ${}^k\mathbf{v}_k$ and angular velocity ${}^k\boldsymbol{\omega}_k$ of the body-fixed frame \mathcal{F}_k , relative to the world frame \mathcal{F}_0 , both resolved in \mathcal{F}_k . It is given in terms of the joint rates $\dot{\vartheta}_i$ as

$$\begin{aligned} \mathbf{V}_k &= \mathbf{J}_{k,1} \dot{\vartheta}_1 + \mathbf{J}_{k,2} \dot{\vartheta}_2 + \dots + \mathbf{J}_{k,k-1} \dot{\vartheta}_{k-1} + \mathbf{J}_{k,k} \dot{\vartheta}_k \\ &= \mathbf{J}_k \dot{\boldsymbol{\vartheta}} \end{aligned} \quad (125)$$

with the geometric Jacobian of body k

$$\mathbf{J}_k = (\mathbf{J}_{k,1}, \mathbf{J}_{k,2}, \dots, \mathbf{J}_{k,k-1}, \mathbf{J}_{k,k}, \mathbf{0}, \dots, \mathbf{0}). \quad (126)$$

Therein, $\mathbf{J}_{k,i}$ is the instantaneous joint screw coordinate vector of joint i represented in \mathcal{F}_k , which is given explicitly as

$$\mathbf{J}_{k,i} = \begin{pmatrix} {}^k\mathbf{e}_i \\ {}^k\mathbf{b}_i \times {}^k\mathbf{e}_i + {}^k\mathbf{e}_i h_i \end{pmatrix} \quad (127)$$

where ${}^k\mathbf{e}_i(\vartheta)$ is a unit vector along the axis of joint i and ${}^k\mathbf{b}_i(\vartheta)$ is the vector to a point on that axis, both measured and resolved in frame \mathcal{F}_k at body k , and h_i is the pitch of the joint. An efficient way to compute $\mathbf{J}_{k,i}$, follows by observing that they can be determined by a frame transformation of the screw coordinates ${}^i\mathbf{X}_i$ current configuration of \mathcal{F}_k , and can thus be calculated as [83]

$$\mathbf{J}_{k,i} = \text{Ad}_{\mathbf{C}_{k,i}} {}^i\mathbf{X}_i, i = 1, \dots, k \quad (128)$$

where the adjoint matrix, which described the transformation of screw coordinates according to the frame transformation $\mathbf{C} \in SE(3)$, is

$$\text{Ad}_{\mathbf{C}} = \begin{pmatrix} \mathbf{R} & \mathbf{0} \\ \tilde{\mathbf{r}}\mathbf{R} & \mathbf{R} \end{pmatrix}, \text{ with } \mathbf{C} = \begin{pmatrix} \mathbf{R} & \mathbf{r} \\ \mathbf{0} & \mathbf{1} \end{pmatrix} \quad (129)$$

and $\mathbf{C}_{k,i} = \mathbf{C}_k^{-1}\mathbf{C}_i$ is the configuration of body i relative to body k . Now for a general tree-topology system, the Jacobian of body k is given by (4), which determines the body-fixed twist as in (3) in terms of $\boldsymbol{\eta}, \dot{\boldsymbol{\eta}}$. The relation (127) indeed applies to any joint, i.e. tree- and cut-joints of the limb.

Consider now the tree-topology system of limb l without platform comprising $n_l = n_l$ bodies. The *system twist vector* is expressed as

$$\mathbf{V}_{(l)} := \begin{pmatrix} \mathbf{V}_1 \\ \vdots \\ \mathbf{V}_{n_l} \end{pmatrix}_{(l)} = \mathbf{J}_{(l)} \dot{\boldsymbol{\vartheta}}_{(l)(l)} \quad (130)$$

in terms of the *geometric system Jacobian*

$$\mathbf{J}_{(l)} = \begin{pmatrix} \mathbf{J}_1 \\ \vdots \\ \mathbf{J}_{n_l} \end{pmatrix}_{(l)}. \quad (131)$$

The latter possesses the factorization

$$\mathbf{J}_{(l)} = \mathbf{A}_{(l)} \mathbf{X}_{(l)}. \quad (132)$$

Assuming a canonical directed spanning tree $\vec{G}_{(l)}$ (assumption 2), matrix $\mathbf{A}_{(l)}(\vartheta)$ is the block-triangular, and $\mathbf{X}_{(l)}$ is the block-diagonal matrix

$$\mathbf{A}_{(l)} = \begin{pmatrix} \mathbf{I} & \mathbf{0} & \mathbf{0} \dots \mathbf{0} \\ & \mathbf{I} & \mathbf{0} \dots \mathbf{0} \\ & & \ddots \vdots \\ & \text{Ad}_{\mathbf{C}_{i,j}} & \mathbf{0} \\ & & & \mathbf{I} \end{pmatrix}_{(l)}, \quad \mathbf{X}_{(l)} = \begin{pmatrix} {}^1\mathbf{X}_1 & \mathbf{0} & \mathbf{0} & \mathbf{0} \\ \mathbf{0} & {}^2\mathbf{X}_2 & \mathbf{0} & \dots & \mathbf{0} \\ \mathbf{0} & \mathbf{0} & {}^3\mathbf{X}_3 & & \mathbf{0} \\ \vdots & \vdots & \ddots & \ddots & \\ \mathbf{0} & \mathbf{0} & \dots & \mathbf{0} & {}^{n_l}\mathbf{X}_{n_l} \end{pmatrix}_{(l)} \quad (133)$$

where $\mathbf{Ad}_{\mathbf{C}_{i,j}} = \mathbf{0}$ if $j \not\prec i$ (body j is not a predecessor of body i), and $i-1$ is the predecessor relation relative to the root-directed tree.

The derivatives of the Jacobian are frequently needed, e.g. for acceleration forward/inverse kinematics. The partial derivatives and the time derivative of the columns of \mathbf{J}_i , i.e. the instantaneous joint screw coordinates in body-fixed representation, can be expressed in closed form by simple vector operation. The non-zero terms are [84, 77]

$$\frac{\partial}{\partial \dot{\theta}_k} \mathbf{J}_{i,j} = \mathbf{ad}_{\mathbf{J}_{i,j}} \mathbf{J}_{i,k}, \text{ if } j \prec k \leq i \quad (134)$$

$$\begin{aligned} \dot{\mathbf{J}}_{i,j} &= \sum_{j \prec k \leq i} \mathbf{ad}_{\mathbf{J}_{i,j}} \mathbf{J}_{i,k} \dot{\theta}_k \\ &= -\mathbf{ad}_{\Delta^i \mathbf{V}_{i,j}} \mathbf{J}_{i,j} \end{aligned} \quad (135)$$

where $\Delta^i \mathbf{V}_{i,j} := \mathbf{V}_i - \mathbf{Ad}_{\mathbf{C}_{i,j}} \mathbf{V}_j$ is the relative twist of body i and j represented in reference frame at body i . The time derivative of the system Jacobian can be expressed as (omitting subscript (l))

$$\dot{\mathbf{J}}(\boldsymbol{\vartheta}, \dot{\boldsymbol{\vartheta}}) = -\mathbf{A}(\boldsymbol{\vartheta}) \mathbf{a}(\dot{\boldsymbol{\vartheta}}) \mathbf{J}(\boldsymbol{\vartheta}) \quad (136)$$

with

$$\mathbf{a}(\dot{\boldsymbol{\vartheta}}) := \text{diag}(\dot{\vartheta}_1 \mathbf{ad}_{\mathbf{X}_1}, \dots, \dot{\vartheta}_{n_l} \mathbf{ad}_{\mathbf{X}_{n_l}}). \quad (137)$$

The adjoint operator matrix, which produces the Lie bracket (screw product), is

$$\mathbf{ad}_{\mathbf{X}_i} = \begin{pmatrix} {}^i \tilde{\boldsymbol{\xi}}_i & \mathbf{0} \\ {}^i \tilde{\boldsymbol{\eta}}_i & {}^i \tilde{\boldsymbol{\xi}}_i \end{pmatrix}, \text{ with } {}^i \mathbf{X}_i = \begin{pmatrix} {}^i \boldsymbol{\xi}_i \\ {}^i \boldsymbol{\eta}_i \end{pmatrix} \quad (138)$$

where $\tilde{\mathbf{x}} \in so(3)$ is the skew symmetric matrix associated to vector $\mathbf{x} \in \mathbb{R}^3$.

B EOM of Tree-Topology System

The dynamics of a rigid body is governed by the NE-equations. They are expressed in compact form as the Euler-Poincaré equations of the rigid body w.r.t. an arbitrary body-fixed reference frame \mathcal{F}_b

$$\mathbf{M} \dot{\mathbf{V}} + \mathbf{G}(\mathbf{V}) \mathbf{M} \mathbf{V} + \mathbf{W}^{\text{grav}} = \mathbf{W} \quad (139)$$

where $\mathbf{W} = (\boldsymbol{\tau}, \mathbf{f})^T \in se^*(3)$ is the body-fixed representation of the wrench acting on the body. The constant 6×6 inertia matrix \mathbf{M} and gyroscopic matrix \mathbf{G} is, respectively,

$$\mathbf{M} = \begin{pmatrix} \boldsymbol{\Theta} & m\tilde{\mathbf{d}} \\ -m\tilde{\mathbf{d}} & m\mathbf{I} \end{pmatrix}, \mathbf{G}(\mathbf{V}) := -\mathbf{ad}_{\mathbf{V}}^T = \begin{pmatrix} \tilde{\boldsymbol{\omega}} & \tilde{\mathbf{v}} \\ \mathbf{0} & \tilde{\boldsymbol{\omega}} \end{pmatrix} \quad (140)$$

with the body-fixed inertia tensor $\boldsymbol{\Theta}$ w.r.t. \mathcal{F}_b , and \mathbf{d} is the position vector of the COM represented in \mathcal{F}_b . The gravity wrench is given by

$$\mathbf{W}_p^{\text{grav}} = -\mathbf{M}_p \mathbf{Ad}_{\mathbf{C}_p}^{-1} \begin{pmatrix} \mathbf{0} \\ \mathbf{g} \end{pmatrix} \quad (141)$$

where \mathbf{g} is the gravity vector resolved in the IFR \mathcal{F}_0 . The classical separated form of the NE-equations is obtained when writing (139) separately for translation and rotation

$$\begin{aligned}\Theta\dot{\omega} + \tilde{\omega}\Theta\omega + m\tilde{\mathbf{d}}(\dot{\mathbf{v}} + \tilde{\omega}\mathbf{v}) &= \boldsymbol{\tau} \\ m(\dot{\mathbf{v}} + \tilde{\omega}\mathbf{v} + (\tilde{\dot{\omega}} + \tilde{\omega}\tilde{\omega})\mathbf{d}) &= \mathbf{f}.\end{aligned}\quad (142)$$

They clearly simplify if the body-fixed reference frame is located at the COM, i.e. if $\mathbf{d} = \mathbf{0}$.

The dynamic EOM of the tree-topology system comprising $n_l = n_l$ rigid bodies can be expressed in closed form as in (72) by means of simple matrix operations [84]. Denote with \mathbf{M}_i the body-fixed mass matrix of body i . The $n_l \times n_l$ generalized matrix $\bar{\mathbf{M}}_{(l)}$ and the matrix $\bar{\mathbf{C}}_{(l)}(\dot{\boldsymbol{\eta}}_{(l)}, \ddot{\boldsymbol{\eta}}_{(l)})$, which determines the generalized Coriolis and centrifugal forces, are

$$\bar{\mathbf{M}}_{(l)} = \mathbf{J}_{(l)}^T \mathbf{M}_{(l)} \mathbf{J}_{(l)} \quad (143)$$

$$\bar{\mathbf{C}}_{(l)} = -\mathbf{J}_{(l)}^T (\mathbf{M}_{(l)} \mathbf{A}_{(l)} \mathbf{a}_{(l)} + \mathbf{b}_{(l)}^T \mathbf{M}_{(l)}) \mathbf{J}_{(l)}. \quad (144)$$

where

$$\begin{aligned}\mathbf{M}_{(l)} &:= \text{diag}(\dots, \mathbf{M}_{i-2}, \mathbf{M}_{i-1}, \mathbf{M}_i, \dots)_{(l)} \\ \mathbf{a}_{(l)}(\dot{\boldsymbol{\eta}}_{(l)}) &:= \text{diag}(\dots, \dot{\eta}_{i-2} \mathbf{ad}_{\mathbf{x}_{i-2}}, \dot{\eta}_{i-1} \mathbf{ad}_{\mathbf{x}_{i-1}}, \dot{\eta}_i \mathbf{ad}_{\mathbf{x}_i}, \dots)_{(l)} \\ \mathbf{b}_{(l)}(\mathbf{V}_{(l)}) &:= \text{diag}(\dots, \mathbf{ad}_{\mathbf{v}_{i-2}}, \mathbf{ad}_{\mathbf{v}_{i-1}}, \mathbf{ad}_{\mathbf{v}_i}, \dots)_{(l)}\end{aligned}\quad (145)$$

with $\mathbf{ad}_{\mathbf{x}_i}$ in (138). The ordering of joint variables is according to the root-directed spanning tree $\vec{G}_{(l)}$. The generalized gravity forces are

$$\mathbf{Q}_{(l)}^{\text{grav}} = -\mathbf{J}_{(l)}^T \mathbf{M}_{(l)} \mathbf{U}_{(l)} \begin{pmatrix} \mathbf{0} \\ \mathbf{g} \end{pmatrix} = -\mathbf{J}_{(l)}^T \begin{pmatrix} \mathbf{M}_1 \mathbf{Ad}_{\mathbf{C}_1}^{-1} \\ \mathbf{M}_2 \mathbf{Ad}_{\mathbf{C}_2}^{-1} \\ \vdots \\ \mathbf{M}_{n_l} \mathbf{Ad}_{\mathbf{C}_{n_l}}^{-1} \end{pmatrix}_{(l)} \begin{pmatrix} \mathbf{0} \\ \mathbf{g} \end{pmatrix} \quad (146)$$

with

$$\mathbf{U}_{(l)}(\mathbf{q}) = \begin{pmatrix} \mathbf{Ad}_{\mathbf{C}_1}^{-1} \\ \mathbf{Ad}_{\mathbf{C}_2}^{-1} \\ \vdots \\ \mathbf{Ad}_{\mathbf{C}_{n_l}}^{-1} \end{pmatrix} \quad (147)$$

Notice that the topology is entirely encoded in matrix $\mathbf{A}_{(l)}$, and thus in $\mathbf{J}_{(l)}$ via (132).

C List of Symbols and Abbreviations

An index (l) on a matrix or vector indicates that all elements are referring to limb l

IFR - Inertial Frame

RL - Representative Limb

FC - Fundamental Cycle (topologically independent loop)

EE - End-Effector

\mathfrak{N}_l - total number of joints in limb l

n_l - number of tree-joints in limb l

L - number of limbs

Γ - topological graph, $\Gamma_{(l)}$ - topological graph of limb $l = 1, \dots, L$
 γ_l - number of FCs of limb l , i.e. of $\Gamma_{(l)}$
 $\Lambda_{\lambda(l)}$ - FC $\lambda = 1, \dots, \gamma_l$ of limb l
 $N_{\lambda,l}$ - number of joint variables associated to FC λ of limb l
 N_l - total number of joint variables in limb l , $N_l = N_{1,l} + \dots + N_{\gamma_l,l}$
 N_{act} - number of actuated joint coordinates, $N_{\text{act}(l)}$ - number of actuated joint coordinates in limb l
 n - total number of joint variables of the tree-topology system according to \vec{G}
 n_l - number of tree-joint variables of limb l
 \bar{n}_l - number of tree-joint variables of limb l when the platform is removed
 \bar{n} - total number of variables of the tree-topology system when the platform is removed, $\bar{n} := \bar{n}_1 + \dots + \bar{n}_L$
 \underline{k} - index of the last body in the path from body k to the ground, i.e. $0 = \underline{k} - 1$
 $\underline{\lambda}$ - cut-edge of Λ_l . It serves as start edge when traversing the FC.
 $\bar{\lambda}$ - last edge when traversing the FC starting from $\underline{\lambda}$
 $\delta_{0,l}$ - number of joint variables of limb l that are not part of a FC of $\Gamma_{(l)}$
 $\delta_{\lambda,l}$ - DOF of FC λ of limb l when disconnected from the platform
 $\sigma_{(\lambda,l)}$ - entries of the fundamental cycle matrix
 $m_{\lambda,l}$ - number of generically independent loop constraints of FC $\Lambda_{\lambda(l)}$ of limb l
 $\eta_{(l)} \in \mathbb{V}^{N_l}$ - overall vector of joint variables $\vartheta_1, \dots, \vartheta_{N_l}$ of limb l (when connected to platform)
 $\vartheta_{(l)} \in \mathbb{V}^{n_l}$ - vector of tree-joint variables $\vartheta_1, \dots, \vartheta_{n_l}$ of limb l (when connected to platform)
 $\bar{\vartheta}_{(l)} \in \mathbb{V}^{\bar{n}_l}$ - vector of tree-joint variables $\vartheta_1, \dots, \vartheta_{\bar{n}_l}$ of limb l (when disconnected from platform)
 ϑ_{act} - vector of actuated joint coordinates
 $\mathbf{q}_{(\lambda,l)}$ - vector of $\delta_{\lambda,l}$ independent variables in terms of which the loop constraints for $\Lambda_{(\lambda,l)}$ can be expressed
 $\mathbf{q}_{(l)}$ - vector of δ_l generalized coordinates of limb l when separated from PKM
 \mathbf{q} - vector of δ generalized coordinates of the PKM
 $\mathbf{y}_{(\lambda,l)}$ - vector of $m_{\lambda,l}$ dependent joint variables of FC $\Lambda_{(\lambda,l)}$ of limb l
 $\mathbf{y}_{(l)}$ - vector of m_l dependent joint variables of limb l when separated from PKM
 $\mathbf{L}_{k(l)}$ - compound geometric Jacobian of body k limb l so that $\mathbf{V}_{k(l)} = \mathbf{L}_{k(l)} \dot{\mathbf{q}}_{(l)}$
 $\mathbf{L}_{p(l)}$ - forward kinematics Jacobian of limb l so that $\mathbf{V}_{p(l)} = \mathbf{L}_{p(l)} \dot{\mathbf{q}}_{(l)}$
 \mathbf{J}_{IK} - inverse kinematics Jacobian of the PKM so that $\dot{\vartheta}_{(l)\text{act}} = \mathbf{J}_{\text{IK}}(\boldsymbol{\eta}_{(l)}) \mathbf{V}_t$
 $\Psi_{\text{IK}(l)}$ - inverse kinematic map of limb l so that $\boldsymbol{\eta}_{(l)} = \Psi_{\text{IK}}(\mathbf{x})$
 Ψ_{FK} - forward kinematic map of mechanism so that $\boldsymbol{\eta} = \Psi_{\text{FK}}(\vartheta_{\text{act}})$
 f_{IK} - inverse kinematic map of PKM so that $\vartheta_{\text{act}} = f_{\text{IK}}(\mathbf{x})$
 $\varphi_{(l)}$ - implicit form of the ODE defining the EOM of limb l . This serves as inverse dynamics solution.
 φ_t - left-hand side of the taskspace formulation of EOM for the PKM

References

- [1] R. Clavel, "Delta, a fast robot with parallel geometry," in *18th Int. Symp. Industrial Robots, Lausanne*, 1988, p. 91–100.
- [2] F. Pierrot, C. Reynaud, and A. Fournier, "Delta: a simple and efficient parallel robot," *Robotica*, vol. 8, no. 2, p. 105–109, 1990.
- [3] J. Angeles, *Fundamentals of robotic mechanical systems*, 3rd ed. Springer, 2007.
- [4] A. Jain, *Robot and Multibody Dynamics*. Springer US, 2011.
- [5] J.-F. Gauthier, J. Angeles, S. B. Nokleby, and A. Morozov, "The kinetostatic conditioning of two-limb schönflies motion generators," *Journal of Mechanisms and Robotics*, vol. 1, no. 1, 2009.
- [6] A. Taghvaeipour, J. Angeles, and L. Lessard, "Constraint-wrench analysis of robotic manipulators," *Multibody System Dynamics*, vol. 29, no. 2, pp. 139–168, 2013.
- [7] O. Altuzarra, A. Zubizarreta, I. Cabanes, and C. Pinto, "Dynamics of a four degrees-of-freedom parallel manipulator with parallelogram joints," *Mechatronics*, vol. 19, no. 8, pp. 1269–1279, 2009.
- [8] P. Wenger and D. Chablat, *Kinematic Analysis of a New Parallel Machine Tool: The Orthoglide*. Dordrecht: Springer Netherlands, 2000, pp. 305–314.

- [9] D. Chablat and P. Wenger, "Architecture optimization of a 3-dof parallel mechanism for machining applications, the orthoglide," *IEEE Transactions on Robotics and Automation*, vol. 19, no. 3, pp. 403–410, 2003.
- [10] A. Wolf, E. Ottaviano, M. Shoham, and M. Ceccarelli, "Application of line geometry and linear complex approximation to singularity analysis of the 3-dof capaman parallel manipulator," *Mechanism and Machine Theory*, vol. 39, no. 1, pp. 75–95, 2004.
- [11] K. Wen, T. S. Nguyen, D. Harton, T. Laliberté, and C. Gosselin, "A Backdrivable Kinematically Redundant (6+3)-Degree-of-Freedom Hybrid Parallel Robot for Intuitive Sensorless Physical Human–Robot Interaction," *IEEE Transactions on Robotics*, 2020.
- [12] J. Wu, J. Wang, L. Wang, and T. Li, "Dynamics and control of a planar 3-dof parallel manipulator with actuation redundancy," *Mechanism and Machine Theory*, vol. 44, no. 4, pp. 835–849, 2009.
- [13] Q. Zou, D. Zhang, X. Luo, G. Huang, L. Li, and H. Zhang, "Enumeration and optimum design of a class of translational parallel mechanisms with prismatic and parallelogram joints," *Mechanism and Machine Theory*, vol. 150, p. 103846, 2020.
- [14] H. Shen, Y. Zhao, J. Li, G. Wu, and D. Chablat, "A novel partially-decoupled translational parallel manipulator with symbolic kinematics, singularity identification and workspace determination," *Mechanism and Machine Theory*, vol. 164, p. 104388, 2021. [Online]. Available: <https://www.sciencedirect.com/science/article/pii/S0094114X21001464>
- [15] A. Klimchik, A. Pashkevich, and D. Chablat, "Stiffness analysis of parallel manipulator navaro with dual actuation modes," in *2018 International Russian Automation Conference (RusAutoCon)*. IEEE, 2018, pp. 1–7.
- [16] C. Baradat, V. Nabat, S. Krut, and F. Pierrot, "Par2: A spatial mechanism for fast planar, 2-dof, pick-and-place applications," in *Proc. 2nd Int Workshop on Fundamental Issues and Future Research Directions for Parallel Mechanisms and Manipulators*, 2009, p. 10.
- [17] O. Company, F. Pierrot, S. Krut, and C. Baradat, "Par2: a spatial mechanism for fast planar two-degree-of-freedom pick-and-place applications," *Meccanica*, vol. 46, p. 239–248, 2011.
- [18] F. Pierrot and O. Company, "H4: a new family of 4-dof parallel robots," in *1999 IEEE/ASME International Conference on Advanced Intelligent Mechatronics (Cat. No.99TH8399)*, 1999, pp. 508–513.
- [19] F. Pierrot, V. Nabat, O. Company, S. Krut, and P. Pognet, "Optimal design of a 4-dof parallel manipulator: From academia to industry," *IEEE Transactions on Robotics*, vol. 25, no. 2, pp. 213–224, 2009.
- [20] F. Pierrot, S. Krut, A. Saenz, O. Company, V. Nabat, and C. Baradat, "Two-Degree-of-Freedom Parallel Manipulator," Aug 2011, patent number: EP2252437 (B1) WO 2009/089916 (A1). Extension : 24/11/10 AR070196 (A1) AT521457 (T) CA2712260 (A1) CN101977737 (A) ES2375074 (T3) JP2011509837 (A) TW200932457 (A) US2011048159 (A1).
- [21] F. Pierrot, T. Shibukawa, K. Morita *et al.*, "Four-degree-of-freedom parallel robot," feb 2003, uS Patent 6,516,681.
- [22] C. Reymond, "Device for the movement and positioning of an element in space," Granted Patent US 4976582 A. [Online]. Available: <https://lens.org/089-198-012-036-824>
- [23] C. Germain, S. Caro, S. Briot, and P. Wenger, "Singularity-free design of the translational parallel manipulator irsbot-2," *Mechanism and Machine Theory*, vol. 64, pp. 262 – 285, 2013.
- [24] N. Rakotomanga, D. Chablat, and S. Caro, "Kinetostatic performance of a planar parallel mechanism with variable actuation," in *Advances in robot kinematics: Analysis and design*. Springer, 2008, pp. 311–320.
- [25] D. Chablat and L. Rolland, "Navaro ii: A new parallel robot with eight actuation modes," in *International Design Engineering Technical Conferences and Computers and Information in Engineering Conference*, vol. 51807. American Society of Mechanical Engineers, 2018, p. V05AT07A043.
- [26] L. Nurahmi and S. Caro, "Type synthesis of two dof hybrid translational parallel manipulators," vol. 836, pp. 48–53, 2016.
- [27] G. Gogu, "Structural synthesis of fully-isotropic translational parallel robots via theory of linear transformations," *European Journal of Mechanics - A/Solids*, vol. 23, no. 6, pp. 1021 – 1039, 2004.
- [28] —, *Structural Synthesis of Parallel Robots: Part 1: Methodology*, ser. Solid Mechanics and Its Applications. Springer Netherlands, 2009.
- [29] X. Kong and C. M. Gosselin, *Type Synthesis of Parallel Mechanisms*. Springer, 2007.
- [30] Z. Huang, Q. Li, and H. Ding, *Theory of Parallel Mechanisms*. Springer Science+Business Media, 2013.
- [31] K. Lee and D. Shah, "Dynamic analysis of a three-degrees-of-freedom in-parallel actuated manipulator," *IEEE Journal on Robotics and Automation*, vol. 4, no. 3, pp. 361–367, June 1988.
- [32] Y. Nakamura and M. Ghodoussi, "Dynamics computation of closed-link robot mechanisms with nonredundant and redundant actuators," *IEEE Transactions on Robotics and Automation*, vol. 5, no. 3, pp. 294–302, June 1989.
- [33] V. Mata, S. Provenzano, J. Cuadrado, and F. Valero, "Inverse dynamic problem in robots using gibbs-appell equations," *Robotica*, vol. 20, no. 1, pp. 59–67, 2002.
- [34] E. Abedloo, A. Molaei, and H. D. Taghirad, "Closed-form dynamic formulation of spherical parallel manipulators by gibbs-appell method," in *RSI/ISM International Conference on Robotics and Mechatronics, Tehran, Iran, October 15-17 2014*, pp. 576–581.

- [35] A. Müller, "Internal preload control of redundantly actuated parallel manipulators –its application to backlash avoiding control," *IEEE Trans. Robotics*, vol. 21, no. 4, pp. 668–677, 2005.
- [36] B. Dasgupta and T. Mruthyunjaya, "A Newton-Euler formulation for the inverse dynamics of the Stewart platform manipulator," *Mechanism and Machine Theory*, vol. 33, no. 8, pp. 1135 – 1152, 1998.
- [37] J. Wang and C. M. Gosselin, "A new approach for the dynamic analysis of parallel manipulators," *Multibody System Dynamics*, vol. 2, no. 3, pp. 317–334, Sep 1998.
- [38] J. Zhao, F. Chu, and Z. Feng, "Kinematics of spatial parallel manipulators with tetrahedron coordinates," *IEEE Transactions on Robotics*, vol. 30, no. 1, pp. 233–243, Feb 2014.
- [39] A. Müller, "Motion equations in redundant coordinates with application to inverse dynamics of constrained mechanical systems," *Nonlinear Dynamics*, vol. 67, no. 4, pp. 2527–2541, 2012.
- [40] A. Müller and T. Hufnagel, "Model-based control of redundantly actuated parallel manipulators in redundant coordinates," *Robotics and Autonomous systems*, vol. 60, no. 4, pp. 563–571, 2012.
- [41] K. Miller and R. Clavel, "The lagrange-based model of delta-4 robot dynamics," *Robotersysteme*, vol. 8, no. 1, pp. 49–54, 1992.
- [42] P. Guglielmetti and R. Longchamp, "A closed form inverse dynamics model of the delta parallel robot," *IFAC Proceedings Volumes*, vol. 27, no. 14, pp. 51–56, 1994, fourth IFAC Symposium on Robot Control, Capri, Italy, September 19-21, 1994.
- [43] J. Brinker and B. Corves, "Lagrangian based dynamic analyses of delta robots with serial-parallel architecture," in *Symposium on Robot Design, Dynamics and Control*. Springer, 2016, pp. 133–141.
- [44] J. Brinker, N. Funk, P. Ingenlath, Y. Takeda, and B. Corves, "Comparative study of serial-parallel delta robots with full orientation capabilities," *IEEE Robotics and Automation Letters*, vol. 2, no. 2, pp. 920–926, 2017.
- [45] M. Bennehar, A. Chemori, M. Bouri, L. Jenni, and F. Pierrot, "A new RISE-based adaptive control of PKMs: design, stability analysis and experiments," *International Journal of Control*, vol. 91, no. 3, pp. 593–607, 2018.
- [46] W. Khalil and O. Ibrahim, "General solution for the dynamic modeling of parallel robots," *Journal of intelligent and robotic systems*, vol. 49, no. 1, pp. 19–37, 2007.
- [47] S. Briot and W. Khalil, *Dynamics of Parallel Robots*. Springer, 2015.
- [48] H. Abdellatif and B. Heimann, "Computational efficient inverse dynamics of 6-dof fully parallel manipulators by using the lagrangian formalism," *Mechanism and Machine Theory*, vol. 44, no. 1, pp. 192 – 207, 2009.
- [49] A. Müller, "Dynamics modeling of topologically simple parallel manipulators: A geometric approach," *ASME Applied Mechanics Review*, vol. 72(3), p. 27 pages, 2020.
- [50] V. Damic and M. Cohodar, "Dynamic analysis of stewart platform by bond graphs," *Procedia Engineering*, vol. 100, pp. 226–233, 2015.
- [51] J. Wu, G. Yu, Y. Gao, and L. Wang, "Mechatronics modeling and vibration analysis of a 2-dof parallel manipulator in a 5-dof hybrid machine tool," *Mechanism and Machine Theory*, vol. 121, pp. 430–445, 2018.
- [52] A. Müller, "Kinematic topology and constraints of multi-loop linkages," *Robotica*, vol. 36, pp. 1641–1663, 2018.
- [53] A. Jain, "Graph theoretic foundations of multibody dynamics, part I: structural properties," *Multibody Syst. Dyn.*, vol. 26, pp. 307–333, 2011.
- [54] J. Wittenburg, *Dynamics of Multibody Systems*, 2nd ed. Springer, 2008.
- [55] L.-W. Tsai and R. Stamper, "A parallel manipulator with only translational degrees of freedom," in *ASME 1996 Design Engineering Technical Conferences, Irvine, CA., 1996*, pp. 96–DETC–MECH–1152.
- [56] L. Tsai, *Robot Analysis: The Mechanics of Serial and Parallel Manipulators*. John Wiley & Sons, Inc., 1999.
- [57] A. Müller, "Review of the Exponential and Cayley Map on $se(3)$ as relevant for Lie group integration of the generalized Poisson equation and flexible multibody systems," *Proceedings of the Royal Society A*, vol. accepted, 2021.
- [58] H. Asada and J. Slotine, *Robot Analysis ad Control*. John Wiley and Sons, 1986.
- [59] J. J. Uicker, B. Ravani, and P. N. Sheth, *Matrix Methods in the Design Analysis of Mechanisms and Multibody Systems*. Cambridge University Press, 2013.
- [60] P. E. Nikravesh, *Computer-aided analysis of mechanical systems*. Prentice Hall, 1988.
- [61] E. Haug, *Computer-Aided Kinematics and Dynamics of Mechanical Systems*. Allyn and Bacon, 1989.
- [62] A. A. Shabana, *Dynamics of Multibody Systems*, 4th ed. Cambridge University Press, 2013.
- [63] A. Müller, "Higher-order constraints for higher kinematic pairs and their application to mobility and shakiness analysis of mechanisms," *Meccanica*, vol. 52, no. 7, pp. 1669–1684, 2017.
- [64] W. Blajer, "Methods for constraint violation suppression in the numerical simulation of constrained multibody systems—A comparative study," *Computer Methods in Applied Mechanics and Engineering*, vol. 200, no. 13-16, pp. 1568–1576, 2011.
- [65] J. C. G. Orden and S. C. Martín, "Controllable velocity projection for constraint stabilization in multibody dynamics," *Nonlinear Dynamics*, vol. 68, no. 1, pp. 245–257, 2012.
- [66] R. Wehage and E. J. Haug, "Generalized coordinate partitioning for dimension reduction in analysis of constrained dynamic systems," *Journal of Mechanical Design*, vol. 104, pp. 247–255, 1982.

- [67] K. T. Wehagea, R. A. Wehageb, and B. Ravani, “Generalized coordinate partitioning for complex mechanisms based on kinematic substructuring,” *Mech. Mach. Theory*, vol. 92, pp. 464–483, 2015.
- [68] P. Nikravesh, “Systematic reduction of multibody equations of motion to a minimal set,” *Int. J. Non-Linear Mechanics*, vol. 25, no. 2, pp. 143–151, 1990.
- [69] W. Blajer, W. Schiehlen, and W. Schirm, “A projective criterion to the coordinate partitioning method for multibody dynamics,” *Archive of Applied Mechanics*, vol. 64, no. 2, pp. 86–98, 1994.
- [70] Z. Terze and J. Naudet, “Structure of optimized generalized coordinates partitioned vectors for holonomic and non-holonomic systems,” *Multibody system dynamics*, vol. 24, no. 2, pp. 203–218, 2010.
- [71] M. Wojtyra, “Joint reactions in rigid body mechanisms with dependent constraints,” *Mechanism and Machine Theory*, vol. 44, no. 12, pp. 2265–2278, 2009.
- [72] J. G. de Jalón and M. D. Gutierrez-Lopez, “Multibody dynamics with redundant constraints and singular mass matrix: existence, uniqueness, and determination of solutions for accelerations and constraint forces,” *Multibody System Dynamics*, vol. 30, no. 3, pp. 311–341, 2013.
- [73] A. Müller, “Semialgebraic regularization of kinematic loop constraints in multibody system models,” *Journal of computational and nonlinear dynamics*, vol. 6, no. 4, 2011.
- [74] —, “Implementation of a geometric constraint regularization for multibody system models,” *Archive of Mechanical Engineering*, pp. 367–383, 2014.
- [75] J. Hervé, “Analyse structurelle des mécanismes par groupe des déplacements,” *Mech. Mach. Theory*, vol. 13, pp. 437–450, 1978.
- [76] J. Herve, “Intrinsic formulation of problems of geometry and kinematics of mechanisms,” *Mech. Mach. Theory*, vol. 17, no. 3, pp. 179–184, 1982.
- [77] A. Müller, “An overview of formulae for the higher-order kinematics of lower-pair chains with applications in robotics and mechanism theory,” *Mechanism and Machine Theory*, vol. 142, p. 103594, 2019.
- [78] L.-W. Tsai, “The Jacobian analysis of a parallel manipulator using reciprocal screws,” in *Advances in Robot Kinematics: Analysis and Control*, J. Lenarčič and M. Husty, Eds. Springer, Dordrecht, 1998, pp. 327–336.
- [79] S. A. Joshi and L.-W. Tsai, “Jacobian analysis of limited-dof parallel manipulators,” *ASME J. Mech. Des.*, vol. 124, pp. 254–258, 2020.
- [80] T. Huang, H. Liu, and D. Chetwynd, “Generalized jacobian analysis of lower mobility manipulators,” *Mechanism and Machine Theory*, vol. 46, no. 6, pp. 831–844, 2011.
- [81] D. Kim and C. W. Kyun, “Analytic formulation of reciprocal screws and its application to nonredundant robot manipulators,” *ASME J. Mech. Des.*, vol. 125, pp. 158–164, 2003.
- [82] A. Müller, “On the terminology and geometric aspects of redundant parallel manipulators,” *Robotica*, vol. 31, no. 1, p. 137–147, 2013.
- [83] A. Müller, “Screw and lie group theory in multibody dynamics —motion representation and recursive kinematics of tree-topology systems,” *Multibody System Dynamics*, vol. 43, no. 1, pp. 1–34, 2018.
- [84] —, “Screw and lie group theory in multibody dynamics –recursive algorithms and equations of motion of tree-topology systems,” *Multibody System Dynamics*, vol. 42, no. 2, pp. 219–248, 2018.
- [85] G. Rodriguez, A. Jain, and K. Kreutz-Delgado, “A spatial operator algebra for manipulator modeling and control,” *The International Journal of Robotics Research*, vol. 10, no. 4, pp. 371–381, 1991.
- [86] A. Jain, “Unified formulation of dynamics for serial rigid multibody systems,” *Journal of Guidance, Control and Dynamics*, vol. 14, pp. 531–542, 1991.
- [87] R. Featherstone, *Rigid Body Dynamics Algorithms*. Springer, 2008.
- [88] F. Park, J. Bobrow, and S. Ploen, “A lie group formulation of robot dynamics,” *The International Journal of Robotics Research*, vol. 14, no. 6, pp. 609–618, 1995.
- [89] F. Park and M. Kim, “Lie theory, riemannian geometry, and the dynamics of coupled rigid bodies,” *Zeitschrift für angewandte Mathematik und Physik (ZAMP)*, vol. 51, no. 5, pp. 820–834, 2000.
- [90] A. Müller, “Recursive second-order inverse dynamics for serial manipulators,” in *2017 IEEE International Conference on Robotics and Automation (ICRA)*. IEEE, 2017, pp. 2483–2489.
- [91] —, “An $O(n)$ -Algorithm for the Higher-Order Kinematics and Inverse Dynamics of Serial Manipulators Using Spatial Representation of Twists,” *IEEE Robotics and Automation Letters*, vol. 6, no. 2, pp. 397–404, 2020.
- [92] K. M. Lynch and F. C. Park, *Modern Robotics*. Cambridge, 2017.
- [93] J. Angeles and S. Lee, “The formulation of dynamical equations of holonomic mechanical systems using a natural orthogonal complement,” *ASME J. Appl. Mech.*, vol. 9, no. 5, pp. 243–244, 1988.
- [94] A. Müller, “On the Hamel Coefficients and the Boltzmann–Hamel Equations for the Rigid Body,” *Journal of Nonlinear Science*, vol. 40, p. 39 pages, 2021.
- [95] P. Voronets, “Equations of motion for nonholonomic systems,” *Matem. Sbornik*, vol. 22, no. 4, 1901.
- [96] P. Voronetz, “Über die Bewegung eines st arren Körpers, der ohne Gleitung auf einer beliebigen Fläche rollt,” pp. 410–453, 1910.

- [97] J. E. Marsden and T. S. Ratiu, *Introduction to mechanics and symmetry: a basic exposition of classical mechanical systems*. Springer Science & Business Media, 2013, vol. 17.
- [98] D. D. Holm, *Geometric Mechanics-Part II: Rotating, Translating And Rolling*. World Scientific, 2011.
- [99] C. Stoeffer, S. Kumar, H. Peters, O. Bröls, A. Müller, and F. Kirchner, "Conceptual design of a variable stiffness mechanism in a humanoid ankle using parallel redundant actuation," in *2018 IEEE-RAS 18th International Conference on Humanoid Robots (Humanoids)*. IEEE, 2018, pp. 462–468.
- [100] J. Y. Luh, M. W. Walker, and R. P. Paul, "On-line computational scheme for mechanical manipulators," 1980.
- [101] A. Mueller, "Code implementation for modeling parallel robots (PKM) with complex loops, and a Delta robot example." *Mendeley Data*, v1, 2021, <https://doi.org/10.17632/2k77vxszb.1>.
- [102] C. E. Bryson and D. C. Rucker, "Toward parallel continuum manipulators," in *2014 IEEE International Conference on Robotics and Automation (ICRA)*. IEEE, 2014, pp. 778–785.